From individuals to species: how natural selection and phenotypic plasticity shape ecomorphological evolution in freshwater mussels

A DISSERTATION
SUBMITTED TO THE FACULTY OF
UNIVERSITY OF MINNESOTA
BY

Sean Michael Keogh

IN PARTIAL FULFILLMENT OF THE REQUIREMENTS FOR THE DEGREE OF
DOCTOR OF PHILOSOPHY

Andrew M. Simons

May 2023

Acknowledgments

This research would not be possible without a tremendous support network. I have been extremely lucky to work with great mentors starting with Andrew Simons (advisor), Stewart Edie & John Pfeiffer (NMNH fellowship advisors), Keith Barker, Sarah Boyer, & Kieran McNulty (committee members), Mark Hove, Sharon Jansa, Sushma Reddy, and Bernard Sietman. I am grateful for the friendship and support of EEB students in the 2018 *cohorde* and beyond. I thank the many museums, collection managers, and curators who allowed me to loan and scan specimens including Bell Museum of Natural History, Amanda Robinson (National Museum of Natural History), Jochen Gerber (Field Museum), Alison Stodola (Illinois Natural History Survey), John Slapcinsky (Florida Museum of Natural History), Charles Randklev (Texas A&M-Natural Resources Institute), and Lily Berniker (American Museum of Natural History). I thank Freya Goetz for assistance scanning specimens and the SI Imaging Facility at the National Museum of Natural History and Brian Bagley at the University of Minnesota for training to operate the computed-tomography scanner in the UMN XRCT lab. I thank Alex Franzen, Ben Minerich, Lindsay Ohlman, Maddie Pletta, Anna Scheunemann, Zeb Secrist, and Bernard Sietman for propagation and husbandry of juvenile mussels as well as assistance in the field. I thank Jess Kozarek, Jiyong Lee, Ben Erickson, Miki Hondzo, and Jeff Marr for assistance and access to the tilting-bed flume at St. Anthony Falls Laboratory. Some computations in my dissertation were conducted on the Smithsonian Institution High Performance Cluster (SI/HPC; https://doi.org/10.25572/SIHPC) and on the Minnesota Supercomputing Institute (University of Minnesota; http://www.msi.umn.edu) High Performance Computing systems.

Dedication

I dedicate this work to my family.

Abstract

Adaptation is the hallmark of evolutionary biology, explaining how species achieve ecological success through natural selection. However, adaptation is challenging to identify leading to frequent 'just-so stories' to explain the adaptive features of organisms. At the core of adaptive studies is the motivation to find the fit between morphological and functional diversity. Here I used the freshwater mussels of North America as a study system to investigate the fit between morphological and ecological traits both within and across species. I used comparative and experimental inferences to identify the evolutionary mechanisms driving ecomorphological patterns. My first chapter identified ecomorphological patterns within and across species between shell thickness, shell anterior thickening, and flow rate. Across species, I found widespread convergence in these traits showing that natural selection produces the following adaptations to riverine flow rates: thick and anteriorly thickened shells in high flow rates (likely for stability in the substratum) and thin and uniformly thickened shells in low flow rates (likely for burrowing efficiency). Additionally, within species, I found a creditably positive relationship between shell thickness and flow rate, effectively mirroring interspecific relationships albeit at different scales. Intraspecific processes may therefore be partially responsible for the evolvability and ecological diversification of the clade. Although I identified this intraspecific ecomorphological pattern, I could not identify the mechanism producing this pattern. To address this, in my second chapter I conducted a common garden experiment on a morphologically variable species, *Pyganodon grandis*. The morphology of this species varies predictably between lake and stream environments and I investigated if this relationship was due to phenotypic plasticity or genetic

differentiation. By rearing siblings from a single female's broodstock, I minimized genetic variation, and released ~6,000 marked individuals into nine sites (four streams, five lakes). Two years after release, I recaptured a total of 70 individuals from both stream and lake sites showing significant shell shape differences between habitats and no shell shape differences between recaptured siblings and wild *P. grandis* reared at the same site, showing definitively that phenotypic plasticity rather than genetic differentiation is driving ecomorphological patterns. In my third and final chapter I ran a fluvial experiment investigating the function of mussel posterior 'ribbed' sculpture. I measured water velocity magnitude, direction, and streambed erosion surrounding mussel models with sculpture and with their sculpture manually removed. In opposition to previous studies, I found more streambed erosion associated with sculptured models. However, mussel orientation to streamflow was the more significant driver to variations in water velocity magnitude, direction, and streambed erosion. This body of work illustrates the complementary nature of phylogenetic comparative methods and experiments to finding the evolutionary mechanisms of phenotypic variation. Lastly, the role of phenotypic plasticity in macroevolutionary outcomes has seldom been investigated but the widespread convergence of ecomorphological traits in chapter 1 and common garden experiment in chapter 2 suggest plasticity may be a key mechanism to macroevolutionary diversification.

Table of Contents

List of Tables

List of Figures

Chapter 1:

Riverine flow rate drives widespread convergence in the shells of imperiled Nearctic freshwater mussels

Introduction

Both contingency and determinism underlie macroevolutionary patterns (Conway Morris 2003, cf. Gould 1989), but the relative contributions of each process can vary in space and time. Historical contingencies often manifest as phylogenetic constraint or extinction constricting phenotypic evolution along particular, and many times unpredictable lines, and determinism as the repeated evolution of high-fitness phenotypes among different selective regimes (Agrawal 2017). A good measure of either's impact on evolution is the frequency and degree of convergence (Burns and Sidlauskas 2019; Rincon-Sandoval et al. 2020), where two or more species evolve similar phenotypes under similar selective pressures independent of their shared ancestry (Carroll 2001; Losos 2011). Phylogenetic comparative approaches across geographically separated but similar habitats (e.g. islands and lakes; Losos et al. 1998; Schluter and Nagel 1995) provide natural experiments to test the frequency and strength of ecomorphological evolution. For strictly aquatic lineages, river basins can limit gene flow and create opportunities for independent diversification across similar hydrological gradients (e.g. Endler 1982). Riverine hydrological dynamics also appear to apply strong selection on phenotypes: fishes have convergently evolved streamlined (i.e. fusiform) body shapes (Lamouroux et al. 2002; Bower et al. 2021); rheophytes, aquatic plants associated with stream habitats, have independently

evolved streamlined leaves and flexible shoots (van Steenis 1981; Karrenberg et al. 2002; Medina et al. 2020; Lytle and Poff 2004); and stream-dwelling snakes have convergently evolved narrow heads to reduce hydrodynamic drag (Hibbitts and Fitzgerald 2005; Segall et al. 2020). Whether this same pressure drives high degrees of convergence for animals that live on or just below the streambed is less clear. Freshwater mussels, a diverse global radiation of filter-feeding bivalves, live at the sediment-water interface across hydrological gradients, from small headwater streams to the largest rivers (Graf and Cummings 2021; Pfeiffer et al. 2022). This broad environmental gradient is hypothesized to be a strong driver of selection for the high morphological disparity of the group (Randklev et al. 2019; Watters 1994), making freshwater mussels a good system to test whether ecomorphological convergence can supersede historical contingencies in evolutionary radiations.

Dislodgment (i.e. displacement by entrainment) of a mussel from its shallowly buried life position exposes it to unsuitable habitats (Sotola et al. 2021) that are detrimental to its survival and fitness (Hastie et al. 2001; Lopez and Vaughn 2021). In large rivers, consistently high flow rates and high shear stress disrupt the streambed by scouring sediment (Sambrook Smith et al. 2010; Curley et al. 2021). In smaller streams, average flow rates are lower, but droughts (Humphries and Baldwin 2003) and flooding (Alila and Mtiraoui 2002) apply infrequent yet stressful disruptions to mussels in the streambed (Hastie et al. 2001). Thus, two evolutionary pathways are hypothesized here to minimize dislodgement: stabilization to maintain life position in the sediment, and mobility to rapidly burrow (vertically or horizontally) during flood and dewatering events. Multiple morphological traits are hypothesized to be under

selection for stabilizing and burrowing functions. For stability and counteracting dislodgement, the mussel becomes better anchored in the substratum with: (a) increased mass from larger shell size (Haag and Rypel 2011); (b) increased density from thicker shells per unit size (Watters 1994); and (c), shifting the shell's center of mass further below the sediment-water interface (as anterior thickening in Figure 1.1, Vermeij and Dudley 1985; Savazzi and Peiyi 1992). For increased burrowing rate: (a) smaller shell sizes reduce mass and (b) thinner shells decrease density, both of which increase burrowing efficiency (Stanley 1970) (left side Figure 1.1). Higher flow rates may apply a more constant dislodgement pressure, selecting for traits that increase stabilization rather than burrowing rate (Stanley 1981, 1970; Johnson 2020; Levine et al. 2014). At lower flow rates, a more infrequent dislodgement pressure from floods or to reposition during drought may select for increased burrowing efficiency rather than stability (Haag 2012). Alternatively, the animal's shell morphology may reflect a functional tradeoff between stabilization and burrowing traits. In any case, the strength of correlated evolution between phenotypes and environments reflects the balance of determinism driving convergence or constraints restricting it.

Here I analyzed shell traits in a phylogenetic context across 164 species including 718 specimens from an environmentally widespread assemblage of North American freshwater mussels (Unionidae & Margaritiferidae) to test: (1) the strength of association between shell morphology and riverine flow rates at both intra and interspecific levels and (2), the frequency and completeness of convergent evolution among similar hydrologic regimes. Given the high fitness cost of dislodgement, I expect that strong selection to maintain a burrowed position will result in a tight

correlation between shell traits and flow rates, with size, overall thickness, and anterior thickening positively correlated with flow rate. I also expect that this selection will result in convergence superseding phylogenetic contingencies, resulting in repeated evolution of functionally similar shell morphologies across transitions into environments with similar flow rates. With their multiple, independent invasions into disjunct river basins across North America (Sepkoski and Rex 1974; Haag 2010), and high morphological and environmental disparity, freshwater mussels are a well-suited system to explore how determinism and contingency shape macroevolution.

Materials and Methods

Sampling, phylogeny, and scanning

As with many studies of evolutionary convergence (e.g. Grossnickle et al. 2020; Serb et al. 2017; Friedman et al. 2016), broad phylogenetic, morphological, and environmental diversity was captured by sampling 164 species (Unionidae + Margartiferidae) comprising over 50% of the extant freshwater mussel diversity of Northern America (Graf and Cummings 2021; http://mussel-project.net/). Of those 164 species, a phylogenetic hypothesis was reconstructed for 150 species (Figure 1.2). Available mitochondrial (COI, NDI, & 16S) and nuclear genes (ITS1 & 28S) were aggregated from GenBank (Table 1.1) in the R package *rentrez* (Winter 2017). Protein-coding genes (COI & NDI) were aligned using MUSCLE in AliView v1.27 and non protein-coding genes were aligned using the E-INS-i method within MAFFT and implemented in Mesquite v3.7 (Edgar 2004, Larsson 2014, Katoh et al. 2005, Maddison and Maddison 2021). Alignments were imported in BEAUTI v2.6.6 and a

substitution model of HKY was used for each codon position of COI and NDI and a single partition for each of the remaining three loci (non protein-coding) (Bouckaert et al. 2019). All partitions (and all loci) were linked to a single tree model with a Yule (pure-birth) model of speciation. To calculate time-relative branch lengths, a relaxed lognormal molecular clock was used for each locus aside from COI and NDI, which were assumed to be evolving together. An ultrametric tree was estimated from combining three runs of 100,000,000 MCMC generations sampling every 5,000 generations in BEAST v2.5.2 (Bouckaert et al. 2019). The monophyly of four taxonomic groups (Unionidae, Amblemini, Lampsilini, and Lampsilini+Popenaidini) were constrained based on previous phylogenetic hypotheses with greater character sampling (Pfeiffer et al. 2019). Tracer v1.7.1 was used to ensure MCMC runs converged and mixed properly (Rambaut et al. 2018). Runs were combined in LogCombiner v2.6.6 and TreeAnnotator v2.6.6 was used to construct a maximum clade credibility tree and assess a 20% burnin (Bouckaert et al. 2019). Five nodes with poor posterior support (<0.5) were collapsed to soft polytomies at https://itol.embl.de/ and collapsed branches were forced to be ultrametric in *phytools::force.ultrametric* (Revell 2012).

Morphological variation was captured by sampling representative specimens from museum collections. Intraspecific sampling maximized sexual, morphological, geographical, and habitat variation. A median of 4 individuals was sampled for 164 species, with only 5 species represented by a single specimen (718 total specimens). One shell valve (hereafter shell) was sampled per specimen; all species sampled are equivalve and aside from interlocking teeth, are mirror images for the traits analyzed

here. All right valves were analytically mirrored about their commissural plane, which defines the point of contact between the two closed valves, to become operational left valves. Shells were scanned using micro-computed tomography at University of Minnesota's X-ray Computed Tomography facility and National Museum of Natural History's Scientific Imaging facility. Three-dimensional, contour mesh models were created from computed tomography image slices in Amira and ORS Dragonfly and then cleaned (filled small holes and made manifold) in Autodesk Meshmixer. The commissural plane and hinge line were digitized in MeshLab per Edie et al. (2022). Because not all 164 species were sampled in the phylogeny, two subsets of data were used across analyses: (1) the 'all-species' dataset (164 spp., 718 specs.), and (2) the 'phylogenetic-species' dataset (150 spp., 668 specs.). All subsequent analyses and data manipulation were done in R (R Core Team 2022).

Shell size, thickness, and anterior thickening

Shell size and thickness were derived from the mesh data. Meshes were split along the commissure line into two sides: 'interior,' facing the soft anatomy, and 'exterior,' facing the external environment (detailed procedure in Edie et al. 2022). Shell size was then determined as the centroid size of 10,000 equally spaced points on the surface of the shell's exterior mesh (via the Poisson disc sampler in *Rvcg::vcgSample*, Schlager 2017). Using only the shell's exterior mesh limits the potential impact of shell thickness on the measurement of size. For shell thickness, 10,000 equally spaced points were placed on both the shell's interior and exterior meshes, and for each interior point, the Euclidean distance to the nearest exterior

point was calculated as a localized measure of shell thickness (Collins et al. 2019). Overall shell thickness was then defined by the median value across measurements.

The anteriorward positioning of shell thickness (hereafter anterior thickening) was determined by measuring shell thickness at each of 400 points arrayed in an equidistant 'grid' placed on the surface of the shell's exterior mesh. The dorsal margin of the grid was aligned to the hinge line, and points were sampled at equal distances along the exterior mesh surface from the anteriormost to posteriormost points along each grid axis (full details and a graphical workflow is provided in Edie et al. 2022, their Supplemental Figure S4). The nearest distance from each grid point to the shell's interior surface mesh were taken, and all distances were then rescaled to 0-1 from the shell's 2% and 98% quantiled thickness values, respectively. This 'thickness map' provides a spatial distribution of relative thickness across the shell that can be compared across specimens. Thickness maps were summarized across individuals using principal components analysis (PCA). The first principal component (PC1) captured the primary gradient between shells with evenly distributed thickness and those with relatively thicker anterior margins (Figure 1.3). Thus, specimen scores along PC1 were used to represent the degree of anterior shell thickening, with more positive values indicating greater relative anterior thickness. Shell thickness and size were natural log transformed for downstream analyses.

Flow rate (within and across species)

Scanned specimens were georeferenced using their recorded latitude and longitude or by estimating the latitude and longitude of their occurrence from locality

metadata. Flow rates encountered across each species were estimated using a larger database of georeferenced occurrences compiled from 45 U.S. natural history collections (Pfeiffer et al. 2022; 89 of those records were changed from *L. teres* to *L. sietmani*). Each occurrence was mapped to the nearest river stretch (i.e. ComID) in the National Hydrography Dataset Plus (NHDPlusV2) which provides flow rates in cubic feet per second (ft^3/s) summarized as annual means in addition to stream slope, and Strahler stream order (USGS 2020). In order to remove lentic habitats, occurrences with non-positive values for flow rate and stream slope were removed. Thus, flow rate was recorded for all 718 sampled individuals in addition to ~217,000 occurrences from the updated Pfeiffer et al. (2022) dataset comprising the 164 species analyzed here. All species had at least twenty occurrences (median: 555, mean: 1,334). Flow rates were summarized for each species using the median flow rate. The median value best represents the 'typical' habitat use in comparison to the mean and mode as it was less biased to multimodal or skewed data distributions. Flow rates were natural log transformed for downstream analyses.

Within-species analyses

Phylogenetic comparative studies frequently assume that species-specific means are biologically relevant but such simplifications can mask meaningful intraspecific level processes (e.g. local adaptation, phenotypic plasticity) and can lead to erroneous results at the interspecific-level (Garamszegi and Møller 2010; Harmon and Losos 2005). Freshwater mussels have intraspecific variation in shell characters and habitat use (Inoue et al. 2013; Zieritz and Aldridge 2009) that can overlap among species

(Keogh and Simons 2019; Pieri et al. 2018). Thus, within-species, specimen-level correlations between morphological traits and flow rate were analyzed first.

Correlation between shell traits

Given the indeterminate, accretionary growth of the bivalve shell, its size, thickness, and anterior thickening may covary. The correlation between traits was modeled using two different Bayesian multilevel models for the all-species dataset (*model 1*, Table 1.2) and the phylogenetic-species datasets (*model 2*). The multilevel structure (i.e. varying-intercept) better accommodates the uneven sampling of individuals per species, giving a less-biased estimate of the correlation between traits (Gelman and Hill 2007). Models were fit using the R package *brms* (Bürkner 2017) with Gaussian response distributions and broad priors; four chains were sampled to convergence. For models that accounted for evolutionary relationships ('*phylo*' term, Table 1.2), a phylogenetic variance-covariance matrix was created in *ape::vcv.phylo* (Paradis and Schliep 2019) assuming a Brownian motion model of evolution.

Effect of flow rate on shell traits

The correlation between shell traits and flow rate was modeled using a series of five Bayesian linear regressions for both the all-species and phylogenetic-species datasets (models *3*, *4*, *5*, *6*, *7*, *8*). Models were fit using the same procedure as the inter-trait regressions above. Model support was evaluated using leave-one-out cross validation to estimate the differences in expected log predictive density (elpd; see R package *loo*, Vehtari et al. 2017).

Species-level analyses

Any adaptive divergence in species' shell traits may be more closely reflected by its modal phenotype in its most commonly occupied (typical) environment. Further, museum collections often capture broad environmental occurrences, which can over-represent rare occurrences and under-represent common ones (Tan et al. 2022). To downweight possible phenotypic and environmental outliers, the form-environment relationship was analyzed for summarized shell traits of individuals occurring in a species' typical habitat. Individuals occurring at flow rates that were within the inner-quartile range (IQR) observed for the species-wide georeferenced dataset were selected to represent the typical phenotypes. For species with no individuals sampled within the species-wide flow rate IQR, the individual with a flow rate nearest the species-wide median was selected (N=37 species). This subset resulted in a median of one individual sampled per species (Figure S5). The median shell trait value was then taken for species with more than one individual occurring within its IQR of flow rate.

Correlation between shell traits and effect of flow rate

Intercorrelation between shell traits was evaluated using a similar approach to the within-species analysis but without the species-level term (models *9*, *10*). The correlations between shell traits and flow rate were then evaluated using a similar series of Bayesian regressions as for the within-species analysis (models *11*, *12*).

Convergence of shell traits in riverine habitats

Convergence was quantified using the 'C-metrics' (C_1, C_2, C_3, C_4) developed in Stayton (2015). C_1 ranges from 0-1 and quantifies the proportion of phenotypic distance reduced by evolution of two or more extant taxa relative to the phenotypes of their ancestors; high values indicate more similar phenotypes relative to estimated ancestral phenotypes. C_2 is the phenotypic distance quantified for C_1. C_3 and C_4 measure the proportion of convergence relative to the total amount of evolution in the smallest clade that contains the tested set of convergent taxa (=C_3) and for the entire clade (=C_4). To reduce computation time, C-metrics were calculated using a modified version of the *convevol::convratsig* function (Stayton 2014) from Zelditch et al. (2017). Significance was tested against a simulated distribution of traits evolving under Brownian motion (1000 iterations). *Convevol* requires *a priori* grouping of species; therefore, stream order was used to assign species to three categorical 'habitat assemblages': small river (stream orders=3-4, N=52), medium river (stream order=5, N=68), and large river (stream order=6-8, N=30) (see correlation between flow rate and stream order in Figure 1.4). As *convevol* can be sensitive to outliers (Grossnickle et al. 2022), two-dimensional phylomorphospaces (Figure 1.5) were created using *deeptime::geom_phylomorpho* (Gearty 2023) to visualize any potential outlier taxa. No evidence of outliers were observed. Thus, the full 150 species phylogenetic dataset was used. Convergence in multivariate morphology (i.e. shell thickness, size, and anterior thickening) was tested for each habitat group.

Results

Within-species trait covariation

Inter-trait correlation

Within species, shell size and thickness are credibly correlated both with and without taking into account phylogenetic relationships among species (Table 1.3, Figure 1.6a). Both models have a low explained variance at the population-level (i.e. the fixed effect holding the group-level effects constant), but high explained variance when including species-level effects (Table 1.3); thus, shell thickness increases with size within species, but species have different mean thickness values. The greater uncertainty of the population-level regression fits for the phylogenetic models (*model 2*, Figure 1.6) derives from the variance in the population-level intercept (Table 1.3), which is influenced by the added variance from the group-level, between-species term (i.e. '1 | *phylo*'). Shell anterior thickening (more positive PC1 scores) increases with shell size and thickness, but with wide uncertainty driven by species-level trait differences (Table 1.3, Figure 1.6b-c). Thus, modeling the effects of flow rate on shell traits accounted for all inter-trait correlations.

Within-species relationships between flow rate and shell traits

Shell size. While accounting for species-level effects, the phylogenetic relatedness of species, and its covariation with shell thickness and anterior thickening, shell size is not likely correlated or weakly anti-correlated with flow rate (Figure 1.7a, Table 1.4). Across all specimens (*model 4*), flow rate has no effect on shell size (95% credible interval brackets zero, Table 1.4). However, the better supported models *5* and *6*, which account for species-level effects, both recover credibly negative effects of flow rate on shell size (Table 1.4), showing that species-level effects bias the among

specimen regression (i.e. *model 4*). Models *7* and *8*, which account for phylogenetic relationships among species, are not directly comparable to models *5* and *6* in terms of their information criteria given the different sizes of the datasets, but these models indicate no correlation between shell size and flow rate (Table 1.4). The effects of flow rate on shell size are similar between the non-phylogenetic and phylogenetic models (Figure 1.7a, Table 1.4), showing that phylogenetic relatedness affects the uncertainty in the inferred relationship but not its direction and magnitude; the standard deviation of the phylogenetic random effect is also similar to the species-level effect ($\sigma_{phylo} \sim \sigma_{species}$, Table 1.4). Models that allow the effect of flow rate to vary by species (models *6* and *8*) are slightly more supported over models that fix the effect of flow rate across species (models *5* and *7*), indicating species-specific effects of flow rate on shell size. However, only 30 of 150 species have a mean effect of flow rate outside the 95% CI of the effect among all individuals (*model 8*, Figure 1.8). Thus, shell size tends to not vary or slightly decrease with flow rate across species, with species-level differences in shell size explaining much of the variance among individuals; the explained variance of the species-effect *model 8* increases from the fixed-effects level ($R^2_{\beta} = 0.38$) to the entire-model level ($R^2_{\text{model}} = 0.86$; Table 1.4).

Shell thickness. While accounting for species-level effects, the phylogenetic relatedness of species, and its covariation with shell size and anterior thickening, shell thickness is positively correlated with flow rate (Figure 1.7b). Across all individuals (*model 4*), shell thickness is positively correlated with flow rate (Table 1.5). That effect is still positive, but decreases when accounting for variation in shell thickness

by species in *model 5* and their relatedness in *model 6* (Table 1.5). Virtually identical effects of flow rate on shell thickness are recovered when accounting for phylogenetic relatedness of species (models *7* and *8*, Table 1.5). As for the models of shell size, models with species-specific effects of flow rate on shell thickness are better supported (compare Δelpd values between models *5* and *6* and for models *7* and *8* in Table 1.5). Models that allow the effect of flow rate to vary by species (models *6* and *8*) are slightly more supported over models that fix the effect of flow rate across species (models *5* and *7*), indicating species-specific effects of flow rate on shell thickness. More species have specific flow rate effects for shell thickness than size, with 78 of 150 species estimated to have a mean effect of flow rate outside the 95% CI of the effect among all individuals (*model 8*, Figure 1.8). However, species-specific effects of flow rate on thickness (varying slopes) have a lower overall effect than species-level differences in thickness (varying slopes; $\sigma_{flow} << \sigma_{species}$, Table 1.5). Thus, shell thickness tends to increase with flow rate within species, but species-level differences in shell thickness explain much more of the variance among individuals; the explained variance of the species-effect *model 7* increases from the fixed effects level ($R^2_{\beta} = 0.37$) to the entire model level ($R^2_{\text{model}} = 0.80$; Table 1.5).

Shell anterior thickening. While accounting for species-level effects, the phylogenetic relatedness of species, and its covariation with shell size and thickness, shell anterior thickening is not correlated with flow rate across all models (Figure 1.7c, Table 1.6).

Species-level trait covariation

Correlation between shell traits

Shell size and thickness are credibly correlated with similar estimated relationships between the non-phylogenetic and phylogenetic models (Table 1.7, Figure 1.9a). Unlike the individual level, shell size does not have a credible effect on shell anterior thickening (Table 1.7, Figure 1.9b). Shell anterior thickening is correlated with shell thickness (Table 1.7, Figure 1.9c). Thus, modeling the effects of flow rate on shell traits at the species level accounted for the inter-trait correlations between size and thickness and between thickness and anterior thickening.

Species-level relationships between flow rate and shell traits

While accounting for the phylogenetic relatedness of species and its covariation with shell thickness, shell size does not correlate with flow rate for species occurrences at typical flow rates (Figure 1.10a, Table 1.8). However, both shell thickness and anterior thickening credibly increase with flow rate (Figure 1.10b-c, Table 1.8) while accounting for intertrait covariation and phylogenetic relatedness.

Convergence testing

Species occurring in small, medium, and large river systems have evolved to be significantly more similar in their shell traits relative to their ancestors (Table 1.9). Evolution has closed between 35.5% to 42.9% of the morphological distance for small, medium, and large river species, respectively (C_1 in Table 1.9, total phenotypic distance as C_2). Convergence is responsible for between 16.8% to 21.2% of the total

morphological evolution in lineages leading from the most recent common ancestor to the tips for each habitat grouping (C_3 in Table 1.9). However, only the large river habitat assemblage had a significant C_3 metric and no habitat assemblage had a significant C_4 metric.

Discussion

Evolutionary adaptations to semi-infaunal lifestyles across riverine flow rates

The positive evolutionary correlation between shell thickness (accounting for size) and flow rate among species is consistent with the hypotheses that thin shells are adapted to burrow quickly in low flow environments and thick shells are adapted for stabilization in high flow environments. At higher flow rates, the shell becomes a denser component of the animal because calcium carbonate greatly outweighs the animal's internal soft anatomy (Eagar 1978). Although no freshwater mussels were tested, Stanley (1970) found that both burrowing time and stability in the substratum increased with shell density for semi-infaunal marine bivalves. The increased anterior thickening with flow rate among species is also consistent with the hypothesis that anterior sequestration of shell thickness pushes mass—and thus the center of gravity—deeper into the substratum, acting like a cemented fence post (Vermeij and Dudley 1985). Thus, the evolutionary form-environment relationships recovered for the semi-infaunal freshwater mussels here likely reflect a functional tradeoff between rapid burrowing and greater stabilization: mussel species typical of low flow environments have poor stability and mussel species typical of high flow environments are poor burrowers. However, against my hypothesis, shell size has no

relationship with flow rate while accounting for its strong covariation with thickness. This suggests that modulation in the mass of freshwater mussels arises mostly from alterations to overall and spatial positioning of shell thickness rather than size. Biomechanical and/or functional equivalency may emerge from modular evolution of shell size, thickness, and anterior thickening, and may explain some of the residual variance in the form-environment relationship. However, I observe little evidence of a many-to-one mapping of functionally equivalent traits (Figure 1.11). Species constrained to develop thin shells may position that thickness anteriorly or grow to larger sizes in higher flow settings, but *Potamilus* species, which occur among the highest flow rates, are relatively thin shelled and show only a modest increase in size with low anterior thickening (Figure 1.11). Instead modifications to shell shape may act to increase stabilization and burrowing efficiency in this genus. Several other lineages that deviate from the positive thickness-flow rate relationship also have similar, laterally compressed and winged (i.e. symphynote) shell shapes (e.g. *Potamilus alatus, Lasmigona complanata, Utterbackiana suborbiculata*). Phylogenetic comparative analyses of shell shape, its sculpture (i.e. ornamentation), and internal soft anatomy will better resolve questions on tradeoffs in freshwater mussel functional morphology (Stanley 1975; Trueman et al. 1966).

Additional ecological and evolutionary processes may underlie the form-environment relationship in freshwater mussels, but the patterns found here suggest that the primary driver of selection is the physical environment, i.e. flow rate. Predation may drive increased shell thickness in freshwater mussels similar to marine bivalves (Smith and Jennings 2000) as has been hypothesized in certain riverine

habitats (Owen et al. 2011; Haag 2012; Daniel and Brown 2013); predation could also select for traits that prevent dislodgement, reinforcing morphological adaptations for stability in the substratum from fluid dynamics. However, predation pressures across habitats are not well-understood (Haag and Warren 1998), making it difficult to evaluate how its direct or indirect effects impact the form-environment patterns observed here. Similarly, gradients in resource availability—levels of calcium, bicarbonate, and food —may correlate with flow rate and thus explain some of the residual morphological variation in the form-environment relationship (Figure 1.7b, Mackie and Flippance 1983; Strayer et al. 2020), but resources are not the primary drivers of phenotypic variation in mussels (Prezant et al. 2022). Further, mussel shells have indeterminate growth, becoming both larger and thicker with age (Heino and Kaitala 1996; Haag and Rypel 2011). If longer-lived individuals are preferentially found in high flow environments, then gradients in ontogenetic age may underlie, but not undermine, the inferred form-environment relationship. For age—and for predation and nutrient availability—shell thickness should be either maximized near the umbo, the oldest part of the shell, or uniformly distributed, but shells in high flow environments thicken across their anterior, suggesting that flow rate is likely the dominant factor acting on mussel shell morphology (Figure 1.10c). Still, adding these other factors into new analyses of functional morphology will help to better understand the exact impact of the environment on the evolution of freshwater mussels. For example, periodic extremes in flow rate (e.g. drought, flooding), rather than its average, may be the primary selective agent. These temporally rare events

could strongly disfavor incompatible phenotypes, analogous to uncommon El Niño events reshaping the beaks of Darwin's finches (Grant and Grant 1993).

Contingency and determinism in the evolution of the freshwater mussel shell

Perhaps initially considered as mutually exclusive factors, both historical contingency and environmental determinism are acting to shape the evolution of major clades (Gould 1989; Conway Morris 2003; Agrawal 2017). In freshwater mussels, repeated independent evolution towards environmentally correlated shell morphologies occurs across riverine flow rates, suggesting a deterministic nature to the clade's radiation across the Nearctic. The frequency and degree of morphological convergence tends to increase with decreasing phylogenetic distance (Stayton 2008; Ord and Summers 2015), but these freshwater mussels are not a shallow radiation, with the most recent common ancestor of Margaritiferidae + Unionidae estimated to be ~210 to 250 Myr (Lopes-Lima et al. 2018; Bolotov et al. 2016). Simple adaptive landscapes, including the one made with the three traits measured here, tend to recover greater degrees of convergence (Zelditch et al. 2017). However, as noted above, the more complex trait of shell shape is likely to show additional, environmentally driven morphological convergence rather than phylogenetic constraint; species with atypical traits for high flow rates appear to have similar shell shapes, which may serve as an alternate functional adaptation to stability in the substratum.

Environmental determinism does not directly scale between the species and individual levels for these mussels. This is most clear for shell anterior thickening,

where flow rate correlates with evolutionary differences among species but not within them (Figure 1.7c, Figure 1.10c, Figure 1.8). Contrary to anterior thickening, shell thickness is ecophenotypic with flow rate, mirroring the positive relationship found across mussel species (Figure 1.7b, Figure 1.10b). Although the strength of relationships differ, parallel ecomorphological relationships at intra and interspecific scales may contribute to the evolvability and ecological diversification of the clade. Highly plastic morphologies increase the probability of establishing interbreeding populations if the environmental conditions differ from the parental ones (Ortmann 1920), and, consequently, increase the propensity for lineage splitting and local adaptation to stream conditions that result in larger species-level differences in traits (see discussion of mechanism in Agrawal 2001). This may be particularly important during episodes of rapid landscape evolution (e.g. vicariance via glacial-interglacial cycles). High morphological variation, presumed to be phenotypic plasticity, could be a consequence or requirement of mussel dispersal (Hinch et al. 1986), which relies (mostly) on fish hosts. Host mediated dispersal of larvae creates a large element of chance generation-to-generation in the environmental conditions of settlement sites (Terui et al. 2017; Watters 1992). Thus, environmental contingency driven by host use stochasticity at microevolutionary scales may explain the ecomorphological mirroring between intra and interspecific levels. Interestingly, this ecomorphological mirroring at intra and interspecific levels is also found in Caribbean *Anolis* lizards, where hindlimb length positively correlates with perch diameter across the radiation and within-species plasticity follows an identical pattern but at a smaller range of values (Calsbeek et al. 2007; Losos et al. 2000; 2001).

Conclusion

Like many of the vertebrates in freshwater rivers, freshwater mussels of North America show widespread convergent evolution. Convergent shell traits across stream environments likely represent structural adaptations for stability in high flows and efficient burrowing in low flows. Environmental determinism of shell morphologies at the species-level also occurs at the intraspecific-level (i.e. shell thickness: Figure 1.7b & Figure 1.10b). This capacity to respond to different environments, either evolutionarily or ecophenotypically, may be critical to the evolutionary resilience of this highly imperiled group. Landscape evolution is accelerating through artificial channelization and damming of waterways, fundamentally altering riverine hydrodynamics. Freshwater mussels seem to have an intrinsic buffering capacity to hydrological changes; yet, imperilment and recent extinctions (Haag and Williams 2014; Ricciardi and Rasmussen 1999) suggest that compounding issues such as deteriorating water quality (Gillis 2011) may be overwhelming the rate of adaptive evolution.

Table 1.1: GI numbers (GenInfo Identifiers) for nucleotide sequences used in phylogenetic analysis. Occasionally, the whole mitochondrial genome was the only NCBI sequence for a given species. In these instances, COI, NDI, and 16S were extracted from the one GI number.

species	**COI**	**NDI**	**16S**	**28S**	**ITS1**
Actinonaias_ligamentina	2006721170	1752319907	56068117	1527230075	1527230159
Actinonaias_pectorosa	1527230242	1527230542	56068118	1527230076	1527230160
Alasmidonta_arcula	1899959323				
Alasmidonta_heterodon	6739293	1381388304	1381388304		
Alasmidonta_marginata	330421377	285027547		18029938	
Alasmidonta_triangulata	1899906822	1280084912	1698812		1280085150
Alasmidonta_undulata	1899906824	148872569			

Alasmidonta_varicosa	1899906830	150251601	2325478630		
Amblema_elliottii	56800558		56068119		
Amblema_plicata	2118838482	1527230546	1625626456	1625626490	1527230162
Anodontoides_ferussaci anus	1280084808	1280085062			1280085225
Arcidens_confragosus	2118838470	1399047675			671706394
Arcidens_wheeleri	671706391	671706425			671706396
Cambarunio_iris	1899907046	90812012	56068173		
Cambarunio_nebulosus	1899907050				
Cambarunio_taeniatus	1899907058	90812030			1374503304
Cumberlandia_monodonta	1389825570	1199890867	1389823675	1389824881	239737245
Cyclonaias_infucata	1509783738	1509782956	11526846		1509782171

Cyclonaias_kieneriana	1509783744	1509782962	56068166		1509782176
Cyclonaias_kleiniana	1509783742	1509782960			1509782175
Cyclonaias_nodulata	1509782990	1509782208			1509782163
Cyclonaias_pustulosa	1509783610	1509782828			1509782179
Cyclonaias_succissa	1509783648	1509782866	11526858		1509782167
Cyclonaias_tuberculata	1625626407	1509782926	1625626460	1625626494	1509782070
Cyprogenia_aberti		1009516545	496208288		
Cyprogenia_stegaria	1527230248	1527230548		1527230079	1527230163
Cyrtonaias_tampicoensis	1910883116	1527230552	1625626477	1625626511	1527230164
Dromus_dromas	56800562	31788633	56068123		
Ellipsaria_lineolata	1752320423	1527230554	1698815	1527230082	1527230165
Elliptio_arca	1899906838				91992209

Elliptio_arctata	1899906844				91992210
Elliptio_complanata	2154332643	1399047667	321267626	338163488	
Elliptio_crassidens	2154393105	1891100516	56068124		1509782130
Elliptio_fisheriana	1563835552	321267940	321267644		
Elliptio_icterina	340509955	321267964	321267657		
Elliptio_lanceolata	1417996019				
Elliptio_producta	1417996021	321267968	321267660		
Elliptio_shepardiana	1899906940				
Elliptio_spinosa	1041668005				1041941090
Elliptoideus_sloatianus	966029121	1891100500	1625626470	1625626504	966029219
Epioblasma_brevidens	5107890	77455941	77456075		78191369
Epioblasma_capsaeformis	56800568	77455929	77456052		78191346

Epioblasma_rangiana	1527230256	1527230558	77456074	1527230084	1527230167
Epioblasma_triquetra	154269423	77455943	77456076		78191370
Eurynia_dilatata	1899906872	1891100508	1698814	18029940	1891100719
Fusconaia_cerina	1417996107	1497512938	56068129		1497513196
Fusconaia_chunii	1497512702	1497513022			1497513228
Fusconaia_cuneolus	1417996127				953835355
Fusconaia_flava	2118838464	1497513124	1719883946	1625626499	1691423768
Fusconaia_masoni	1417996287	1497513136			1497513264
Fusconaia_mitchelli	1891100395	1891100606			1891100748
Fusconaia_subrotunda	1678503923	338832690	1719883944		1691423770
Glebula_rotundata	1527230260	1527230562	1625626478	1625626512	1527230169
Gonidea_angulata	2307875938	2191686844	514255626	823960667	

Hamiota_altilis	1899906948	90811966	18157625		
Hamiota_subangulata	1899906992	1527230566	18157621	1527230088	1527230171
Hemistena_lata	1891100317	1891100512	56068136		1891100721
Lampsilis_bracteata	1752320093	1752319659			1752319445
Lampsilis_cardium	2006704465	1752319911	1104599461	1527230089	1752319529
Lampsilis_cariosa	1899906958	148872553	2386959188		
Lampsilis_dolabraeformis	1899959881	1527230572		1527230091	1527230174
Lampsilis_fasciola	2006728953	90811970			
Lampsilis_floridensis	1917889360	2050646634			1917469379
Lampsilis_higginsii	285027464	285027569			
Lampsilis_hydiana	2168650634	2168650666	6180029		1752319493
Lampsilis_ornata	1899906978	31788629	18157629		

Lampsilis_ovata	2075442940	2191686852	56068138	1527230093	1527230176
Lampsilis_radiata	1899906982	321268042	321267702		
Lampsilis_satura	1752320449	1752319917	6180035	1527230095	1752319536
Lampsilis_sietmani	2118838458				1678209050
Lampsilis_siliquoidea	2168650642	2168650662	496208287		1752319542
Lampsilis_splendida	1899959424				
Lampsilis_straminea	1899906986				1752319544
Lampsilis_teres	2118838466	2050646850	18157630		1917469387
Lampsilis_virescens	1752320477				1752319546
Lasmigona_complanata	330421415	285027573	29838623		
Lasmigona_compressa	330421429	336441856	29838625		
Lasmigona_costata	1376009483	336441858	40748062		

Lasmigona_decorata	6739305	2213905519			
Lasmigona_holstonia	56800578				
Lasmigona_subviridis	330421443	302702188	302702188		3916716
Leaunio_lienosus	2118838474	1752319951	1493555935		1752319554
Leaunio_umbrans	1899907062	90812076			
Leaunio_vanuxemensis	1899907076	90812094	56068174		
Lemiox_rimosus	1527230282	1527230584	56068139	1527230097	1527230180
Ligumia_recta	1527230300	1527230602	146261971	1527230106	1527230189
Margaritifera_falcata	2307875954	331746775	50897879	50897911	
Margaritifera_marriana e	1073722337		1073722283	1073722424	
Medionidus_acutissimus	56800585	1621573802	56068144		1104417565
Medionidus_conradicus	1527230304	1527230606	496208286	1527230108	1527230191

Megalonaias_nervosa	1509783724	1509782942	1625626464	1625626498	1509782131
Obliquaria_reflexa	2118838448	1527230610	56068145	1527230110	1527230193
Obovaria_arkansasensis	2118838472	541904721			
Obovaria_olivaria	1941988064	541904769	11526849		
Obovaria_unicolor	541904369	541904862	11526848		1374503308
Paetulunio_fabalis	78172546	90811992			
Parvaspina_collina	1417996313	172055320	56068151		172055334
Plectomerus_dombeyanus	1527230316	1527230618	56068147	1527230114	1527230197
Plethobasus_cyphyus	1891100319	1731598978	56068148		1891100722
Pleurobema_clava	1900450499		56068150		91992221
Pleurobema_cordatum	1678504009		1719883947		1691423772
Pleurobema_decisum	1899907004	91992241	11526838		91992226

Pleurobema_oviforme	1899907006	1804034214	56068158		953835375
Pleurobema_plenum	1678504081		1719883945		1691423775
Pleurobema_pyriforme	1899907010	91992243	1698830		966029241
Pleurobema_sintoxia	1888660476	285027605			93484061
Pleurobema_strodeanum	1417996667		1625626466	1625626500	966029243
Pleuronaia_barnesiana	1891100315	1891100510	1625626467	1625626501	1891100720
Popenaias_popeii	1910883096	1527230624	1625626455	1625626489	1527230200
Potamilus_alatus	1527230332	1527230634	823960829	1527230122	1527230205
Potamilus_capax	1527230340	1527230642		1527230126	1527230209
Potamilus_fragilis	2118838454	2019293674	29838619	1527230100	1861356639
Potamilus_leptodon	1527230290	1527230592	56068140	1527230101	1527230184
Potamilus_ohiensis	1527230538	1527230842		1527230134	1527230217

Potamilus_purpuratus	2118838460	2019293804	1698831	1527230158	1861356638
Pseudodontoideus_subv exus	1280084776	1280085030	56068167		1280085209
Ptychobranchus_fasciol aris	1527230366	1527230668	496208279	1527230139	1527230222
Ptychobranchus_occidentalis		496208327	496208269		
Ptychobranchus_subtentus		496208359	496208285		
Pyganodon_grandis	2118838446	1399047671	170284238	12584116	1280085163
Quadrula_fragosa	Generated sequence	Generated sequence			Generated sequence
Quadrula_quadrula	2118838480	1804034212	1625626461	1625626495	1509782128
Reginaia_ebenus	1527230370	1527230672	1625626458	1625626492	1527230224
Sagittunio_nasutus	1563835570	803360318	146261973		32481748

Sagittunio_subrostratus	1752320481	1390626219	146261974		1752319547
Simpsonaias_ambigua	1928140685	1928140683		1069429878	
Strophitus_radiatus	1280084878	1280085132	1698810		1280085227
Strophitus_undulatus	2192709799	1390626217	29838627		1280085228
Theliderma_cylindrica	2216500195	31788733			
Theliderma_intermedia		31788699			
Theliderma_johnsoni	1804034351				
Theliderma_metanevra	1509783726	1509782944	1698835		1509782135
Toxolasma_lividum	1752320489	1752319943		1527230144	1527230226
Toxolasma_parvum	2118838462	1390626225	29838618		
Toxolasma_texasiense	2118838476	1399047669	56068168		
Tritogonia_nobilis	1804034342	1804034281			

Tritogonia_verrucosa	2118838478	1509782934	56068169		1509782125
Truncilla_donaciformis	2077530048	1527230684		1527230148	1527230230
Truncilla_macrodon	2077530133	1752319947		1527230151	1752319552
Truncilla_truncata	2077530234	1527230694	56068170	1527230153	1527230234
Uniomerus_carolinianus			321267715		
Uniomerus_declivis	966029193		1625626462	1625626496	966029255
Uniomerus_tetralasmus	2118838452	1509782958	1493555949		1509782174
Utterbackia_imbecillis	2118838450	1399047687	29838622		
Utterbackiana_couperiana	1280084626	1280084880	1698807		1280085134
Utterbackiana_implicata	1563835636	148872563			

Utterbackiana_suborbic ulata	2118838468	1280084884			1280085136
Venustaconcha_ellipsifo rmis	1527230392	1527230696	56068172	1527230154	1527230235
Villosa_delumbis	1899959570	90811990	1698839		
Villosa_vibex	1899907080	90812044			

Table 1.2: Bayesian multilevel model descriptions. Parameters: $trait_1$, $trait_2$, and $trait_{covar}$ are either ln shell size (mm), ln median shell thickness (mm), or relative anterior thickening (PC1 scores); *species* is the species of an individual; and *phylo* is the variance-covariance matrix from the species level phylogeny.

MODEL	FORMULA	DESCRIPTION
Within-species models		
	Correlation between shell traits	
Model 1:	$trait_1 \sim trait_2 + (1 \mid species)$	species as varying intercept (random effect)
Model 2:	$trait_1 \sim trait_2 + (1 \mid species) + (1 \mid phylo)$	species and their phylogenetic covariance as varying intercepts (random effects)
	Correlation between shell traits & flow rate	

Model 3:	*trait* ~ 1	null, intercept-only
Model 4:	*trait* ~ $trait_{covar}$ + *flow*	population-level, i.e. only fixed effects, accounting for any covarying traits
Model 5:	*trait* ~ $trait_{covar}$ + *flow* + (1 | *species*)	species as random effect, accounting for any covarying traits
Model 6:	*trait* ~ $trait_{covar}$ + *flow* + (*flow* | *species*)	allow flow rate to vary by species, accounting for any covarying traits
Model 7:	*trait* ~ $trait_{covar}$ + *flow* + (1 | *species*) + (1 | *phylo*)	species and their phylogenetic covariance as varying intercepts (random effects), accounting for any covarying traits
Model 8:	*trait* ~ $trait_{covar}$ + *flow* + (*flow* | *species*) + (1 | *phylo*)	allow flow rate to vary by species, accounting for phylogenetic covariance and any covarying traits
Species-level models		

	Correlation between shell traits	
Model 9:	$trait_1 \sim trait_2$	trait correlation
Model 10:	$trait_1 \sim trait_2 + (1 \mid phylo)$	trait correlation, accounting for phylogenetic relatedness of species
	Correlation between shell traits & flow rate	
Model 11:	$trait \sim trait_{covar} + flow$	population-level, i.e. only fixed effects, accounting for any covarying traits
Model 12:	$trait \sim trait_{covar} + flow + (1 \mid phylo)$	accounting for phylogenetic relatedness and any covarying traits

Table 1.3: Correlations between shell traits among individuals. The 'Model' field gives the number corresponding to the formulae in Table 1.2. The '$trait_1$' and '$trait_2$' fields give the response and predictor, respectively. $\beta_{trait\text{-}2}$ is the population-level effect (fixed effect) of the predictor on the response, expressed as the median posterior value with 95% CI in brackets. $\sigma_{species}$ and σ_{phylo} are the respective standard deviations of the random effects (group-level varying intercepts) of species and the phylogenetic covariance among species. '$R^2_{trait\text{-}2}$' is the explained variance of the model of $trait_2$ conditioned on the mean group-level effects (i.e. species or phylo). 'R^2_{model}' is the explained variance using all terms.

Model	***trait*$_1$**	***trait*$_2$**	$\beta_{intercept}$	$\beta_{trait\text{-}2}$	$\sigma_{species}$	σ_{phylo}	$R^2_{trait\text{-}2}$	R^2_{model}
1	shell thickness	shell size	-7.91 [-8.65,-7.17]	1.11 [1.01,1.20]	0.55 [0.50,0.62]	–	0.30	0.89

2	shell thickness	shell size	-8.51 [-9.42,-7.60]	1.16 [1.06,1.25]	0.22 [0.16,0.30]	0.32 [0.26,0.39]	0.31	0.89
1	shell anterior thickening	shell size	-103.95 [-141.92,-64.80]	13.31 [8.21,18.24]	25.13 [22.47,28.36]	–	0.03	0.83
2	shell anterior thickening	shell size	-120.76 [-166.83	14.49 [9.29,19.62]	12.45 [9.04,16.21]	15.60 [12.28,19.24]	0.03	0.83

			,-75.11]					
1	shell anterior thickening	shell thickness	-9.97 [-13.31,-6.73]	13.16 [10.25,16.06]	20.32 [18.09,23.02]	–	0.12	0.82
2	shell anterior thickening	shell thickness	-13.94 [-32.56, 4.68]	10.78 [7.78,13.73]	13.04 [9.89,16.57]	12.32 [9.02,15.84]	0.08	0.82

Table 1.4: Effect of flow rate on shell size. Model numbers correspond to formulations in Table 1.2. β_{thick} and $\beta_{ant\text{-}hick}$ are the fixed effects of shell thickness and anterior thickening on shell size, expressed as the median posterior value with 95% CI in brackets. β_{flow} is the fixed effect of flow rate on shell size. R^2_{β} is the explained variance of the model of the fixed effects (β) conditioned on mean group-level effects (σ). $\sigma_{species}$ is the standard deviation of the random effect (group-level varying intercept) of species. σ_{flow} is the standard deviation of the random effect (group-level varying slope) of flow rate. σ_{phylo} is the standard deviation of the random effect (group-level varying intercept) of the phylogenetic covariance among species. 'R^2_{model}' is the explained variance using all terms. 'Δelpd' is the change in expected log predictive density from the best supported model (i.e. elpd=0); 's.e. Δelpd' is the standard error of Δelpd. '–' marks not-applicable. Gray rows highlight models that take into account phylogenetic relatedness (their elpd is not directly comparable to the non-phylogenetic models, see main text results for details).

Model	β_{thick}	$\beta_{ant\text{-}thick}$	β_{flow}	R^2_{β}	$\sigma_{species}$	σ_{flow}	σ_{phylo}	R^2_{model}	**Δelpd**	**s.e. Δelpd**

8	0.38 [0.35,0.42]	0.0008 [-0.0001, 0.0017]	-0.0052 [-0.011, 0.0008]	0.38	0.15 [0.064,0.21]	0.015 [0.0054, 0.023]	0.20 [0.17,0.24]	0.87	0	0
7	0.38 [0.35,0.42]	0.0007 [-0.00018,0.0016]	-0.0042 [-0.00900, 0.00071]	0.38	0.091 [0.038,0.14]	–	0.20 [0.17,0.24]	0.86	-9.3	3.7
6	0.38 [0.34,0.41]	0.0004	-0.0079 [-0.014,-0.0020]	0.37	0.29 [0.24,0.34]	0.017 [0.0085, 0.025]	–	0.87	0	0

		[-0.0005, 0.0013]								
5	0.37 [0.34,0.41]	0.0002 [-0.0008, 0.0011]	-0.0058 [-0.011,-0.0010]	0.36	0.30 [0.27,0.34]	–	–	0.86	-13	4.8
4	0.37 [0.33,0.41]	-0.0053	0.0009 [-0.0070,0.0089]	–	–	–	–	0.34	-487	26

		[-0.0061, -0.0043]								
3	–		–	–	–	–	–	–	-632	25

Table 1.5: Effect of flow rate on shell thickness; formatted as in Table 1.4.

Model	β_{size}	$\beta_{ant\text{-}thick}$	β_{flow}	R^2_{β}	$\sigma_{species}$	σ_{flow}	σ_{phylo}	R^2_{model}	**Δelpd**	**s.e. Δelpd**
8	1.090 [0.99, 1.19]	0.0031 [0.0016,0.0046]	0.018 [0.0079, 0.029]	0.36	0.20 [0.035,0.33]	0.030 [0.016,0.043]	0.25 [0.19,0.33]	0.89	0	0
7	1.096 [0.99, 1.20]	0.0033 [0.0018,0.0048]	0.016 [0.0079, 0.024]	0.37	0.23 [0.17,0.30]	–	0.27 [0.21,0.34]	0.88	-8.5	4.4
6	1.021	0.0046	0.022	0.39	0.41	0.034	–	0.90	0	0

	[0.92, 1.12]	[0.003, 0.0061]	[0.012, 0.033]		[0.33,0.50]	[0.019,0.048]				
5	1.01 [0.91, 1.11]	0.0050 [0.0034, 0.0066]	0.019 [0.011, 0.028]	0.40	0.45 [0.39,0.51]	–	–	0.88	-14.4	5.3
4	0.84 [0.75, 0.93]	0.013 [0.011, 0.014]	0.042 [0.031, 0.054]	–	–	–	–	0.58	-387	25
3	–		–	–	–	–	–	–	-695	25

Table 1.6: Effect of flow rate on shell anterior thickening; formatted as in Table 1.4.

Model	β_{size}	β_{thick}	β_{flow}	R^2_{β}	$\sigma_{species}$	σ_{flow}	σ_{phylo}	R^2_{model}	**Δelpd**	**s.e. Δelpd**
7	2.67 [-4.67,10.11]	9.89 [5.58,14.18]	-0.28 [-0.72,0.15]	0.07	12.98 [9.73,16.53]	–	12.82 [9.14,16.61]	0.83	0	0
8	3.36 [-4.27,10.85]	9.60 [5.25,14.00]	-0.28 [-0.77,0.20]	0.07	13.20 [7.49,18.68]	0.73 [0.036,1.70]	12.97 [9.28,16.76]	0.83	-1.2	1.7
5	-4.82 [-11.74,1.96]	15.30 [11.32,19.42]	-0.21 [-0.64,0.21]	0.14	19.88 [17.41,22.71]	–	–	0.82	0	0
6	-4.53	15.22	-0.21	0.14	20.65	0.55	–	0.82	-0.7	1.2

	[-11.35, 2.44]	[11.096, 19.25]	[-0.67,0.27]		[17.30,25.12]	[0.024,1.55]				
4	-28.88 [-33.91, -23.86]	30.41 [27.55,33.30]	0.37 [-0.22, 0.96]	–	–	–	–	0.42	-325	24
3	–		–	–	–	–	–	–	-520	23

Table 1.7: Correlations between shell traits of species from typical flow rate occurrences. The 'Model' field gives the number corresponding to the formulae in Table 1.2. The $trait_1$ and $trait_2$ fields give the response and predictor, respectively. $\beta_{trait\text{-}2}$ is the population level effect (fixed effect) of the predictor on the response with the 95% credible interval in brackets. R^2_β is the explained variance of the model of the fixed effects (β) conditioned on mean group-level effects (σ). R^2_{model} is the explained variance using all terms. '–' marks not-applicable. Gray rows highlight models that take into account phylogenetic relatedness.

Model	***trait*$_1$**	***trait*$_2$**	**$\beta_{trait\text{-}2}$ mean [95% CI]**	**σ_{phylo}**	**R^2_β**	**R^2_{model}**
9	shell thickness	shell size	0.78 [0.52,1.03]	–	–	0.19
10	shell thickness	shell size	0.98 [0.75,1.21]	0.30 [0.23,0.37]	0.26	0.78

9	shell anterior thickening	shell size	-6.88 [-18.9,5.01]	–	–	0.01
10	shell anterior thickening	shell size	1.11 [-6.41,8.59]	14.39 [10.80,18.26]	0.003	0.64
9	shell anterior thickening	shell thickness	23.8 [18.4,29.3]	–	–	0.30
10	shell anterior thickening	shell thickness	11.60 [6.02,17.20]	12.11 [8.29,15.99]	0.09	0.62

Table 1.8: Effect of flow rate on shell traits of species occurring at typical flow rates; formatted as in Table 1.4.

trait	**model**	β_{size}	β_{thick}	$\beta_{ant\text{-}thick}$	β_{flow}	σ_{phylo}	R^2_{model}	**Δelpd**	**s.e. Δelpd**
shell size	12	–	0.37 [0.28,0.47]	–	-0.020 [-0.058,0.018]	0.19 [0.16, 0.23]	0.31	–	–
	11	–	0.27 [0.17,0.37]	–	-0.020 [-0.063,0.023]	–	0.20	0	0
	3	–	–	–	–	–	–	-15.3	5.3

shell thickness	12	0.77 [0.57,0.97]	–	0.0058 [0.0027, 0.0089]	0.14 [0.085,0.19]	0.18 [0.11, 0.26]	0.53	–	–
	11	0.70 [0.52,0.88]	–	0.0095 [0.0067, 0.012]	0.14 [0.089,0.19]	–	0.61	0	0
	3	–	–	–	–	–	–	-74.1	10.3
shell anterior thickening	12	–	6.33 [0.35,12.31]	–	5.68 [2.98,8.37]	10.84 [6.78,14.71]	0.21	–	–
	11	–	15.58 [8.65,22.62]	–	5.31 [2.36,8.17]	–	0.36	0	0

	3	–	–	–	–	–	–	-34.2	7.5

Table 1.9: Convergence statistics of freshwater mussel morphology (combination of shell size, thickness, and anterior thickening) within river types. Headers correspond to 'C-metrics' from R package *convevol*, see text for details. Significant convergence scores are bolded.

Habitat assemblage	**C_1**	**C_2**	**C_3**	**C_4**
Small river - stream order 3-4	**0.378**	**13.871**	0.184	0.003
p-value	**0.041**	**0.011**	0.090	0.515
Medium river - stream order 5	0.355	**12.150**	0.168	0.0008
p-value	0.135	**0.011**	0.403	0.908
Large river - stream order 6-8	**0.429**	**16.718**	**0.212**	0.001
p-value	**0.004**	**<0.001**	**0.003**	0.547

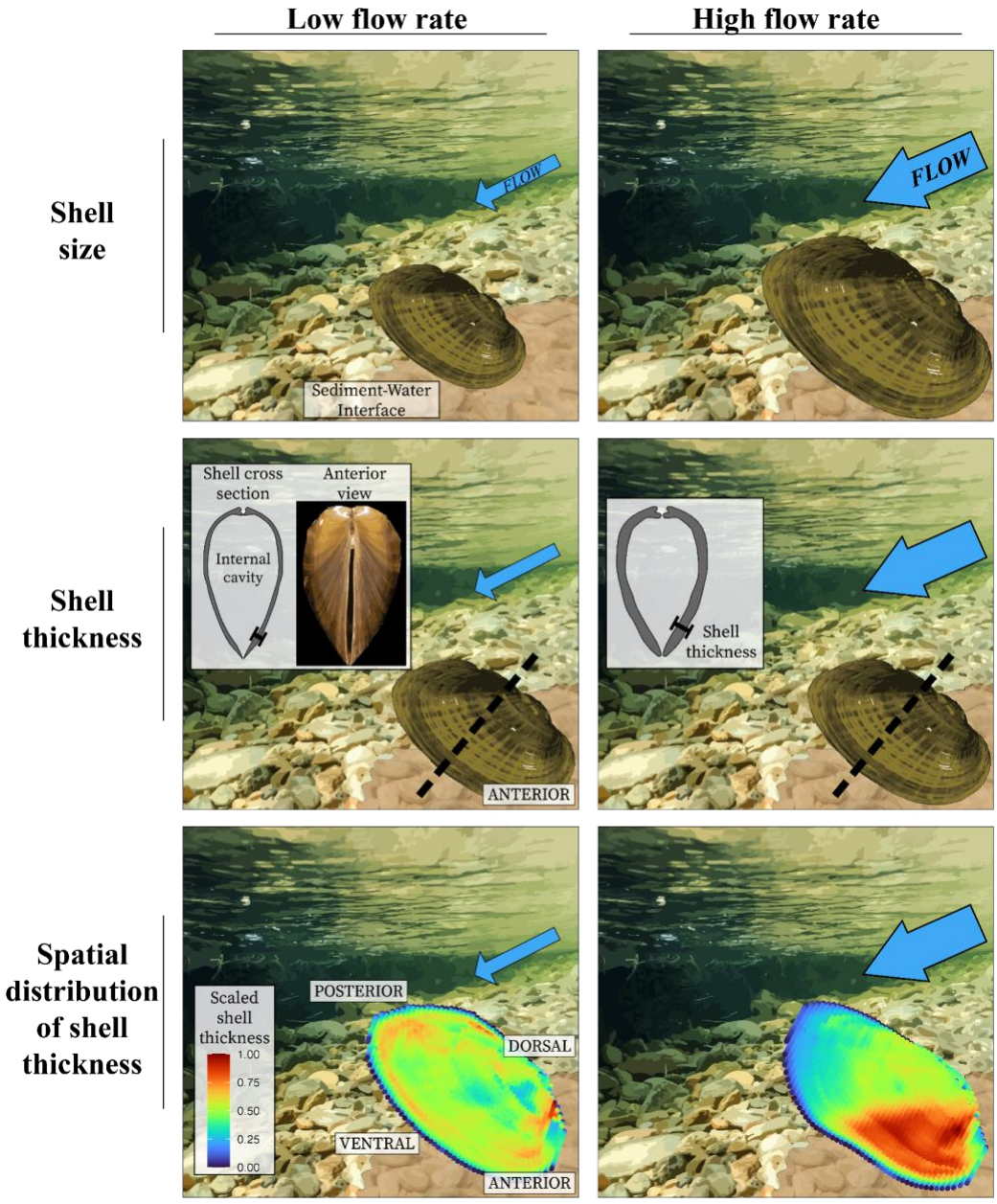

Figure 1.1: Hypothesized morphological adaptations (shell size, thickness, and spatial distribution of shell thickness, i.e. anterior thickening) across low and high riverine flow rates (left and right panels, respectively).

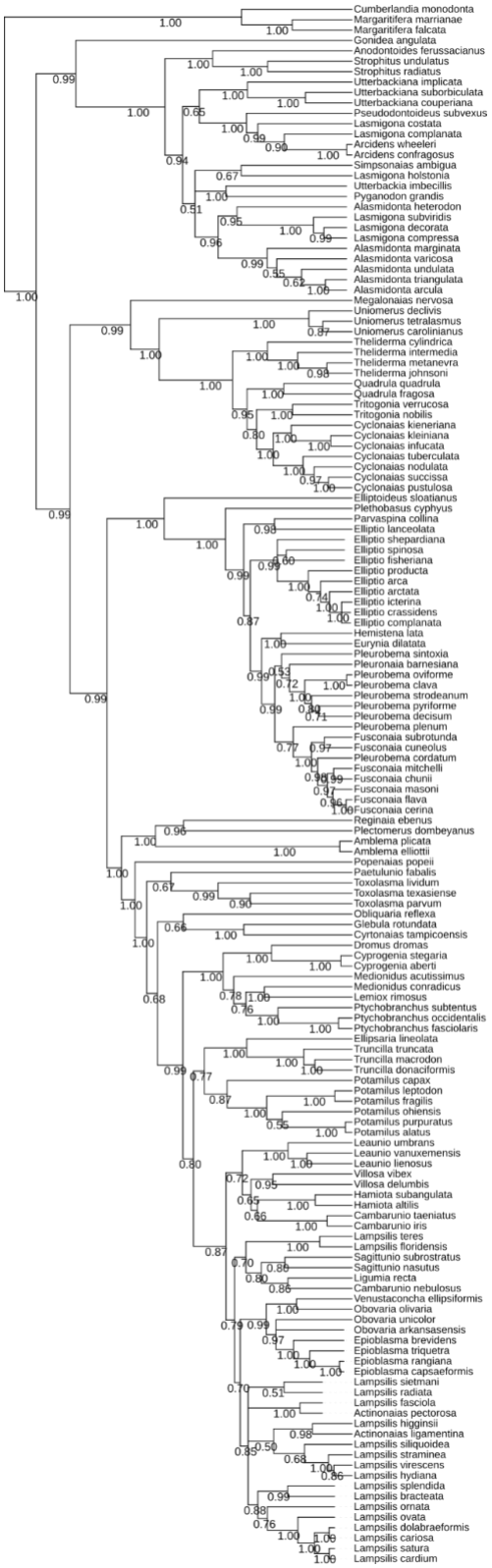
Cumberlandia monodonta
Margaritifera marrianae
Margaritifera falcata
Gonidea angulata
Anodontoides ferussacianus
Strophitus undulatus
Strophitus radiatus
Utterbackiana implicata
Utterbackiana suborbiculata
Utterbackiana couperiana
Pseudodontoideus subvexus
Lasmigona costata
Lasmigona complanata
Arcidens wheeleri
Arcidens confragosus
Simpsonaias ambigua
Lasmigona holstonia
Utterbackia imbecillis
Pyganodon grandis
Alasmidonta heterodon
Lasmigona subviridis
Lasmigona decorata
Lasmigona compressa
Alasmidonta marginata
Alasmidonta varicosa
Alasmidonta undulata
Alasmidonta triangulata
Alasmidonta arcula
Megalonaias nervosa
Uniomerus declivis
Uniomerus tetralasmus
Uniomerus carolinianus
Theliderma cylindrica
Theliderma intermedia
Theliderma metanevra
Theliderma johnsoni
Quadrula quadrula
Quadrula fragosa
Tritogonia verrucosa
Tritogonia nobilis
Cyclonaias kieneriana
Cyclonaias kleiniana
Cyclonaias infucata
Cyclonaias tuberculata
Cyclonaias nodulata
Cyclonaias succissa
Cyclonaias pustulosa
Elliptoideus sloatianus
Plethobasus cyphyus
Parvaspina collina
Elliptio lanceolata
Elliptio shepardiana
Elliptio spinosa
Elliptio fisheriana
Elliptio producta
Elliptio arca
Elliptio arctata
Elliptio icterina
Elliptio crassidens
Elliptio complanata
Hemistena lata
Eurynia dilatata
Pleurobema sintoxia
Pleuronaia barnesiana
Pleurobema oviforme
Pleurobema clava
Pleurobema strodeanum
Pleurobema pyriforme
Pleurobema decisum
Pleurobema plenum
Fusconaia subrotunda
Fusconaia cuneolus
Pleurobema cordatum
Fusconaia mitchelli
Fusconaia chunii
Fusconaia masoni
Fusconaia flava
Fusconaia cerina
Reginaia ebenus
Plectomerus dombeyanus
Amblema plicata
Amblema elliottii
Popenaias popeii
Paetulunio fabalis
Toxolasma lividum
Toxolasma texasiense
Toxolasma parvum
Obliquaria reflexa
Glebula rotundata
Cyrtonaias tampicoensis
Dromus dromas
Cyprogenia stegaria
Cyprogenia aberti
Medionidus acutissimus
Medionidus conradicus
Lemiox rimosus
Ptychobranchus subtentus
Ptychobranchus occidentalis
Ptychobranchus fasciolaris
Ellipsaria lineolata
Truncilla truncata
Truncilla macrodon
Truncilla donaciformis
Potamilus capax
Potamilus ieptodon
Potamilus fragilis
Potamilus ohiensis
Potamilus purpuratus
Potamilus alatus
Leaunio umbrans
Leaunio vanuxemensis
Leaunio lienosus
Villosa vibex
Villosa delumbis
Hamiota subangulata
Hamiota altilis
Cambarunio taeniatus
Cambarunio iris
Lampsilis teres
Lampsilis floridensis
Sagittunio subrostratus
Sagittunio nasutus
Ligumia recta
Cambarunio nebulosus
Venustaconcha ellipsiformis
Obovaria olivaria
Obovaria unicolor
Obovaria arkansasensis
Epioblasma brevidens
Epioblasma triquetra
Epioblasma rangiana
Epioblasma capsaeformis
Lampsilis sietmani
Lampsilis radiata
Lampsilis fasciola
Actinonaias pectorosa
Lampsilis higginsii
Actinonaias ligamentina
Lampsilis siliquoidea
Lampsilis straminea
Lampsilis virescens
Lampsilis hydiana
Lampsilis splendida
Lampsilis bracteata
Lampsilis ornata
Lampsilis ovata
Lampsilis dolabraeformis
Lampsilis cariosa
Lampsilis satura
Lampsilis cardium

Figure 1.2: Molecular phylogeny of Unionidae + Margaritiferidae with posterior support labels at each node. Nodes with <0.50 posterior support were collapsed to soft polytomies.

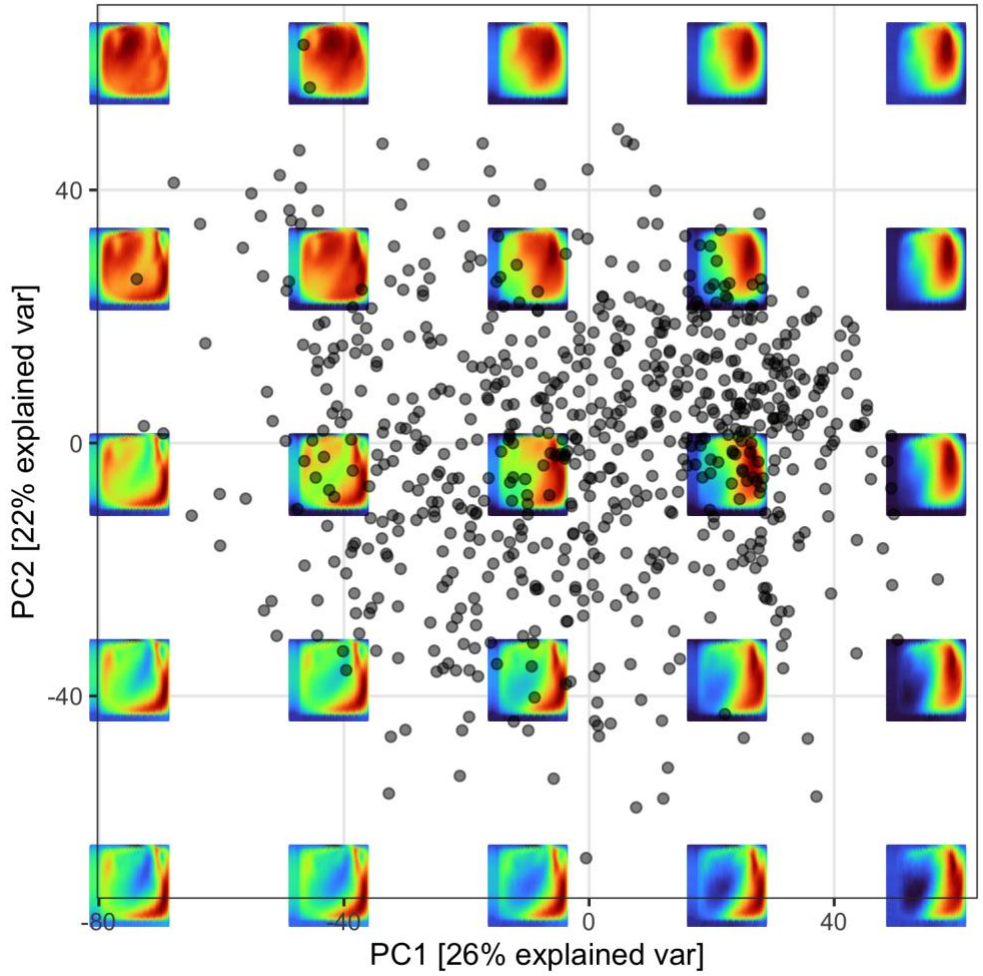

Figure 1.3: Principal components analysis of scaled thickness measurements across the shell. Points are individual shells and images show the distribution of scaled thickness, with relatively thicker areas marked in red and thinner in blue.

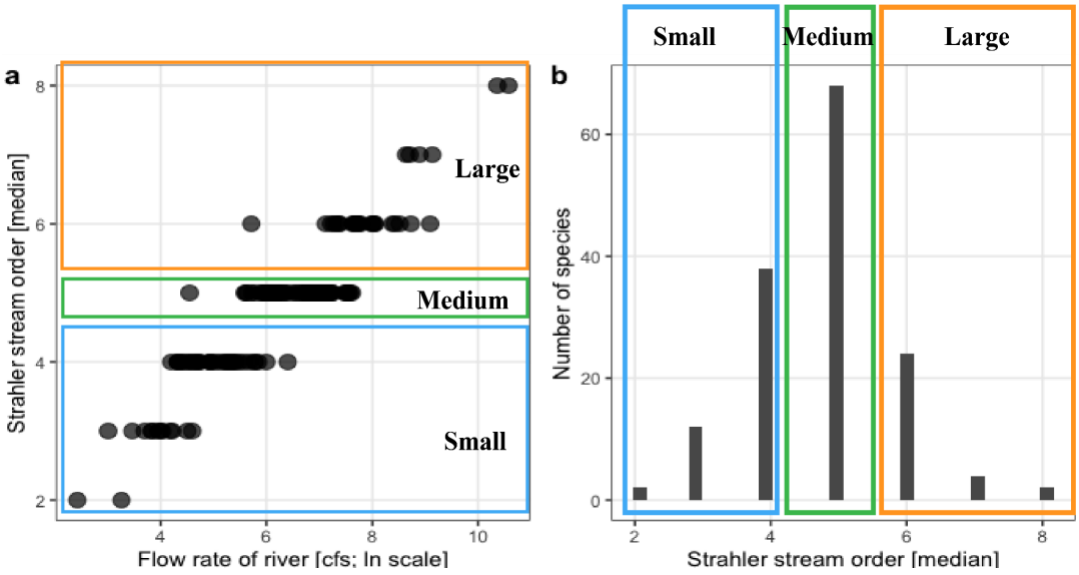

Figure 1.4: (a.) Median Strahler stream order occupancy versus median flow rate for species; (b.) Frequency of species Strahler stream order occupation. Species were grouped into stream size categories: small, medium, and large for *convevol* analysis.

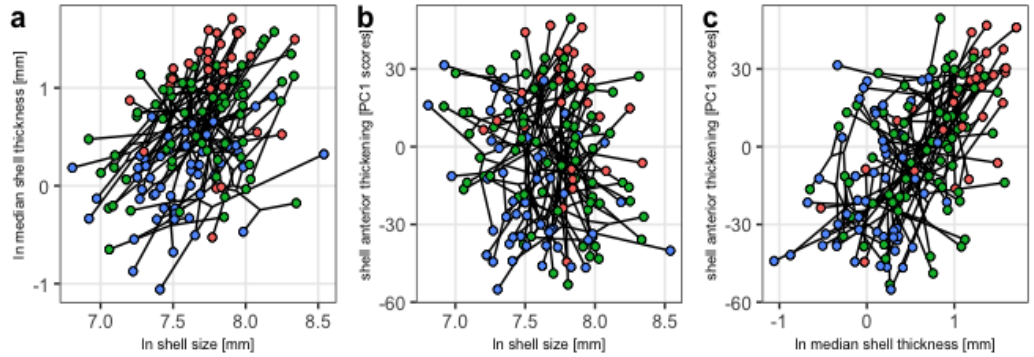

Figure 1.5: Two-dimensional phylomorphospaces of morphological trait combinations with points (species) colored by stream size categories: small = blue, medium = green, and large = red.

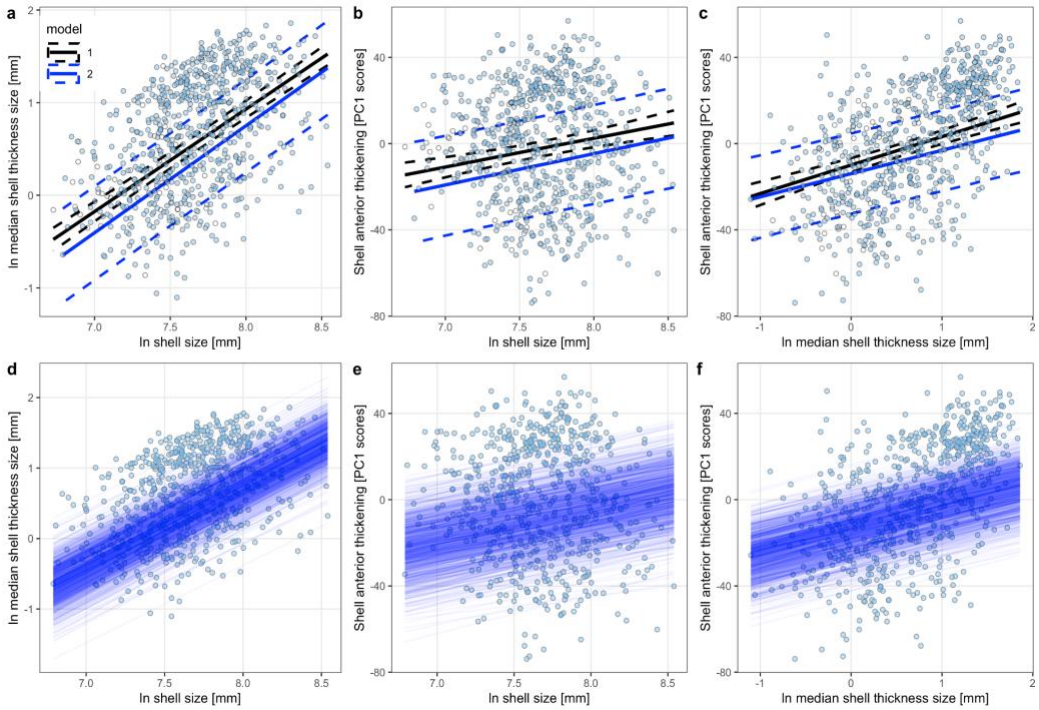

Figure 1.6: Correlations between shell traits. Hollow black points mark the all-species dataset and light blue points mark the subsetted phylogenetic-species dataset. Solid lines show the expected value of the posterior distribution and dashed lines show the 95% CI for the all-species (black) and phylogenetic-species (blue) datasets. (a) Credibly positive effect of shell size on shell thickness. (b) Credibly positive effect of shell size on anterior thickening. Positive PC1 scores correspond to greater anterior thickening (see Figure 1.3). (c) Credibly positive effect of shell thickness on anterior thickening. (d-f) 1000 draws of the expected value of the posterior distribution show that added uncertainty in the phylogenetic model (Model 2) compared to Model 1 is in the intercept term, not the slope term.

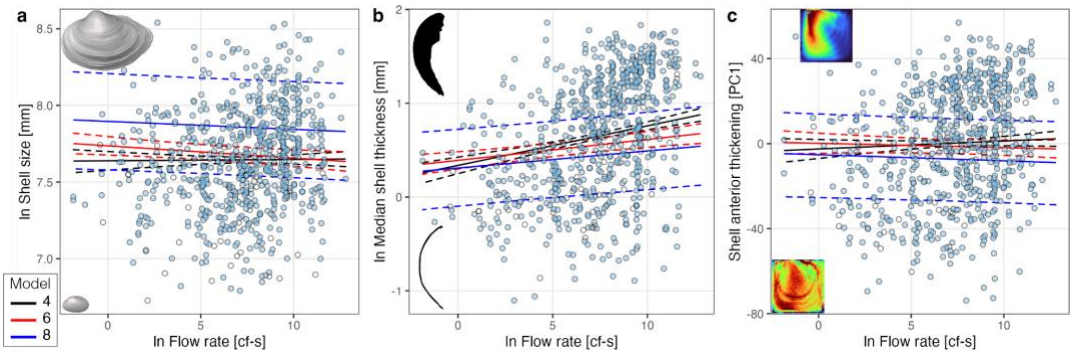

Figure 1.7: Marginal effects of flow rate on shell traits within species. Hollow black circles mark the all-species dataset and blue points mark the phylogenetic-species dataset. Regression lines with ribbons give the expected slope from the posterior distribution with 95% CI for the all-species dataset (models *4*, *6*) and phylogenetic-species dataset (*model 8*). (a) No correlation (models *4*, *8*) or weakly negative (*model 6*) marginal effect of flow rate on shell size. (b) Credibly positive effect of flow rate on shell thickness. (c) No credible effect of flow rate on shell anterior thickening. Graphics along y-axes are bounds of variation in shell traits: (a) scans of *Pyganodon grandis* (top), *Toxolasma corvunculus* (bottom); (b) shell thickness silhouettes of *Ptychobranchus occidentalis* (top), *Utterbackia imbecillis* (bottom); (c) shell 'thickness maps' of *Pleurobema sintoxia* (top), *Utterbackiana couperiana* (bottom).

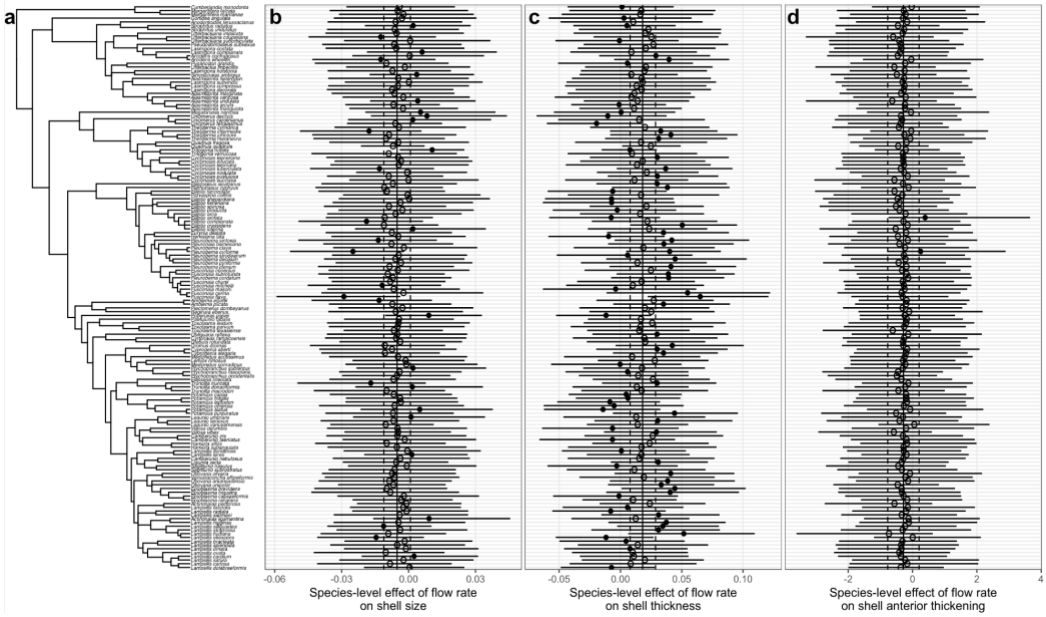

Figure 1.8: Within-species effects of flow rate on shell traits as the species-level slopes from model 8 for the phylogenetic dataset. The vertical black line shows the population-level slope (i.e. the fixed effect), with dashed vertical black lines giving its 95% CI. Solid black points show the median estimate per species that lie outside the uncertainty in the population-level slope, with horizontal black bars giving the 95% CI (open circles are within the population-level slope uncertainty). Values above 0 indicate an increase in the trait value with increasing flow rate. (a) Molecular phylogeny of species in the phylogenetic-species dataset. (b) Within-species effect of flow rate on shell size. (c) Within-species effect of flow rate on shell thickness. (d) Within-species effect of flow rate on shell anterior thickening.

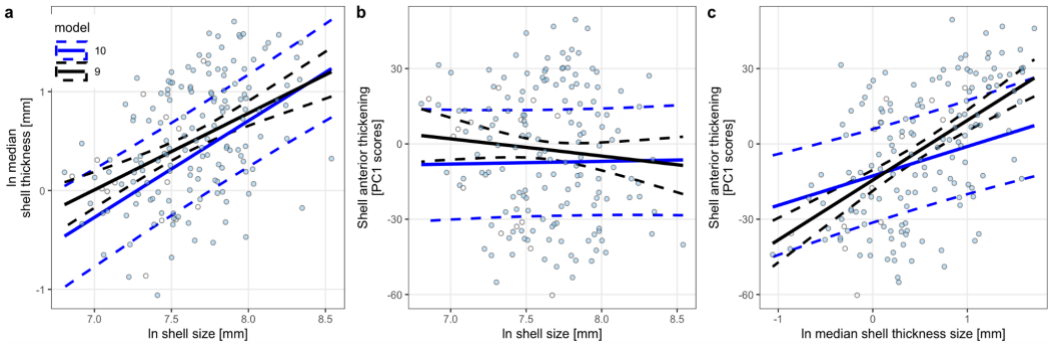

Figure 1.9: Correlations between species-level shell traits at the species' typically encountered flow rate. Hollow black points mark the all-species dataset and light blue points mark the subsetted phylogenetic-species dataset. Solid lines show the mean estimated slope and dashed lines show the 95% CI for the all-species (black) and phylogenetic-species (blue) datasets. (a) Credibly positive effect of shell size on shell thickness. (b) No credible effect of shell size on anterior thickening when accounting for phylogenetic relationships among species. (c) No credible effect of shell thickness on anterior thickening when accounting for phylogenetic relationships among species. Positive PC1 scores correspond to greater anterior thickening (see Figure 1.3).

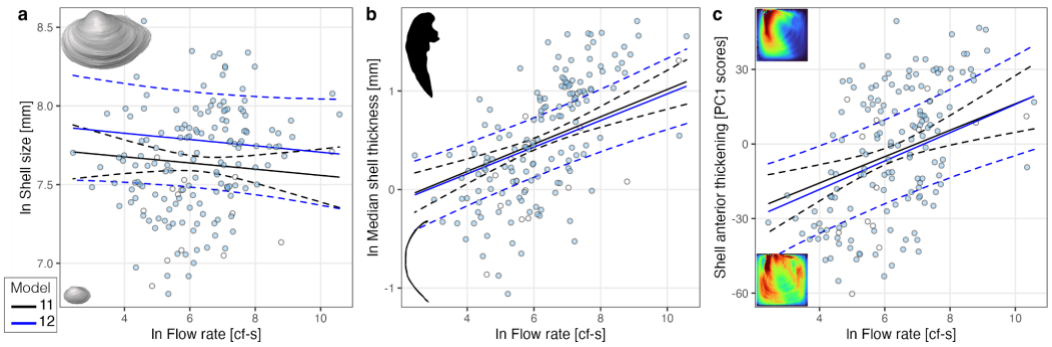

Figure 1.10: Marginal effects of flow rate on shell traits of species occurring at typical flow rates. Hollow black circles mark the all-species dataset and blue points mark the phylogenetic-species dataset. Regression lines with ribbons give the expected slope from the posterior distribution with 95% CI for the all-species dataset (*model 11*) and phylogenetic-species dataset (*model 12*). (a) No credible effect of flow rate on shell size. (b) Credible, positive effect of flow rate on shell thickness. (c) Credible, positive effect of flow rate on shell anterior thickening. Graphics along y-axes are bounds of variation in shell traits: (a) scans of *Pyganodon grandis* (top), *Toxolasma lividum* (bottom); (b) shell thickness silhouettes of *Pleurobema cordatum* (top), *Utterbackia imbecillis* (bottom); (c) shell 'thickness maps' of *Pleurobema sintoxia* (top), *Alasmidonta atropurpurea* (bottom).

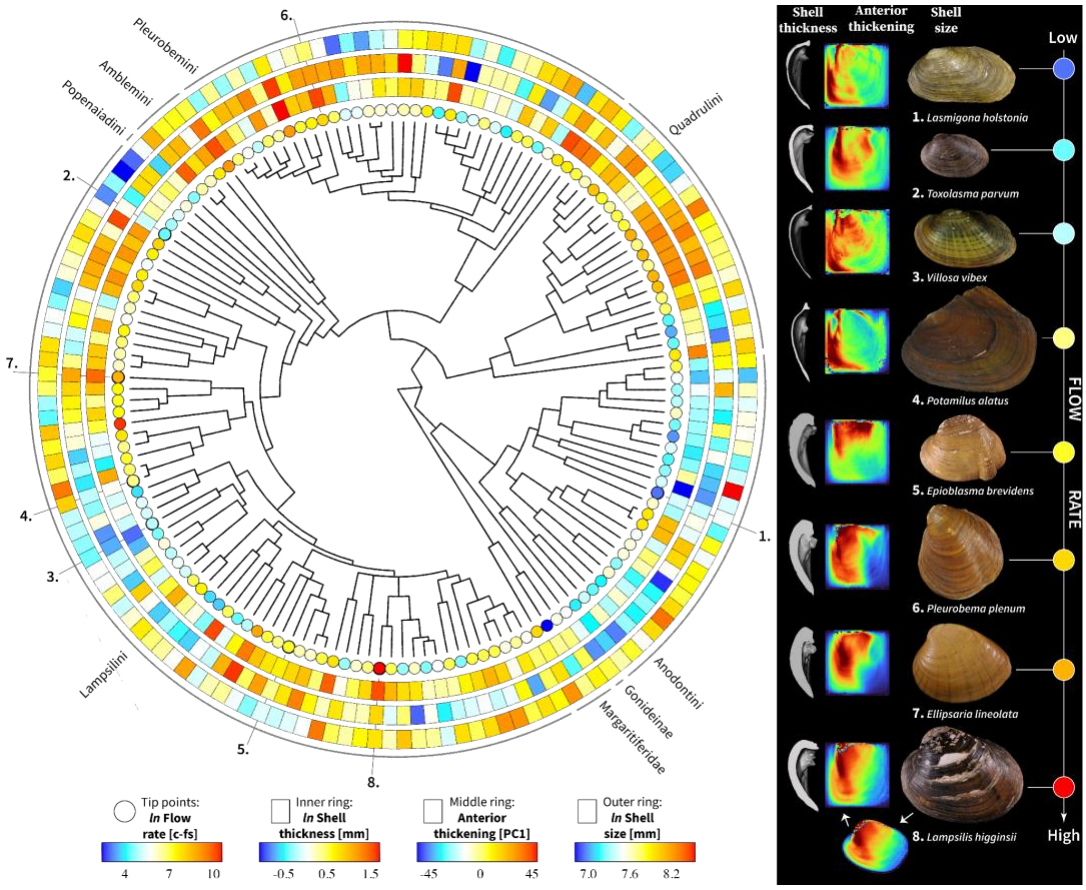

Figure 1.11: Trait evolution of flow rate (natural log transformed; tip points), shell thickness (natural log transformed; inner rectangles), anterior thickening (PC1 scores; middle rectangles), and shell size (natural log transformed; outer rectangles). Species traits on the right panel are organized vertically by flow rate occupation (low to high) and traits left to right: cross section of scanned shell (thickness), anterior thickening map, and shell photographs are scaled to centroid size. All shells and anterior thickening maps are oriented with anterior on the left and dorsal on top. Tree visualized using code from Ghilardi et al. (2021) and *ggtree* (Yu et al. 2017). Besides *Potamilus alatus*, shell photographs are of type specimens provided with the permission of the National Museum of Natural History, Smithsonian Institution

(https://collections.nmnh.si.edu/). Top to bottom: USNM 86320, 85312, 85155, 85349, 84677, 84475, 84823.

Chapter 2:

Field experimentation in lake-stream gardens reveal dramatic phenotypic plasticity in sibling freshwater mussels (Unionidae: *Pyganodon*)

Introduction

Identifying the mechanisms that produce phenotypic variation is fundamental to understanding how organisms adapt to their environments. When species exist across heterogeneous environments, evolutionary processes can produce localized phenotypic variants creating a tight phenotype-environment fit within-species that may reflect adaptation to local conditions (Hendry 2016). Regardless of whether this ecophenotypic variation is adaptive or not, two major pathways exist to explain this pattern. First, localized genetic evolution across populations in different habitat types can result in genotypic differentiation, producing divergent phenotypes. Second, ecophenotypic variation can be the result of phenotypic plasticity where a single genotype produces different phenotypes dependent on environmental cues. Identifying the relative contribution of each process in empirical systems requires experimentation, typically through common garden (organisms from different environments reared in the same environment) or reciprocal transplant (organisms reared in one environment then transferred to another environment). By controlling the environment, these approaches measure phenotypic differences or the 'reaction norm' either between individuals (common garden) or between environments (reciprocal transplant) thus separating the environmental versus genetic effects on phenotypic variation (Pfennig 2021). A similar but more strict approach standardizes

genetic variation through genetic clones or siblings. The reaction norms of clones or family groups can then be measured across environmental variation and then compared to wild populations in shared environments to not only separate genetic versus plastic effects but assess their relative roles in ecophenotypic outcomes.

Freshwater mussels from the family Unionidae are notorious for their high intraspecific variation in shell form (Graf 2007). Much of this diversity varies predictably with the environment (Haag 2012; Zieritz and Aldridge 2009). For example, many species possess clinal variation in shell morphology in response to stream size (Ortmann 1920). Shells become more inflated (shell width relative to length), taller (shell height relative to length), thicker, and more asymmetrical (umbo positioned more anteriorly) with increasing stream size. In addition to this shell form-stream size gradient, shell shape also varies between lentic (lakes, wetlands, and reservoirs) and lotic (streams) habitats. Within multiple species, populations in lentic habitats ('lakes' hereafter) possess a more inflated shell shape relative to their conspecifics in lotic habitats ('streams' hereafter) (Ortmann 1919; Grier 1920). These ecophenotypic patterns are expressed across highly divergent lineages and therefore are assumed to be adaptive in habitat specific functions (e.g. stability, burrowing, floatation) (Watters 1994). Importantly, an underlying process explaining these common ecophenotypic patterns is unknown. Freshwater mussels are among the most imperiled aquatic groups globally and understanding if ecophenotypes are the result of speciation, genetic differentiation, or phenotypic plasticity is critical to successful conservation management (Ferreira-Rodríguez et al. 2019). Multiple integrative systematic studies using morphometric and molecular phylogenetic inferences have

disproved the speciation hypothesis of ecophenotypic variation (Cyr et al. 2007; Olivera-Hyde et al. 2020; Inoue et al. 2013; Pieri et al. 2018). Additionally, population genetic analyses of three species exhibiting lake-stream ecophenotypy showed no genetic association between ecophenotypic forms (Zieritz et al. 2010). These findings have led to the incorrect identification of phenotypic plasticity as the mechanism for ecophenotypic patterns in freshwater mussels and has led to the default explanation for any intraspecific variation (Inoue et al. 2013; Zieritz et al. 2010; Hornbach et al. 2010; Jeratthitikul et al. 2019; Wu et al. 2022). Although these molecular studies provide compelling evidence supporting phenotypic plasticity, they do not sequence markers involved in shell production and thus genetic mechanisms (e.g. convergent evolution) cannot be ruled out. What is needed is an experimental approach where the environment and/or genetic variation is standardized to separate genetic differentiation from phenotypic plasticity. Only one experiment has been conducted assessing the mechanism of morphology-habitat correlation in freshwater mussels. Hinch et al. (1986) conducted a reciprocal transplant experiment of *Lampsilis radiata* mussels between sand and mud substrates within Lake Erie. They found transplanted mussels from sand to mud substrates grew taller (shell height relative to length) relative to control (unmoved mussels) and mud to sand transplants showing that the environment and phenotypic plasticity can alter shell shape. However, the mechanisms of many ecophenotypic patterns remain unknown including the shared ecophenotypic pattern expressed across species occupying both stream and lake habitats.

I conducted a field experiment to understand the mechanism(s) producing ecophenotypic variation in freshwater mussels. I performed the experiment using *Pyganodon grandis*, a species that relative to other freshwater mussels grows quickly (Kesler and Van Tol 2000) and is easily propagated in the laboratory (M. Bradley, pers. comm.). *Pyganodon grandis* shares the ecophenotypic pattern of increased shell inflation in lake systems with other species (e.g. *Amblema plicata*, *Eurynia dilatata*, *Fusconaia flava*, *Ligumia recta*, *Pleurobema sintoxia*, *Lampsilis siliquoidea*) (Grier 1920; Ortmann 1919) but also becomes more circular in shell outline in lakes and more elongated in streams (Haag 2012) (Figure 2.1a). Ecophenotypy is so extreme in *P. grandis* that historically these variations were recognized as separate species or subspecies (Baker 1928). The experiment consisted of sibling mussels placed in one of two sets of wild common gardens: stream or lake habitat types comprising multiple field sites per habitat type. Mussels were reared from a single broodstock to minimize genetic variation and therefore isolate genetic versus environmental effects on morphology. After two years of growth, I measured and compared the morphology of sibling mussels between sites and habitat types and finally to wild *P. grandis* populations from the same sites. I asked five related questions: Among recaptured siblings, (1) does morphology differ between rearing site, (2) habitat type, or (3) between sites with the same habitat type? Additionally, to assess the potential bounds of plasticity I compared experimental mussels to wild populations to ask (4) to what extent do siblings morphology match the morphology of wild *P. grandis* reared within the same site and (5) habitat type?

Materials and Methods

Experimental subjects & design

I collected a single gravid female *P. grandis* from Chub Creek in southeastern Minnesota, USA (Cannon River drainage; 44.522, -93.2) on April 25, 2020. The mussel was promptly transported to the Center for Aquatic Mollusk Programs and held on oxygen for four days. *Pyganodon grandis*, like most freshwater mussels, is an obligate parasite on freshwater fishes during the larval life stage. Many fish species serve as hosts for *P. grandis* (Clarke and Berg 1959; Penn 1939; Trdan and Hoeh 1982; Wilson 1916). However, to eliminate the possibility that host use may influence intraspecific morphological variation of *P. grandis*, I used a single host, *Perca flavescens* (Yellow perch), to rear sibling mussels. Eighteen *P. flavescens* were manually inoculated with the broodstock of the collected *P. grandis* individual using standard freshwater mussel-fish host inoculation protocols (Zale and Neves 1982; Sietman et al. 2018). Briefly, viable glochidia (larvae) were manually extracted and suspended in aerated water baths along with *P. flavescens* hosts. I visually inspected the fin margins of hosts to confirm glochidia attachment and subsequently fish were moved to recirculating aquaria. Aquaria were monitored at regular intervals for sloughed glochidia and juvenile transformation. Juvenile mussels began dropping off fish twelve days after inoculation and continued for ten days (May 11-20, 2020). I aggregated approximately 14,766 juveniles in aerated buckets and transferred metamorphosed mussels to the Minnesota Zoo mussel propagation facility. Mussels were held at the zoo in mesh-lined (400um) baskets with sand (grain size 0.35-

0.45mm) in a flow-through trough and fed a commercial algae diet (Nanno 3600 and Shellfish Diet 1800) along with filtered lake water (200um screen).

Three months later (August 2020) mussels reached a size range (10-15mm) where they could be safely marked. I marked both valves of approximately 5,860 mussels with a black cyanoacrylate glue dot and cured with an accelerant (StewMac Inc. super glue and brush-on accelerator). I found nine suitable release sites (four streams, five lakes) in the same drainage (Cannon) and as close to the collection site as the mother *P. grandis* (Figure 2.2). I released 420-1,500 mussels at each of the nine sites over a five week period (mid-August-September). In addition, ~800 mussels were aggregated in a single mesh-lined basket and the basket was placed in a lake behind the zoo's propagation facility (same water source used to feed all mussels). Mussels were transported to release sites in five gallon buckets and acclimated to release sites with a 50% water change over thirty minutes. At deeper lake sites, I set up ten meters of lead line spread between PVC pipes and a cinder block between them to landmark release location. At stream sites, I scattered mussels over approximately 100 meters of stream distance but preferentially in deeper water.

Recapture & data collection

Two years following release (August 2022), I returned to the field sites and attempted recapture of released individuals using standard field collecting methods (e.g. wade, snorkel, SCUBA) over a three-week period. Recaptured individuals were immediately placed on ice and transported to the University of Minnesota where they were phenotyped, a tissue sample was taken, and were stored in a ultracold freezer (-

80C). I phenotyped each individual using three standard caliper (Mitutoyo electronic caliper) measurements frequently used in freshwater mussel morphometrics: maximum length (mm), maximum height (measured perpendicular to length centered on umbo; mm), and maximum width (mm) (Figure 2.1b). In addition to recaptured mussels in wild field sites, I quantified shell morphology for individuals that were kept at the Minnesota Zoo (in a mesh-lined basket with ~0.3um sand placed in a lake). Lastly, at all sites I successfully recaptured experimental (marked) individuals, I also collected and quantified the morphology of natural populations of *P. grandis*. Collection of wild individuals occurred both at time of release and recapture although only vouchered (deposited at JFBM) specimens were measured during time of release to prevent pseudo replication.

Statistical analysis

All analyses were performed in R v4.2.1 (R Development Core Team 2022) using packages *tidyverse* (Wickham et al. 2019), *car* (Fox and Weisberg 2019), and *multcomp* (Hothorn et al. 2008). I first visualized morphological variation using boxplots. In this instance morphology data were size corrected using shell length (height/length, width/length) and natural log transformed. I then ran linear regressions predicting height or width dependent on length. Regressions were ran for each site and habitat type. Finally, I constructed ANCOVA (analysis of covariance) models to test a series of questions below. I used type III sums of squares and $\alpha \leq 0.05$ was used to assess significance. For each model, shell height or width was used as a dependent variable with shell length as a covariate.

Question 1: Do sibling mussels reared at different sites have different shell morphology?

A first order analysis to test if the environment has an effect on shell morphology was to perform ANCOVAs to test if rearing sites had significantly different shell morphology (size relative height and width). Only recaptured sibling mussels were included but models were constructed with and without individuals reared at the zoo for the duration of the experiment.

Question 2: Do sibling mussels reared in streams versus lakes have different shell morphology?

Secondly, I wished to test what environmental factor(s) were causing any morphological differences between rearing sites. Therefore, I aggregated siblings reared at different sites but in comparable habitats, stream and lake, and tested for a significant effect of habitat type on shell morphology. As with question 1, only recaptured siblings were included. Although the zoo reared individuals were technically reared in a lake environment, because they were in a densely packed enclosure, zoo mussels were excluded from downstream analyses.

Question 3: Do sibling mussels reared at different sites but same habitat (stream vs. lake) have different shell morphology?

To test if rearing site had an effect on shell morphology among siblings reared in comparable habitats, I constructed ANCOVA models consisting of only stream or

lake reared individuals with site used as the predictor variable. I then used pairwise *post hoc* testing (Tukey method) to assess significant differences between each site comparison. Because only one site was a lake environment, this test was only done for stream sites.

Question 4: Do experimental mussels morphology differ from wild P. grandis reared at the same site?

If shell shape is purely determined by environmental factors in *P. grandis*, then sibling mussel morphology should match the morphology of wild caught individuals reared at the same site. Therefore, I aggregated experimental (siblings) and wild collected mussels at each site and tested for morphological differences.

Question 5: Do experimental mussels morphology differ from wild P. grandis reared in the same habitat (stream vs. lake)?

Lastly, I combined all lake and stream reared mussels into two separate datasets and tested for morphological differences between experimental (siblings) and wild mussels. Because only one site was a lentic environment, this test was only done for the stream habitat type.

Results

Recaptured and wild caught mussels

I recaptured mussels at four sites including one lake (Shields Lake: 44.37, -93.43) and three streams (Belle Creek: 44.424, -92.768; Chub Creek: 44.522, -93.2; Maple

Creek: 44.0958, -93.15). The Chub Creek recapture site was the same site the mother was collected from. In total, 70 individuals were recaptured including 26 from the single lake site and 44 from the three stream sites. These samples exclude the 305 experimental mussels kept at the zoo for the duration of the experiment. In addition to the experimental (sibling) mussels, 145 wild *P. grandis* were collected from the four sites. See Table 2.1 for more details on sample sizes and site information.

Statistical analysis

I found dramatic differences in relative shell height and width (Figure 2.3, Figure 2.4) across sites but particularly between stream and lake habitat types. These results were confirmed through linear regression (Figure 2.5) and ANCOVA models (Table 2.2). Sibling mussels and wild *P. grandis* reared in the same environment generally had no discernable difference in shell morphology with exception to one site, see below.

Q1: Do sibling mussels reared at different sites have different shell morphology?

I found a significant effect of rearing site (Table 2.2, Q1) on shell height and width while accounting for covariation with shell length showing that some aspect of the environment can modulate shell morphology. The results were largely agnostic to the inclusion or the exclusion of zoo individuals although the sum of squares (SS) increased for the model including zoo individuals (389.13 & 290.68 vs. 269.6 & 270.44).

Q2: Do sibling mussels reared in streams versus lakes have different shell morphology?

When lumping the recaptured individuals from each site into stream and lake habitat types, I found a significant difference in both relative height and width between habitats (Table 2.2, Q2) suggesting that the environmental cue responsible for morphological differences by site is tied to habitat type.

Q3: Do sibling mussels reared at different sites but same habitat (stream vs. lake) have different shell morphology?

Our ANCOVA models failed to find shell morphology differences between the three stream sites. This result was supported by the pairwise *post hoc* tests which found all pairwise combinations of lotic sites produced no significant differences in shell morphology. This further supports habitat type as the primary driver of morphological variation in *P. grandis*.

Q4: Do experimental mussels' morphology differ from wild P. grandis reared at the same site?

Separate ANCOVAs for each site generally produced non-significant differences between sibling and wild caught shell morphology at each site (Table 2.2). The one exception was at Belle Creek, where both relative shell height and width were significantly different between sibling and wild mussels. This model assumes wild caught mussels are from divergent gene pools relative to siblings but this may not be true, especially at Chub Creek where the source broodstock was collected from.

Q5: Do experimental mussels morphology differ from wild P. grandis reared in the same habitat (stream vs. lake)?

Although this test was only performed for the stream habitat type, the results followed those of question 4. When the ANCOVA included Belle Creek mussels it found significant morphological differences between sibling and wild mussels in lotic habitats. When the Belle Creek individuals were removed a weakly significant effect was still found for relative shell height but no difference was found for relative width.

Discussion

The results of my field experiment (Figure 2.3) show extreme shape divergence among sibling mussels reared in different sites and habitat types (Table 2.2; Figure 2.4), thereby revealing phenotypic plasticity as the primary mechanism producing shape variation in *P. grandis*. The combined evidence of shell shape differences between sites (Q1) and habitat types (Q2) as well as a lack of differentiation across the three stream sites (Q3) shows that plasticity in shell shape responded most robustly and predictably to habitat type (lake-stream) (Table 2.2). Ecophenotypic expressions of sibling mussels match previous field observations (Ortmann 1919; Clarke 1973) and the phenotypes of wild captured mussels from these habitats (Table 2.2; Figure 2.5) when accounting for allometry. Morphological differences between stream and lake habitats include size relative shell height, width (inflation), as well as shell coloration. Specifically across the three stream sites, shells were more elongated

in the anterior-posterior orientation, laterally deflated, and periostracum (i.e. outermost shell layer) color was dark brown. Whereas at Shields Lake, shells were more circular in both the longitudinal (anterior-posterior) and axial (width) planes with a bright yellow-green periostracum. Although the breadth of phenotypic expression of siblings mussels generally mirrored the variance of wild collected mussels, the morphology of wild caught mussels from Belle Creek was distinct from sibling mussels reared there (Table 2.2, Q4). This mismatch between experimental and wild mussels suggests that genetic differentiation and possibly local adaptation, may still play a role in ecophenotypic outcomes. Belle Creek was the only site where high sample sizes of first and second year-old wild caught mussels were collected. Because sibling mussels largely spent their first growing season (May-August 2020) in laboratory conditions, there may be a developmental lag or shape difference when comparing sibling and wild caught mussels of the same age. Therefore, this mismatch may reflect environmental differences during the first growing season rather than genetic differentiation and local adaptation. I discuss the implication of these findings from both basic and applied perspectives and propose next steps in the investigation of the roles of phenotypic plasticity and local genetic adaptation in the evolution of ecomorphology in freshwater mussels.

Environmentally mediated phenotypes

Phenotypic plasticity is expected to evolve in lineages that experience high spatial and temporal variation in environmental conditions as well as have high dispersal capabilities (Hendry 2016; Pfennig 2021. Temporary parasites, who rely on their

hosts for dispersal may uniquely fit these criteria. Freshwater mussels are obligate parasites during the larval life-stage, relying on an aquatic vertebrate (typically fish) host for dispersal. Given their sessile lifestyle as adults, the mobility of the host is the primary determinant of dispersal distance and habitat use generation-to-generation (Terui et al. 2017; Watters 1992). Host specificity varies greatly across freshwater mussels (Hewitt et al. 2019) including host specialists (Sietman et al. 2017; 2018) and hosts generalists including *P. grandis* who can successfully transform on over 40 fish species from 14 taxonomic families (Hewitt et al. 2019). Intuitively, host generalism would only seem to increase environmental uncertainty and dispersal variance. *Pygandon grandis* uses large, highly migratory fishes including *Cyprinus carpio* (Common carp), *Alosa chrysochloris* (Skipjack herring) but also smaller, more localized fish hosts including *Fundulus diaphanous* (Banded killifish) and *Etheostoma nigrum* (Johnny darter) (Lefevre and Curtis 1910; Surber 1913; Trdan and Hoeh 1982). Therefore, host generalism may be a predisposition to phenotypic plasticity as has been proposed in other systems (Brown et al. 2012; Leggett et al. 2013). Alternatively, host generalism may be a product of plasticity as adaptive phenotypic plasticity would increase the environmental variation occupied by a species and thus increase interactions with potential hosts in novel habitats. With their high variance in host specificity and documented phenotypic plasticity here, freshwater mussels may be a uniquely suited system to test these causal relationships. Habitat type was the biggest determinant of shape variation for both sibling and wild caught *P. grandis*. However, the specific environmental cue(s) initiating phenotypic expression is unclear. Hydrology is the most obvious environmental difference

between lake and stream field sites and quantification of within-species ecophenotypic relationships between morphology and water velocity (Balla and Walker 1991), flow rate (i.e. discharge) (Graf 1998), Reynolds number (i.e. hydraulic energy) (Simeone et al. 2022), and Strahler stream order (Ortmann 1920) suggest that freshwater mussels can reliably respond to hydrologic changes. However, the zoo population, reared in a basket enclosure within a lake, had drastically different morphology with more 'stream-like' relative heights and widths (Figure 2.4). These mussels were reared alongside baskets of other freshwater mussel species and to ensure adequate dissolved oxygen, air pumps were used surrounding the baskets. Further, the basket was densely packed with upwards of ~700 mussels with an average length of 42 mm in a ~1.5 meters^2 area. Hydrologic agitations caused by either neighboring mussels or air pumps could have been enough to falsely trigger the 'stream-form' phenotype. Importantly, there was very little morphological variance among the 305 individuals measured at the zoo showing that they were all responding to identical signal(s). In addition to hydrology, substrate type (Hinch et al. 1986) and turbidity (Tuttle-Raycraft and Ackerman 2020) have both been shown to illicit plastic phenotypic responses in freshwater mussels. Yet, anecdotally, substrate was not noticeably different between Shields Lake and the stream sites. At stream sites, mussels were collected from clay, silt, sand, and gravel and at Shields Lake, silt and sand. Turbidity and other water quality parameters are unlikely determinants of shell shape as 'lake-form' and 'stream-form' phenotypes can be collected meters away within the same contiguous waterbody. For example, above and below dams (Haag 2012; also observed in this study). More common garden experiments, preferably in

laboratory conditions where environmental variation can be more finely manipulated, are necessary to illuminate the specific environmental cue(s) *P. grandis* are responding to.

Phenotypic plasticity can produce neutral, maladaptive, or adaptive morphologies. Whether fitness advantages are tied to shell shape variation in *P. grandis* remains an unanswered question but the shared phenotypic expression of shell inflation in lake habitats and shell deflation in stream habitats across multiple divergent lineages (Grier 1920) suggests phenotypic plasticity is adaptive in *P. grandis*. Watters (1994) hypothesized that shell inflation in lakes is an adaptation for buoyancy in soft substrates (e.g. silt). Shell inflation increases surface area perpendicular to the burrowing axis and life position, which along with thin shells, may decrease sinking in low-density substrates. As noted above, soft substrates can occur in stream habitats as well but Watters (1994) suggested shell inflation is deleterious in stream habitats because hydrologic conditions can cause dislodgement of inflated shells. Alternatively, Eager (1978) proposed that the 'stream-form' and 'lake-form' phenotypic gradient reflects a tradeoff between stability in hydrodynamically demanding stream environments versus metabolic efficiency. Released from the physical constraints of streamflow, shell growth and morphology in lake populations may reflect a optimization of energy allocation towards internal soft anatomy involved in feeding, respiration, and reproduction rather than shell excretion. As Eager (1979) points out, an optimal way to reduce surface area and thus shell production while increasing internal volume is to become more spherical, as the 'lake-form' clearly does (Figure 2.3). If Eager's hypothesis is correct, internal

anatomical modifications should be evident between stream and lake populations. Lastly, the spherical shape divergence in lake habitats may be an anti-predator adaption to more quickly escape the gape of molluscivore fishes. Despite releasing more animals in lakes and having more lake sites than streams, I only recaptured mussels from a single lake site. My recapture efforts likely reflect lower survival in lake versus stream habitats and predation may be the underlying cause. Integrative approaches including performance assays and metabolomics will be fruitful endeavors in understanding the potential adaptive significance of phenotypic plasticity in *P. grandis* and freshwater mussels generally.

Conservation implications

In the face of widespread imperilment, the evolution of phenotypic plasticity in freshwater mussels has significant conservation implications. First, extreme ecophenotypy in species, like *P. grandis*, reflects their evolutionary potential. Regardless if this variation is adaptive, it illustrates that plastic freshwater mussel species have the ability to respond to changing environments: a trait that may provide resilience to anthropogenically modified habitats and climate change (Reed et al. 2011). Second, the identification of phenotypic plasticity rather than genetic differentiation as the mechanism for ecophenotypic patterns is highly convenient for conservation managers. The most popular resource used to combat mussel imperilment is captive-rearing propagation (Haag and Williams 2014). Propagation depends on field collection of gravid individuals, captive-rearing and culture of juveniles, and release of reared individuals into novel habitats, frequently different

than the locality of the collected female (Gum et al. 2011). The identification of phenotypic plasticity in a given lineage allows managers some flexibility in release location and ontogenetic timing as plastic species like *P. grandis* are highly acclimatized to environmental heterogeneity generation-to-generation and possibly within lifetimes. Cultured mussels spend variable amount of time in captivity and the timing of release into novel (Pletta pers. comm.), wild localities may be particularly important if developmental plasticity is fixed beyond a certain life point. However, no discernable variation in shape was detected when mussels were initially released into wild sites (three months old) but the shape divergence observed after two years shows that developmental plasticity does not become fixed in *P. grandis*, at least not early in life. Finally, the prevalence of propagation programs in North America are now being leveraged for basic science, including the research conducted here but also in ecotoxicology (Buczek et al. 2017, Popp et al. 2018), thermal tolerance (Pandolfo et al. 2010; Archambault et al. 2013), and life-history (Lefevre and Curtis 1910; Coker et al. 1921; Howard 1922; Sietman et al. 2017; 2018), which may be just as valuable to mussel conservation as stocking.

Conclusion

Experimental results from this study and others (Hinch et al. 1986; Tuttle-Raycraft and Ackerman 2020) show that freshwater mussels can conditionally express their anatomical features in response to environmental cues and phenotypic plasticity may be a common feature of mussels given the strong ecophenotypic variation in other species (Grier 1920; Ortmann 1920; Ball 1922; Agrell 1948; Graf

1998; Balla and Walker 1991; Zieritz and Aldridge 2009). Given their high and predictable morphological variation, *Pyganodon grandis* may be an ideal model system to study phenotypic plasticity and moreover, the functional genomics of shell shape in bivalves. I reared nearly ~7,000 individuals to three months of age from a single broodstock and found that they grew quickly and were robust to environmental changes. Additional investigation is needed to identify the environmental cues and adaptive significance of shell shape variation. Integrative and experimental inferences such as combining RNA-sequencing, morphometrics, and additional common garden experiments will be fruitful avenues of research.

Table 2.1: Sample sizes for recaptured siblings and wild caught *P. grandis* by sampling site and habitat type.

Site	Habitat type	Siblings/Wild	Samples	Notes
Belle Creek	Stream	Siblings	21	Includes 1 deceased at time of recapture
Belle Creek	Stream	Wild	104	
Chub Creek	Stream	Siblings	18	Includes 1 deceased at time of recapture
Chub Creek	Stream	Wild	44	Does not include mother
Maple Creek	Stream	Siblings	5	
Maple Creek	Stream	Wild	23	
Shields Lake	Lake	Siblings	26	Includes 1 deceased at time of recapture
Shields Lake	Lake	Wild	5	
Zoo	Experimental	Siblings	305	

Table 2.2: Results of ANCOVAs (questions 1-5) including degrees of freedom (df), sum of squares (SS), F statistic (*F*), and p-value. P-values that were not significant (>0.05) are denoted NS.

Model	**df**	**SS**	***F***	***P*-value**
Q1 Site effects on siblings				
Relative shell height	3	269.6	54.94	<0.001
Relative shell width	3	270.44	43.07	<0.001
Q1 Site effects on siblings (including zoo)				
Relative shell height	4	389.13	127.78	<0.001
Relative shell width	4	290.68	85.45	<0.001
Q2 Habitat effects on siblings				
Relative shell height	1	254.88	141.09	<0.001
Relative shell width	1	256.83	114.96	<0.001
Q3 Site effects within same habitat on siblings				
Lotic				

Relative shell height	2	5.4	1.64	NS
Relative shell width	2	0.75	0.24	NS
Q4 Genetic (wild vs. siblings) effects at same site				
Shields Lake				
Relative shell height	1	11.08	3.18	NS
Relative shell width	1	0	0.0008	NS
Maple Creek				
Relative shell height	1	4.61	1.25	NS
Relative shell width	1	2.6	1.31	NS
Chub Creek				
Relative shell height	1	14.8	2.8	NS
Relative shell width	1	3.1	0.56	NS
Belle Creek				
Relative shell height	1	139.9	22.49	<0.001
Relative shell width	1	47.4	8.35	0.005
Q5 Genetic (wild vs. siblings) effects in same habitat				
Lotic				
Relative shell height	1	219	30.9	>0.001

Relative shell width	1	51.8	9.8	0.001

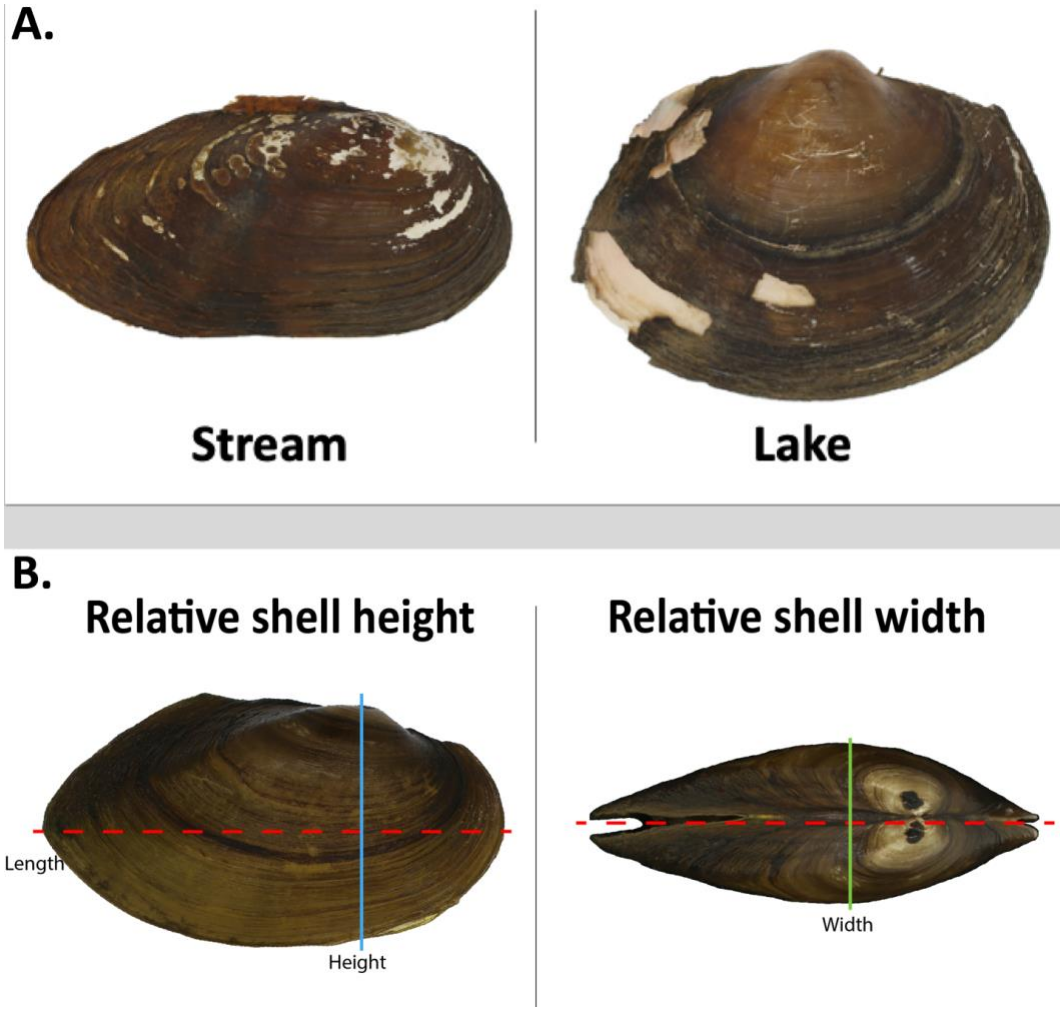

Figure 2.1: (a.) Typical shell shape variation of *P. grandis* between stream and lake habitats (Ortmann 1919; Grier 1920; Haag 2012). (b.) Morphological measurements shell length, height, and width (mm) quantified in this study.

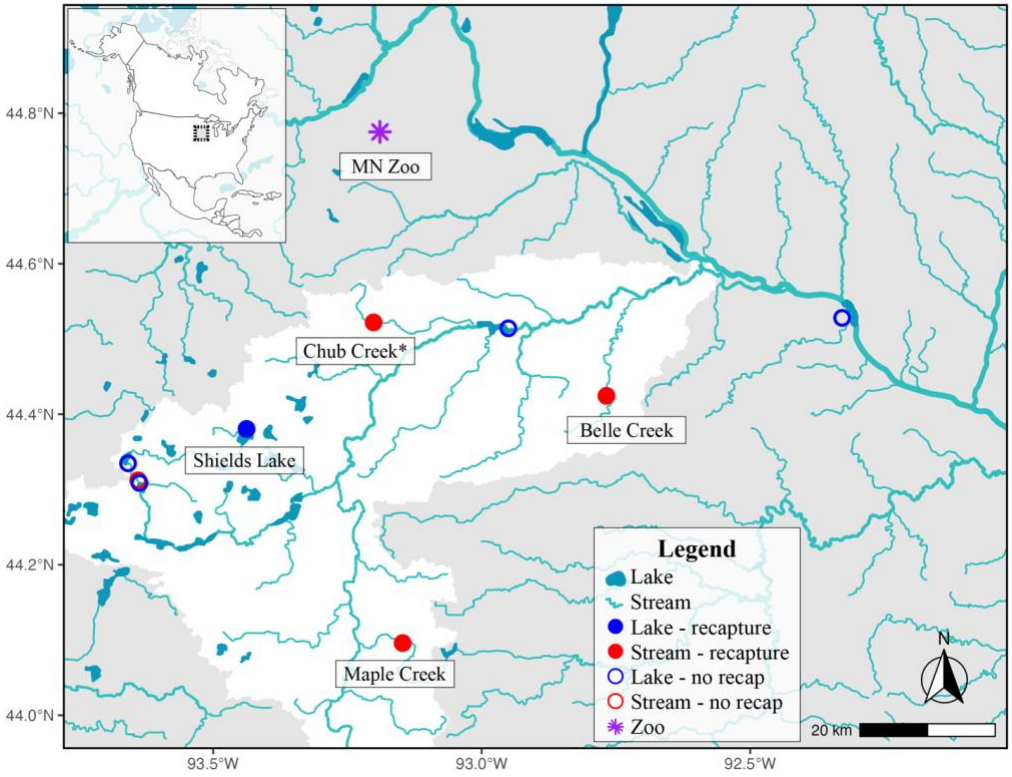

Figure 2.2: Map of the Cannon River drainage in southeastern Minnesota, USA (white). Circular points denote release sites: hollow = no recapture, solid = recaptures. *Denotes the location of the gravid female's field collection (Chub Creek).

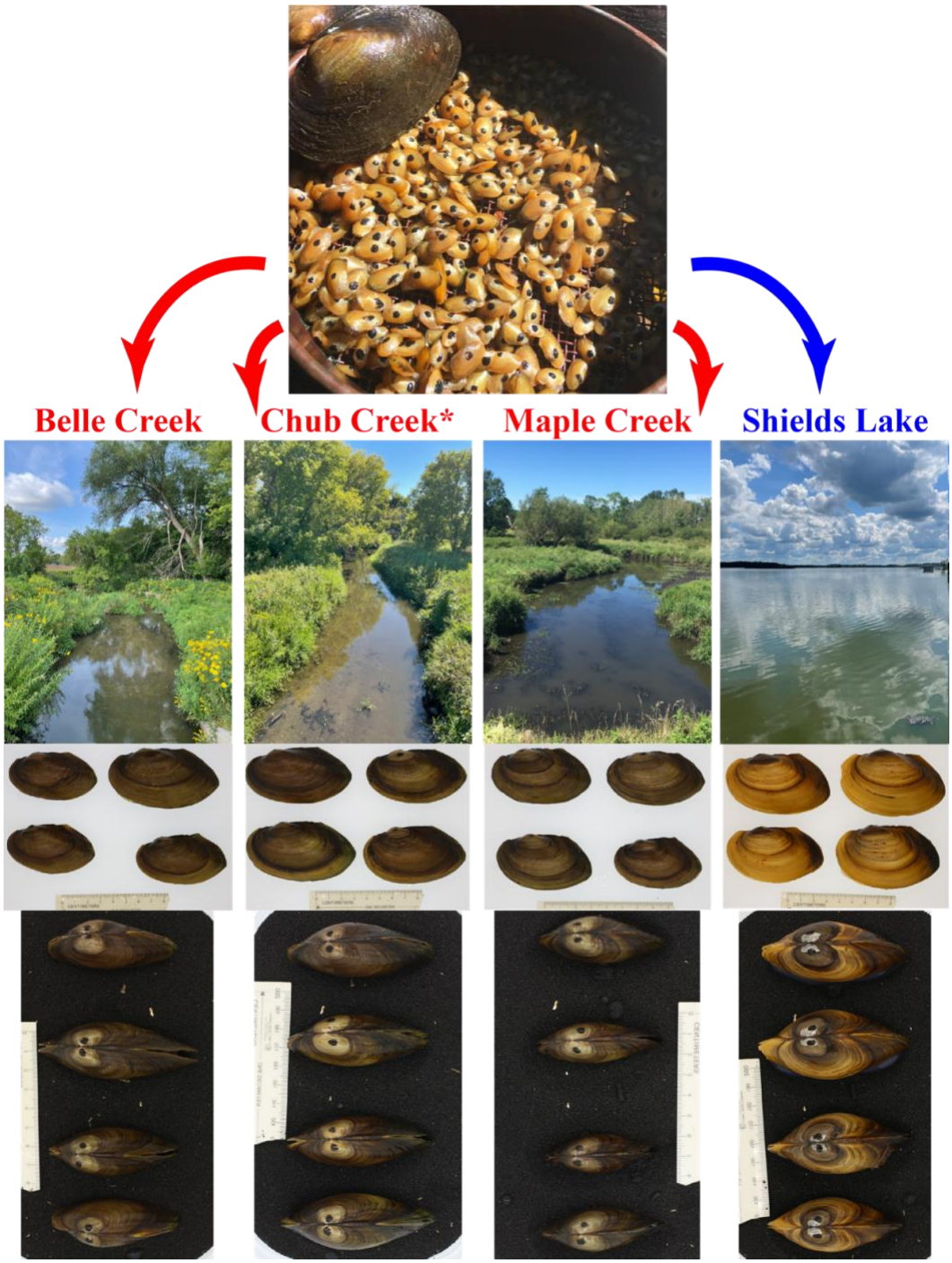

Figure 2.3: Layout of experimental design and shell morphology of recaptured siblings for four field sites including two habitats. Top photo shows marked siblings at three months of age immediately prior to field release with an adult *P. grandis* for

scale. Second row shows each field site at time of recapture. Third and fourth rows show four representative mussels from each recapture site: lateral view (top) and dorsal view (bottom).

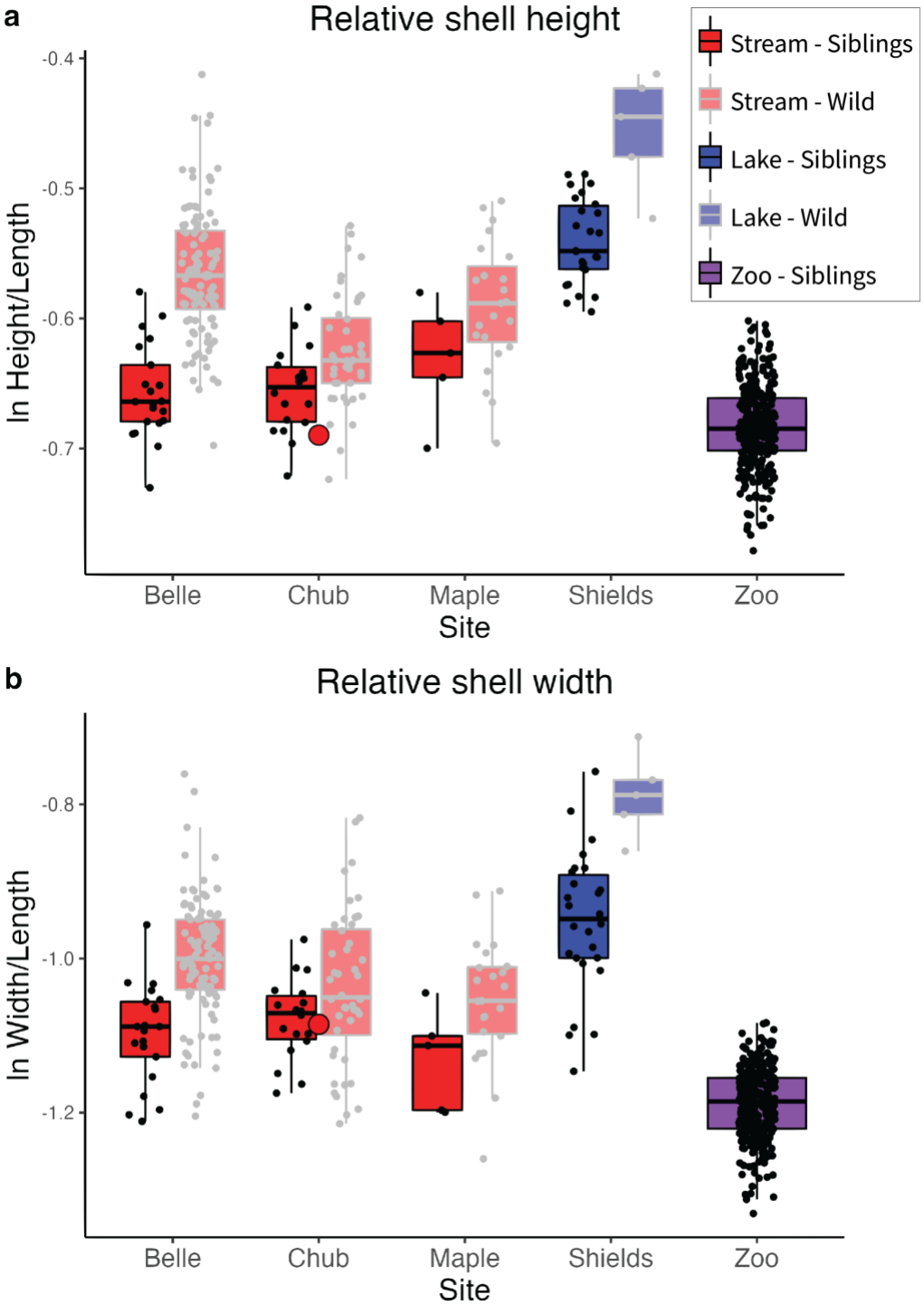

Figure 2.4: Boxplots of (a.) relative shell height (ln(height/length) and (b.) relative shell width (ln(width/length) for each site including sibling (black outlines) and wild (gray outlines) populations. Each boxplot is colored by habitat type: stream (red), lake (blue), and zoo enclosure (purple). Large red point in Chub Creek is the gravid female's (mother) morphology.

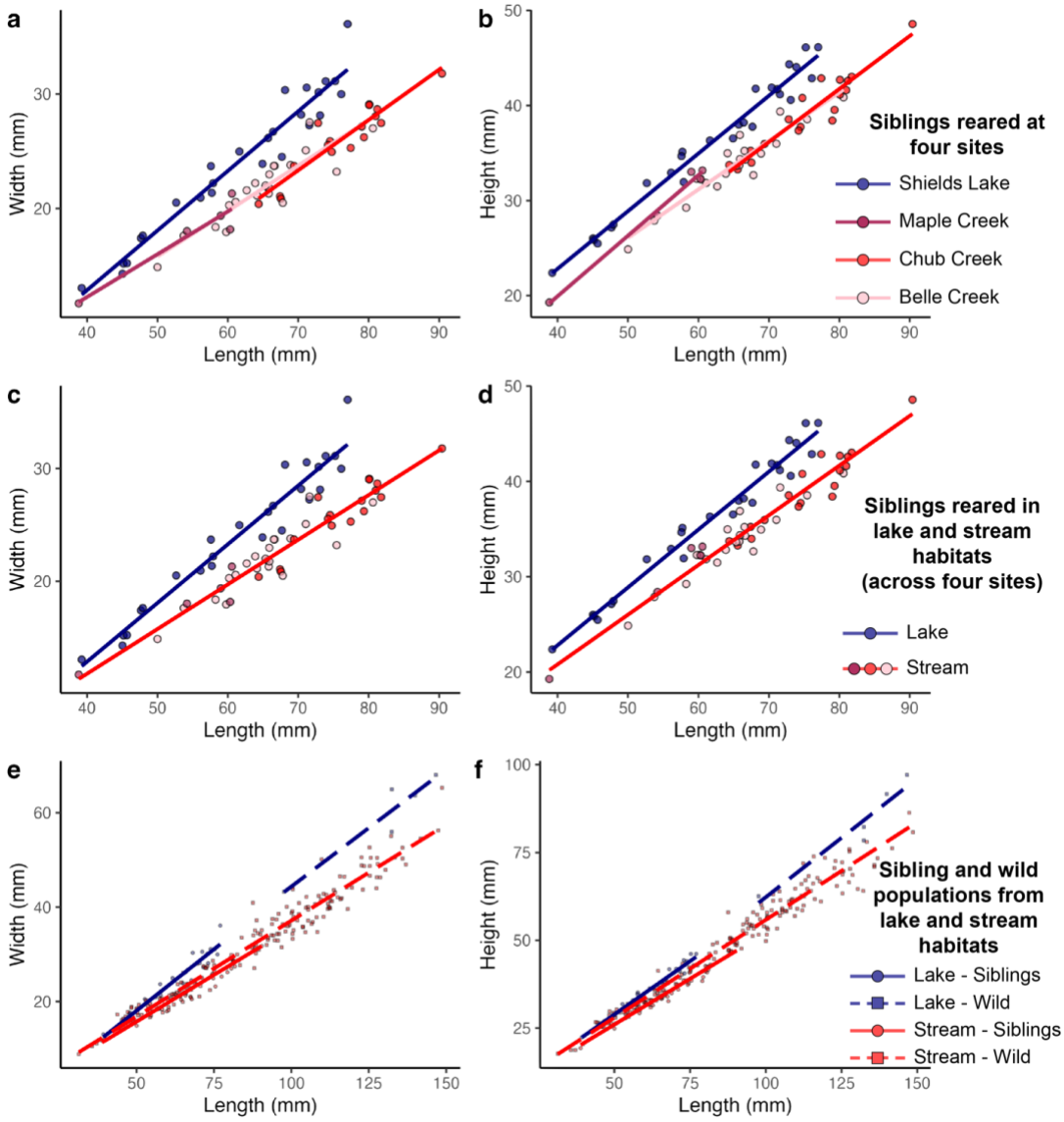

Figure 2.5: Linear regression of shell width (left panels) and shell height (right panels) as a function of shell length (i.e. growth trajectories). Top row (a. & b.):

siblings reared at each site have a separate regression line. Second row (c. & d.): growth regressions for each habitat type. Bottom row (e. & f.): growth regressions for each habitat type. Bottom row (e. & f.): growth regressions for wild and sibling populations in each habitat type.

Chapter 3:

Fluvial experiment investigating the effects of freshwater mussel posterior sculpture and orientation on hydrodynamics and streambed erosion (Unionidae: *Quadrula*)

Introduction

Identifying and quantifying the interactions between fluid dynamics and biological surfaces is imperative to understand how organisms adapt as well as manipulate flow in aquatic environments (Lauder et al. 2016). In fluvial settings, like streams and rivers, hydrodynamics are influenced by flow-induced forces as well as reaction forces by the biotic community (Nikora 2010). Organismal phenotypic traits, such as behavior, morphology, and physiology, have fundamental hydrological consequences in aquatic systems and are molded by evolutionary processes (Constantinescu et al. 2013; Hawkins et al. 2022; Rivera 2008; Trontelj et al. 2012). The relationship between phenotypic traits and the environment should be relatively tight as natural selection shapes phenotypic variation to maximize survival and reproduction (Arnold 1983). As such, organismal traits of biotic communities in fluvial ecosystems are both constrained by hydrodynamics through natural selection and manipulate it through ecological interactions. Despite the importance of phenotypic-hydrodynamic interactions on both ecological conditions of biological communities and the evolution of species comprising such communities, they have seldom been studied and quantified for many stream dwelling organismal groups.

The semi-infaunal freshwater mussels (Order Unionoida) occur at the sediment-water interface in streams and rivers across all continents aside from Antarctica (Graf and Cummings 2021). Given their abundance in fluvial ecosystems and their relatively large body size (Haag and Rypel 2011), they dominate benthic habitats, often comprising more than 50% of biomass (Haag 2012; Hanson et al. 1988; Negus 1966; Strayer et al. 1994). Freshwater mussels are relatively sessile but use their foot to find suitable habitat and burrow within the streambed. These bivalves do not have true siphons and generally expose the posterior end of their shell, containing incurrent and excurrent apertures, for respiration, feeding, waste excretion, etc. (Nichols et al. 2005; Strayer 2014; Vaughn et al. 2008). Further, freshwater mussels are long-lived organisms, (some species reaching ages >100 years old; Anthony et al. 2001) which exposes them to frequent, strong flow-induced forces during flood events. Displacement by entrainment, hereafter dislodgment, of freshwater mussels from the streambed is highly costly to mussel fitness as it transports them to potentially unsuitable downstream habitats, disrupts feeding, respiration, & reproduction, and constant reburial is energetically expensive (Curely et al. 2021; Hastie et al. 2001; Lopez and Vaughn 2021; Sotola et al. 2021). However, freshwater mussels are hypothesized to have evolved several adaptations to limit dislodgment events within their fluvial habitats (Watters 1994).

Shell morphology and behavior of freshwater mussels have both been shown to alter either streambed erosion (i.e. scour) or hydrodynamics (Allen and Vaughn 2011; Sansom et al. 2018; Sansom et al. 2020; Wu et al. 2020. Shell sculpturing along the dorsal-posterior margin (typically exposed to flow) has been shown to reduce

streambed erosion in freshwater mussels (Allen and Vaughn 2011; Daniel and Brown 2014; Watters 1994) and marine bivalves in fluvial experiments (Stanley 1981). However, streambed erosion was only coarsely quantified (% change) or not at all in these studies. Further, the influence that shell sculpture has on hydrology, including water velocity and direction, which ultimately influences streambed morphology, is unknown. In addition to shell morphology, mussel behavior, including orientation to flow, can significantly alter hydrological conditions surrounding mussels (Kumar et al. 2019; Wu et al. 2020). Yet no study has quantified how mussel orientation within the streambed effects streambed erosion. Therefore large gaps in knowledge exist in explaining how freshwater mussel morphology and orientation influence both hydrology and streambed morphology. My objectives in the study are to (1) quantify the effect shell sculpture has on water velocity magnitude, direction, and streambed morphology, (2) quantify the effect mussel orientation has on water velocity magnitude, direction, and streambed morphology, (3) identify additive and/or nonadditive effects of sculpture and orientation on hydrological and bathymetry metrics, and (4) identify patterns between hydrological parameters and streambed morphology to link potential causative hydrological factors on streambed morphology (e.g. erosion, deposition). Consistent with previous research, I hypothesize that regardless of mussel orientation, the presence of shell sculpture will significantly alter water velocity magnitude and direction and result in less streambed erosion surrounding mussels.

Materials and Methods

Flume

I performed experiments in a tilting bed flume at the Saint Anthony Falls Laboratory (SAFL), University of Minnesota (Table 3.1; Figure 3.1A) (Lee et al. 2022). The 14.6 m long flume had a width of 0.91 m filled with a sand/small gravel sediment (1.25 mm median grain size) that was approximately 0.13 m deep and a slope of 0.03%. The flume was outfitted with a computer-controlled data acquisition (DAQ) carriage that slid in the streamwise direction above the flume channel. The position of velocity and topography measurements were dictated by the DAQ carriage. At the start of each experiment and when the flume sediment was dry, I smoothed the streambed to a uniform height using a fixed height board that slid on the flume walls in the downstream direction. I gradually filled the flume (back-filled to start) to a depth of 0.12 m and discharge of 0.039 m^3/s. Once the proper flume depth was reached I used a Vectrino Acoustic Doppler Velocimeter (ADV; Nortek, Boston, MA) to collect three-dimensional water velocity at 5 m downstream of the flume and a depth of 0.072 m (60% of the total depth). When the streamwise velocity at this location reached 0.35-0.36 m/s the experiment began. Each experiment lasted six hours in addition to a flume fill time of approximately 45 minutes.

I ran four experimental trials with identical flume specifications. In each experiment two mussel models were partially buried (to mimic their life position) along the midline of the flume at 7 m and 9 m downstream. Two treatments were applied to the mussel models one at a time across the four trials. Mussel models were oriented ventrally downstream in experiment 1 and ventrally upstream in experiment

2. In between experiments 2 and 3, I used a file and sandpaper to remove posterior sculpture that was exposed, effectively making the 'ribbed' posterior sculpture smooth. No changes in shell shape or shell punctures were made. In experiment 3, smoothed models were oriented ventrally downstream and vice versa in experiment 4.

Mussel models

The shells of two *Tritogonia nobilis* (Gulf Mapleleaf) specimens from the Bell Museum of Natural History were used to construct mussel models for flume experiments. The first model (JFBM 22856.4) was collected from the Tennessee River (AL, USA) with a shell length of 61.09 mm (height = 51.38 mm; width = 19.52 mm), hereafter referred as the 'small' model. The second model (JFBM 22855.7) was collected from the Alabama River (AL, USA) and was 89.33 mm in shell length (height = 67.33 mm; width = 21.93 mm), hereafter referred as the 'large' model. To create each model, I articulated the shells of each specimen, filled the internal cavity with a small amount of gravel to mimic the natural weight of a mussel, and used a waterproof adhesive to fix each specimen in the closed position. I placed each model in the midline of the flume and the same streamwise position across the four experimental trials (small model at 7 m downstream and large model at 9 m downstream). Each mussel model was partially buried at a 55 degree angle to expose posterior sculpture and mimic their life position (e.g. expose regions of the shell where incurrent and excurrent apertures would filter-feed). Therefore, across all trials the same regions of shell morphology were buried and exposed (above the sediment-

water interface) for each model. See Table 3.1 for dimensions of shell exposure for each model.

To visualize morphological differences, specifically differences in shell sculpture before and after manual sculpture removal, I scanned the right valves from each specimen before the start of the experiment using micro-computed tomography (micro-CT) at the University of Minnesota's X-ray Computed Tomography facility. At the end of the experiment, I scanned entire models (two shells articulated) using micro-CT at the National Museum of Natural History's Scientific Imaging facility. I used Amira and ORS Dragonfly to create three-dimensional mesh models from the image stacks produced from each scan in Autodesk Meshmixer.

Acoustic Doppler Velocimetry (ADV)

To test for flow velocity differences across experimental trials, I used Acoustic Doppler Velocimetry which was attached and manipulated by the DAQ carriage. The Vectrino Profiler ADV captures instantaneous velocity in three-dimensions. Three-dimensional velocity was taken at a sampling volume of 5.5 mm and 50 mm immediately beneath the ADV probe. I collected ADV measurements at a sampling rate of 50-200 Hz for 120 s. All ADV measurements were taken along the midline (i.e. center) of the flume at twelve streamwise (x) locations (six surrounding each mussel model). For each mussel model, ADV measurements were taken at streamwise locations: 100 mm upstream of the leading edge of protruded models, immediately above the middle of the streamwise exposure of models, above models at 75% of its streamwise exposure, at the descending edge of models plus 5 mm to

avoid flow obstruction with models, downstream of models at a distance of 75% of the models' protruded height, and downstream a full length of models' protruded height. At each of these six streamwise positions, I took ADV measurements at various depth (z) locations. For streamwise locations not obstructed by the model, I took ADV measurements at five depths: 5.5 cm, 7.2 cm, 9.6 cm, 10.8 cm, and 11.5 cm from the water surface. The minimum depth was constrained by the ADV probe being fully submerged and the reading occurring 5 cm below the probe. The maximum depth was taken 5 mm above the streambed to account for any obstruction due to streambed movement. The three depths between the minimum and maximum were taken at 60%, 80%, and 90% of the total water depth (12 cm). For the remaining two streamwise ADV locations which were directly above the mussel models I used the protrusion height of the model as a proxy for the streambed location and measured velocity 5 mm above the model and at 80% and 90% of the total water depth between the model and water surface. I did not take a measurement at 60% of the total water depth for these streamwise locations as the minimum depth (5.5 cm) was nearly 60% of the water depth over each mussel model. Across the four experimental trials and two models per trial, 224 ADV measurements were taken. I started ADV measurements 90 minutes into each six hour trial. I converted ADV files in Vectrino Plus v2.0.2 and processed and filtered (i.e. 'despiked') in MATLAB using the modified phase space thresholding technique (Parsheh et al. 2010). At each ADV location, I time averaged velocity in each of the three-dimensions. For downstream analyses, I used Pythagorean theorem to transform three-dimensional velocity measurements to a single magnitude as well as find the hypotenuse of velocity

vectors in the streamwise (x) and stream depth (z) as a measure of velocity direction. Stream span (y) velocity was essentially 0 at all locations and therefore its influence on velocity direction was ignored.

Bathymetry

I measured streambed topography, hereafter bathymetry, using a flume channel wide, 2 mm thick laser sheet attached the DAQ carriage. The laser sheet scanned the length of flume channel and a high speed camera (SICK) captured the laser location in the x, y, and z direction with a spatial resolution of 2 mm as the DAQ cart slid in the streamwise direction. Scans were taken before and after each experiment. Before the experiment, I scanned the streambed after smoothing the streambed and positioning mussel models prior to filling the flume. I scanned the streambed again after draining the flume resulting in two scans per trial (pre and post scans). I processed bathymetry data in MATLAB while taking into account the slope (0.03%) of the flume and subtracted the streambed heights (z) between the before and after scans for each experiment. I then assessed differences to the streambed across experimental treatments.

Statistical analyses

All statistical analyses were performed in R v4.2.1 (R Development Core Team 2022) using packages *tidyverse* (Wickham et al. 2019) and *car* (Fox and Weisberg 2019). I constructed ANCOVA (analysis of covariance) models to test a series of

questions. I used type III sums of squares and $\alpha \leq 0.05$ was used to assess significance.

I first tested for differences in the starting conditions of experimental trials. Water velocity (velocity in three directions was transformed to a single magnitude) and direction 10 cm upstream of each mussel model are assumed to be unaffected by the mussel models, therefore these measurements should be close to identical across all trials. I tested this using ANCOVA using covariates experimental trial, streamwise (x) position, and stream depth (z). Additionally I used the bathymetry scans taken prior to the start of each trial to quantify any difference in the positioning, angle, and protrusion of mussel models. Aside from differences in sculpture, mussel models in trials 1 & 3 and trials 2 & 4 should be positioned and orientated identically. For each mussel model and orientation (four pairwise comparisons) I isolated a small region of the bathymetry scan corresponding to the maximum streamwise and stream span dimensions of mussel models and ran ANCOVA models to test for differences in starting conditions. I then extracted topographical differences for each experiment by subtracting bathymetry scans post-experiment from scans taken pre-experiment and isolated streambed regions surrounding mussel models (streamwise (x) distance = 3 times the exposed length of mussel models and stream span (y) distance = 2 times the exposed width of mussel models) to quantify changes in the streambed (e.g. erosion, deposition). Ithen constructed ANCOVA models to test for bathymetry differences based on both mussel sculpture and orientation treatments using streamwise (x) and stream span (y) locations as covariates. Lastly, I constructed ANCOVA models to test for water velocity magnitude and direction differences between sculpture and

orientation treatments using streamwise (x) and stream depth (z) positions as covariates.

Results

Differences in experimental starting conditions

The ANCOVA models testing for differences in upstream water velocity magnitude and direction found no significant differences across experimental trials (magnitude: p-value=0.66, direction: p-value=0.62) indicating the hydrologic conditions across trials were not significantly different. Conversely, ANCOVA models testing for differences in the placement of mussel models across trials with the same orientation, were all significant (p-value ≤ 0.05) besides one comparison (small model, upstream orientation). Experimental trials (3 & 4) with sculpture removed from models consistently had models that were placed deeper into the streambed (shorter protrusion height) and differences between protrusion heights were as large as ~10 mm (Figure 3.2).

Bathymetry

Qualitatively, I observed greater variation in bathymetry, specifically streambed erosion, associated with the large mussel model (left column of Figure 3.3). Further, the location of streambed erosion appears to be correlated with mussel orientation. Mussels orientated downstream (Figure 3.3A-B,E-F), have a horseshoe shaped streambed erosion immediately in front of the model or contained to the sides. Mussels orientated upstream (Figure 3.3C-D,G-H), have ‘v’ shaped streambed

erosion immediately upstream with large and fairly deep holes downstream of models. Sculptured models appear to produce larger and deeper streambed erosion at least for the large mussel model. ANCOVA models found both the orientation and the presence/absence of shell sculpture to significantly effect streambed morphology (Table 3.2).

Water velocity magnitude & direction

Across all trials water velocity magnitude decreases with stream depth (z) and water velocity direction is consistently in the streamwise (x) direction aside from the six ADV measurements taken directly behind models in each trial (Figure 3.4). The effects of shell sculpture on water velocity magnitude and direction were not apparent (Figure 3.4A vs. E, B vs. F, C vs. G, D vs. H) with the ANCOVA model (Table 3.2) finding no significant differences between sculpture treatments. Mussel orientation (facing upstream vs. downstream) however influenced both water velocity magnitude and direction. With few exceptions, models orientated in the downstream direction had lower water velocity magnitudes (except Figure 3.4E) at points behind models and water velocity direction tended to point upwards at these locations whereas they were pointed downward when models were oriented upstream (Figure 3.4C-D, G-H). ANCOVA models found both water velocity magnitude and direction were significantly different between the two orientations (Table 3.2).

Discussion

Contrary to my hypothesis that shell sculpture would alter water velocity magnitude and direction resulting in less streambed erosion, I found no significant effects of shell sculpture on water velocity magnitude and direction (Table 3.2; Figure 3.4) but increased, rather than decreased, streambed erosion associated with shell sculpture (Table 3.2; Figure 3.3). However, increased streambed erosion may be due to differences in the starting placement of mussel models between sculptured and unsculptured trials (Figure 3.2). In three of the four pairwise comparisons (Figure 3.2A-C), the sculptured models had a taller protrusion height (e.g. more of the mussel model was exposed to flow), which may explain the increased streambed erosion surrounding sculptured models. Conversely to sculpture, model orientation had significant effects on water velocity magnitude, water velocity direction, and streambed erosion (Table 3.2). When mussels were oriented downstream (ventral downstream), streamflow was obstructed by the blunt dorsal edge of mussel models, creating streambed erosion immediately upstream of the model (Figure 3.3A) and/or around the sides of mussel models (Figure 3.3B,E,F). Conversely, when models were oriented upstream (ventral upstream), streamflow wrapped around mussel models and created large and often deep (~10 mm) streambed erosion holes immediately downstream of models (Figure 3.3C,D,G,H). Further, the shape of exposed mussel models appeared to guide water velocity in predictable directions (Table 3.2). When oriented in the downstream position, the blunt dorsal edge along with the posterior slope, appears to direct water velocity magnitude away from the streambed downstream (Figure 3.4A,B,E,F), which may explain the absence of streambed

erosion downstream (Figure 3.3A,B,E,F). When oriented upstream, I observed the opposite pattern, where the direction of water velocity magnitude was directed towards the streambed downstream of models (Figure 3.4C,D,G,H), resulting in erosion holes (Figure 3.3C,D,G,H).

Shell sculpture

I found no evidence that the presence of shell sculpture functions as an anti-scouring mechanism (Figure 3.3). In fact, I found the presence of shell sculpture to increase streambed erosion. However, as mentioned above, variation in protrusion height (the amount of shell exposed from the streambed) between sculptured and unsculptured experimental trials may be responsible for my unexpected results (Figure 3.2). Additionally, I ran each treatment for each model once, lacking replication. Without replication it is difficult to assess whether bathymetry results are genuine or due to error in starting conditions. Further, there are many experimental differences between previous shell sculpture-streambed erosion studies and the study conducted here. I chose to use shell models rather than live animals to exert greater control on experimental conditions. Watters (1994) used shell models similarly and even used closely related species: *Quadrula quadrula* and *Tritogonia verrucosa*. However, water velocity was much lower at 0.05 m/s (compared to 0.1-0.4 m/s, Figure 3.4) and streambed grain size was <0.42 mm compared to a median grain size of 1.25 mm used here (Table 3.1). Given the discrepancy of results, replication of Watters' (1994) experimental methods using quantitative methods is needed. Although I used shell models for fine-tuned control, the use of live freshwater

mussels in fluvial experiments is important as it considers behavior and better mimics natural conditions. Allen and Vaughn (2011) and Daniel and Brown (2014) both used live mussels to assess streambed stability associated with sculptured and unsculptured species in fluvial experiments. Both experiments found sculptured species to generally decrease streambed erosion or even increase deposition around sculptured species. Sculptured species may behave differently to unsculptured species including orientation to flow (Di Maio and Corkum 1997), burrowing angle, depth, and activity (Allen and Vaughn 2009; Sansom et al. 2022), substrate preference (Goodding et al. 2019), or possess more hydrodynamic shell shapes. Additionally, I used only two mussel models in each trial and placed them two meters apart to minimize their interaction. However, freshwater mussels tend to occur in aggregations, called 'mussel beds' (Strayer 1981; 2008), which have been shown to increase the surface roughness of streambeds and result in decreased near-bed water velocity (Sansom et al. 2018). In fluvial experiments, sculptured species in monoculture at high densities were found to have significantly decreased streambed erosion or even deposition (Allen and Vaughn 2011), suggesting that shell sculpture functions as an anti-scouring mechanism for the mussel bed rather than the individual.

Mussel orientation

My experiment shows conclusively that freshwater mussel orientation significantly effects water velocity magnitude, direction, and streambed erosion (Table 3.2; Figure 3.3-4). These results appear to be partially relating the asymmetrical morphology along the dorsal-ventral axis (Figure 3.1B). Flow direction

(vectors in Figure 3.4) downstream of mussel models follows the slope of exposed shell shape creating downstream streambed erosion holes when oriented upstream and upstream and peripheral streambed erosion when oriented downstream (Figure 3.3). Further, regardless of upstream or downstream orientation, relative to the mussel, stream erosion is always taking place dorsally. Therefore, despite obvious differences in water velocity magnitude, direction, and streambed erosion, it is unclear if these differences are biologically significant.

There is currently conflicting evidence in the literature that freshwater mussels orient themselves to streamflow (Haag 2012). Historically they were understood to orient themselves to flow in the upstream direction (ventral upstream) (Baker 1928; Coker 1921) as this prevents incurrent filtration of waste products from the excurrent aperture as the excurrent aperture is downstream of the incurrent aperture in this position. However, field studies and experiments have found mussel orientation to be highly context dependent. Perles et al. (2003) measured the orientation of *Lampsilis siliquoidea* in an artificial stream as well as multiple species at a field site over a three month period. Although *L. siliquoidea* in the artificial stream were generally oriented within ~30 degrees of an upstream position, there was no pattern to the orientation of mussels found at the field site. These findings mirror the results of Di Maio and Corkum (1997) who found vastly different mussel orientations between two stream sites. In a stream with highly variable flow rates (i.e. discharge), mussels were generally oriented in the upstream direction but in a stream with more stable flow rates mussels were randomly oriented. Clearly mussel orientation is complex and

context dependent and may be highly species-specific and/or change with fluctuations in flow rate and water velocity.

Conclusion

My results of increased streambed erosion associated with shell sculpture are in opposition to a suite of studies (Allen and Vaughn 2011; Daniel and Brown 2014; Stanley 1981; Watters 1994) who found decreased streambed erosion surrounding sculptured mussels. However, this result may be due to experimental error (e.g. differences in starting conditions, Figure 3.2) or a lack of experimental replication. Therefore, I am not suggesting that shell sculpture does not serve an anti-scouring function as currently hypothesized. Regardless, my results do suggest that other factors, namely mussel orientation but also protrusion height, and/or shell morphology, are stronger determinants of streambed erosion and hydrodynamics than shell sculpturing (Table 3.2; Figure 3.3-4). In addition to increased trials, future experiments should explore the interactions of shell sculpture, orientation, shell shape, and protrusion height on hydrodynamics and streambed morphology. Different species or even populations within species are likely interacting with streamflow in unique ways. Broadening the scope of experimental fluvial studies to additional taxa of both model and live specimens will further illuminate how mussels interact and manipulate streamflow on ecological timescales as well as the evolutionary ramifications of hydrodynamics on mussel morphology.

Table 3.1: Experimental parameters and details.

Flume Parameters	**Values**
Wetted length	14.6 m
Wetted width	0.91 m
Water depth	0.12 m
Sediment depth	0.13 m
Median sediment grain size	0.00125 m
Flow discharge	0.039 m^3/s
Water surface slope	0.03%
Streamwise location of small mussel model	7 m downstream
Streamwise location of large mussel model	9 m downstream
Maximum height of exposed small mussel model	0.014 m
Maximum height of exposed large mussel model	0.025 m
Maximum width of exposed small mussel model	0.029 m
Maximum width of exposed large mussel model	0.038 m
Maximum length of exposed small mussel model	0.051 m

Maximum length of exposed large mussel model	0.072 m
Burrowing angle of mussel models	~55°

Table 3.2: Results of ANCOVAs testing for the effects of shell sculpture and mussel orientation respectively on streambed changes and hydrology including parameters degrees of freedom (df), sum of squares (SS), F statistic (*F*), and p-value. Significant p-values (<0.05) are bolded.

Model	**df**	**SS**	***F***	***P*-value**
Sculpture effects				
Streambed changes	1	14493	4905.7	**<0.001**
Water velocity magnitude	1	0.002	0.98	0.32
Water velocity direction	1	0.002	0.16	0.69
Orientation effects				
Streambed changes	1	115	32.4	**<0.001**
Water velocity magnitude	1	0.007	4.5	**0.03**

Water velocity direction	1	9E-08	9.1	**0.003**

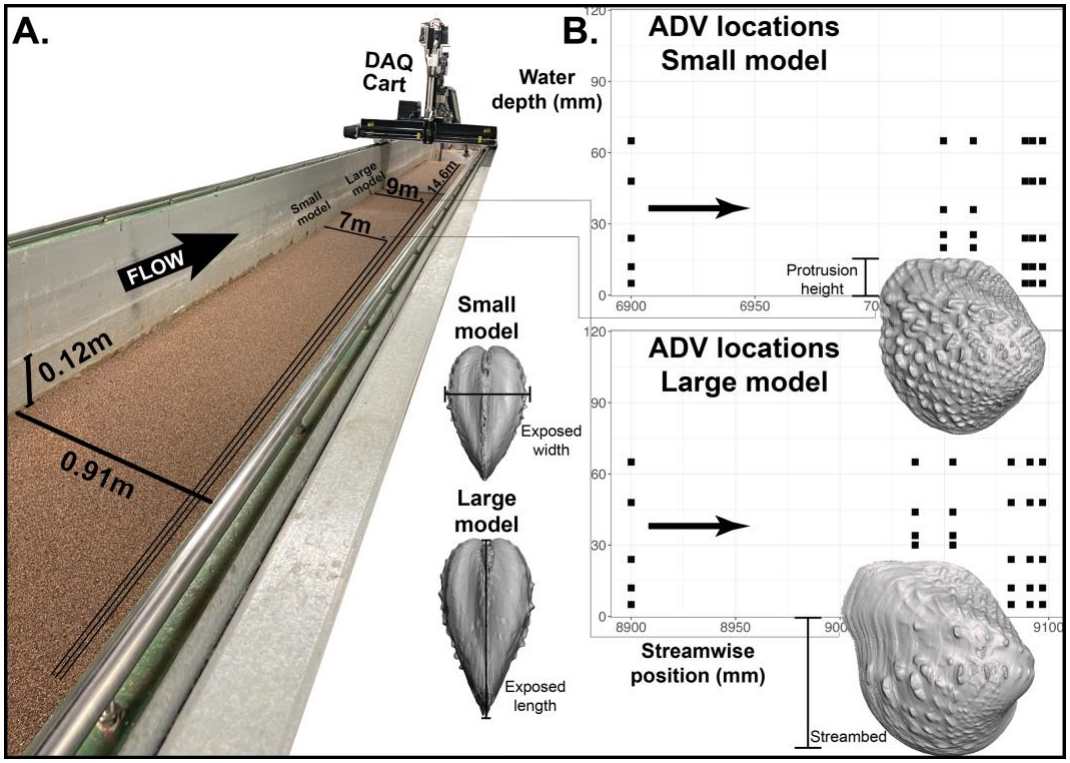

Figure 3.1: (A.) Photograph of experimental channel (flume) with DAQ cart, flume width, wetted length, water depth, and streamwise positions of small and large mussel models. (B.) Plots showing the streamwise and stream depth locations of ADV measurements (black squares) surrounding small and large models. Water depth is 120 mm and ADV measurements were taken along the midline (center) of flume and mussel models. Computed-tomography scans show the location of buried models as

well as their protrusion height, exposed width, and exposed length. Arrows indicate the direction of streamflow.

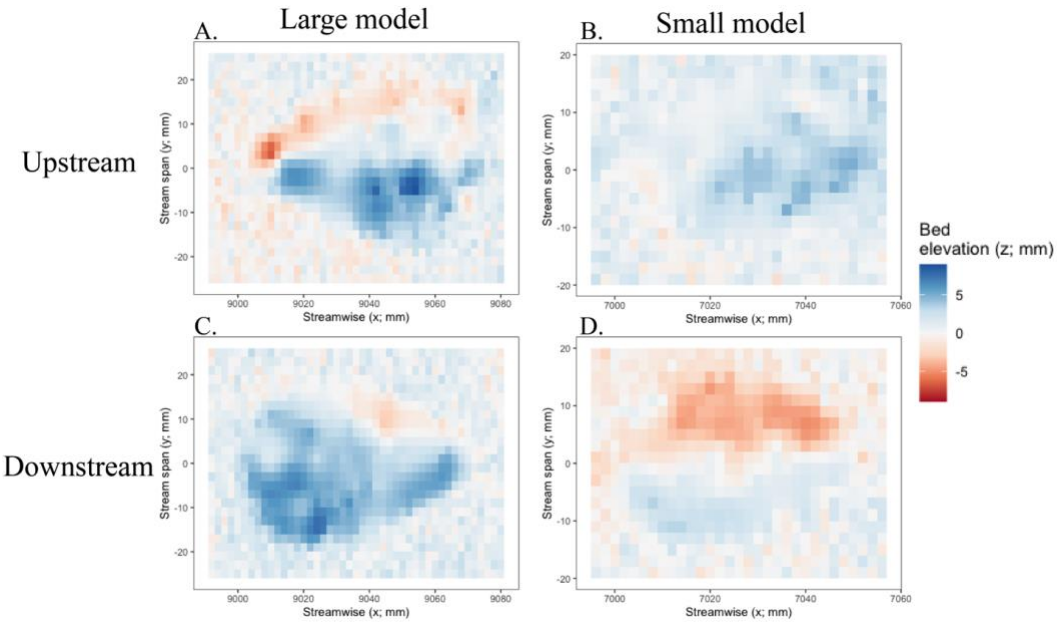

Figure 3.2: Differences in the starting conditions and placement of mussel models. The difference between the placement of the large (A.) and small (B.) mussel model between experiment 2 and 4. Positive values (blue) indicate a higher mussel protrusion height in experiment 2. The difference between the placement of the large (C.) and small (D.) mussel model between experiment 1 and 3. Positive values (blue) indicate a higher mussel protrusion height in experiment 1.

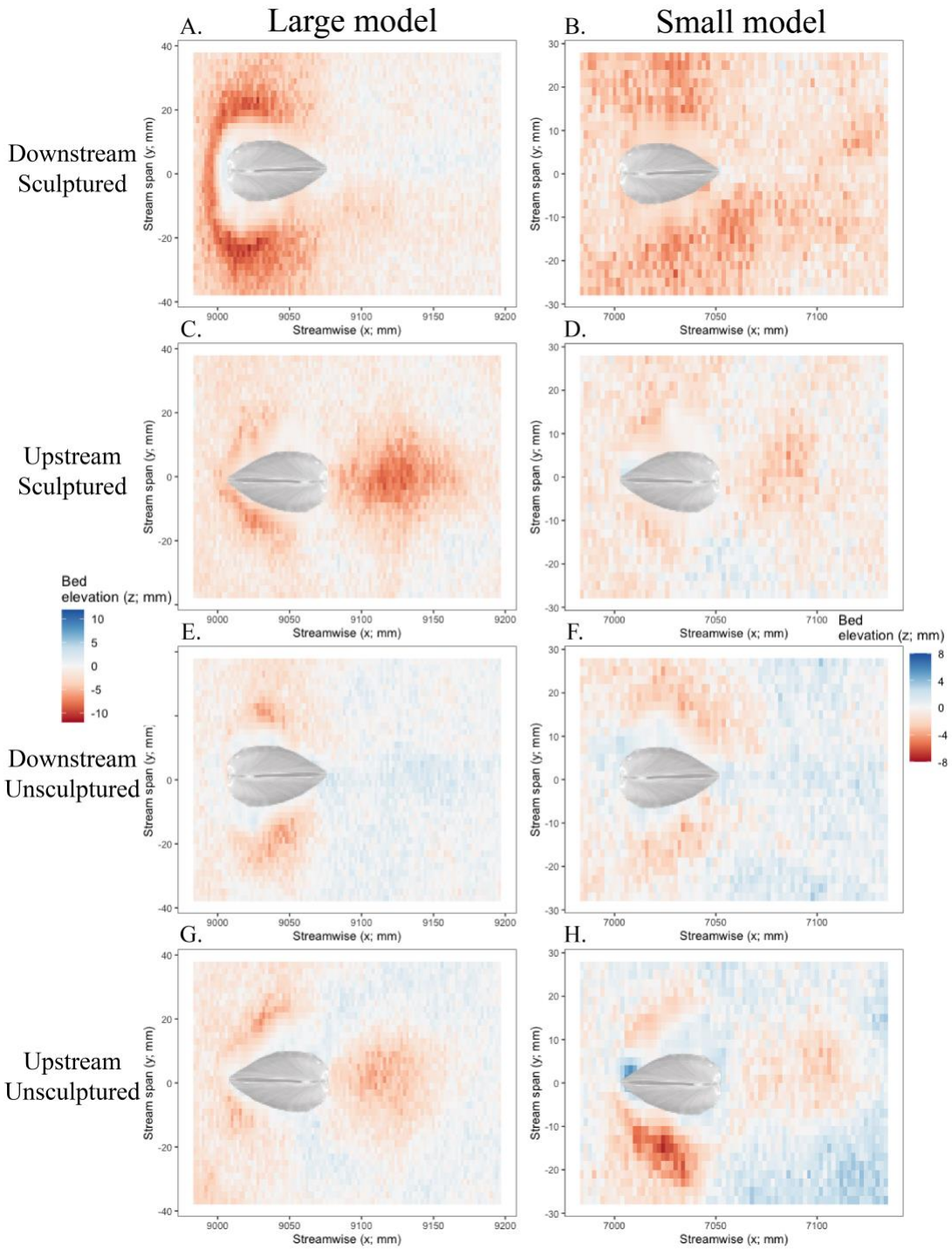

Figure 3.3: Net streambed erosion and deposition after each experimental trial and for each mussel model: large (left) and small (right) for all treatments (orientation and sculpture). Note the different scales of bed elevation between the two columns of

plots. A mussel model schematic was superimposed in the approximate location of the model in each plot. Streamflow is from left to right.

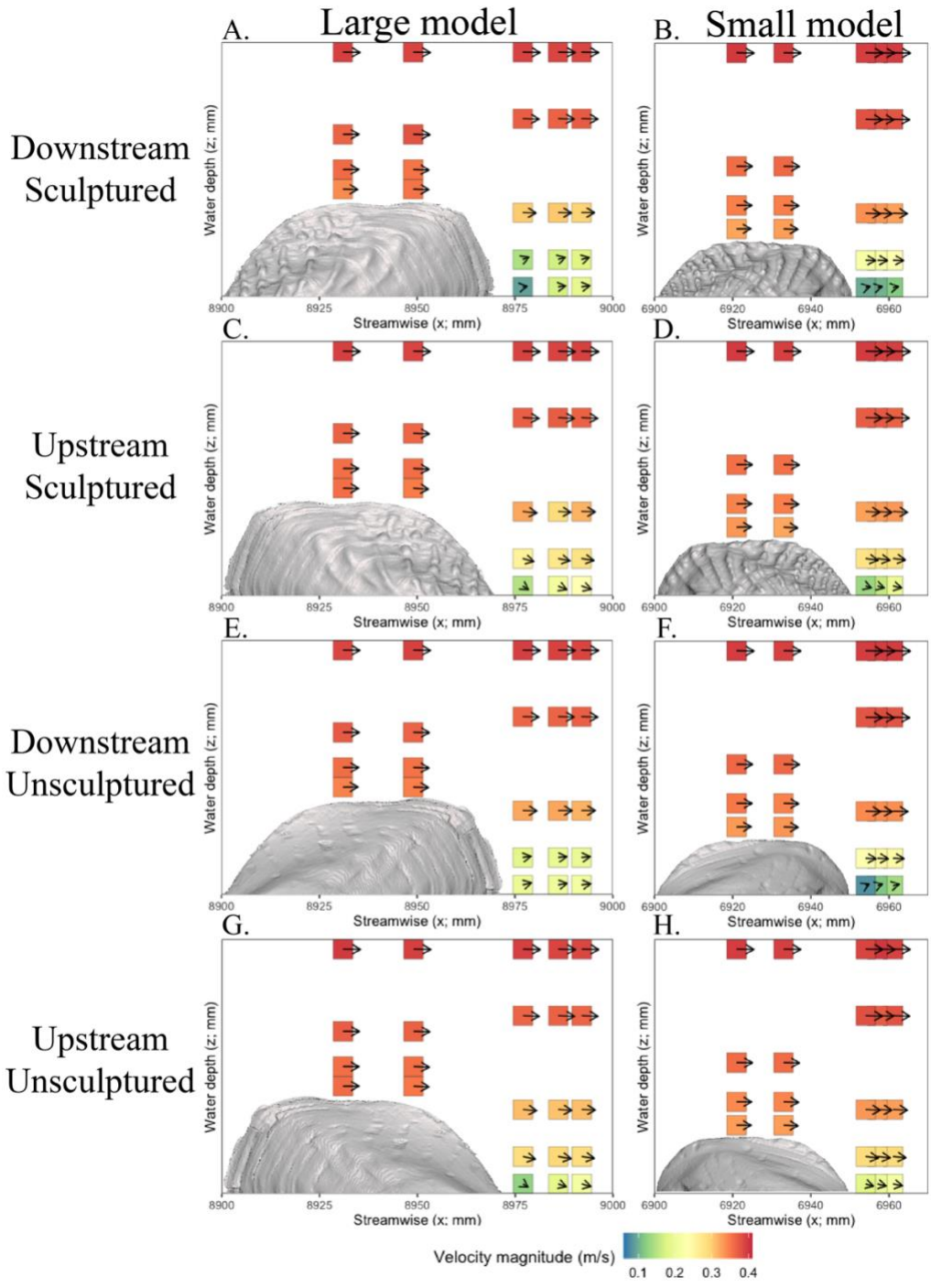

Figure 3.4: Water velocity magnitude (tiled colors and length of vectors) and direction (angle of vectors) taken from ADV measurements for each experimental

trial and each mussel model: large (left) and small (right) for all treatments (orientation and sculpture). Water is flowing from left to right. The CT-scan of each mussel model (and treatment) was superimposed in the approximate location for each trial. ADV measurements taken from 10 cm upstream of models were omitted from plots to save space and as they were shown to not differ between trials.

Bibliography

Agrawal AA. 2001 Phenotypic plasticity in the interactions and evolution of species. Science **294**, 321-6. (doi:10.1126/science.1060701)

Agrawal AA. 2017 Toward a predictive framework for convergent evolution: integrating natural history, genetic mechanisms, and consequences for the diversity of life. The American Naturalist **190**, S1-2. (doi:10.1086/692111)

Agrell I. 1948 The shell morphology of some Swedish unionids as affected by ecological conditions. Arkiv För Zoologi **41**, 1-30.

Allen DC, Vaughn CC. 2009 Burrowing behavior of freshwater mussels in experimentally manipulated communities. Journal of the North American Benthological Society **28**, 93-100. (doi:10.1899/07-170.1)

Allen DC, Vaughn CC. 2011 Density-dependent biodiversity effects on physical habitat modification by freshwater bivalves. Ecology **92**, 1013-1019. (doi:10.1890/10-0219.1)

Anthony JL, Kesler DH, Downing WL, Downing JA. 2001 Length-specific growth rates in freshwater mussels (Bivalvia: Unionidae): extreme longevity or generalized growth cessation?. Freshwater Biology **46**, 1349-1359. (doi:10.1046/j.1365-2427.2001.00755.x)

Archambault JM, Cope WG, Kwak TJ. 2014 Influence of sediment presence on freshwater mussel thermal tolerance. Freshwater Science **33**, 56-65. (doi:10.1086/674141)

Baker FC. 1928 Fresh Water Mollusca of Wisconsin.

Ball GH. 1922 Variation in fresh-water mussels. Ecology **3**, 93-121. (doi:10.2307/1929144)

Balla SA, Walker KF. 1991 Shape variation in the Australian freshwater mussel *Alathyria jacksoni* Iredale (Bivalvia, Hyriidae). Hydrobiologia **220**, 89-98. (doi:10.1007/BF00006541)

Bolotov IN, Vikhrev IV, Bespalaya YV, Gofarov MY, Kondakov AV, Konopleva ES, Bolotov NN, Lyubas AA. 2016 Multi-locus fossil-calibrated phylogeny, biogeography and a subgeneric revision of the Margaritiferidae (Mollusca: Bivalvia: Unionoida). Molecular Phylogenetics and Evolution **103**, 104-121. (doi:10.1016/j.ympev.2016.07.020)

Bouckaert R, Vaughan, TG, Barido-Sottani, J, Duchêne, S, Fourment, M, Gavryushkina, A, Heled, J, Jones, G, Kühnert, D, De Maio, N, Matschiner, M. 2019 BEAST 2.5: an advanced software platform for Bayesian evolutionary analysis. PLoS Computational Biology **15**, e1006650. (doi:10.1371/journal.pcbi.1006650)

Bower LM, Saenz DE, Winemiller KO. 2021 Widespread convergence in stream fishes. Biological Journal of the Linnean Society **133**, 863-79. (doi:10.1093/biolinnean/blab043)

Brown SP, Cornforth DM, Mideo N. 2012 Evolution of virulence in opportunistic pathogens: generalism, plasticity, and control. Trends in microbiology **20**, 336-342. (doi:10.1016/j.tim.2012.04.005)

Buczek SB, Cope WG, McLaughlin RA, Kwak TJ. 2017 Acute toxicity of polyacrylamide flocculants to early life stages of freshwater mussels. Environmental toxicology and chemistry **36**, 2715-2721. (doi:10.1002/etc.3821)

Bürkner PC. 2017 *brms*: an R package for Bayesian multilevel models using Stan. Journal of Statistical Software **80**, 1-28. (doi:10.18637/jss.v080.i01)

Burns MD, Sidlauskas BL. 2019 Ancient and contingent body shape diversification in a hyperdiverse continental fish radiation. Evolution **73**, 569-587. (doi:10.1111/evo.13658)

Calsbeek R, Smith TB. Bardeleben C. 2007 Intraspecific variation in *Anolis sagrei* mirrors the adaptive radiation of Greater Antillean anoles. Biological Journal of the Linnean Society, **90,** 189-99. (doi:10.1111/j.1095-8312.2007.00700.x)

Carroll SB. 2001 Chance and necessity: the evolution of morphological complexity and diversity. Nature **409**, 1102-9. (doi:10.1038/35059227)

Clarke AH. 1973 The freshwater molluscs of the Canadian Interior Basin. Malacologia **13**, 1-509.

Clarke AH, Berg CO. 1959 The freshwater mussels of central New York with an illustrated key to the species of northeastern North America. Cornell University Agricultural Experiment Station Memoir **367**, 1-79.

Coker RE, Shira AF, Clark HW, Howard AD. 1921 Natural history and propagation of freshwater mussels. Bulletin of the United States Bureau of Fisheries **37**, 75-181

Collins KS, Edie SM, Gao T, Bieler R, Jablonski D. 2019 Spatial filters of function and phylogeny determine morphological disparity with latitude. PLoS ONE **14**, e0221490. (doi:10.1371/journal.pone. 0221490)

Conway Morris S. Life's Solution: Inevitable Humans in a Lonely Universe. Cambridge University Press, Cambridge, U.K. (doi:10.1017/CBO9780511535499)

Constantinescu G, Miyawaki S, Liao Q. 2013 Flow and turbulence structure past a cluster of freshwater mussels. Journal of Hydraulic Engineering **139**, 347-358. (doi:10.1061/(ASCE)HY.1943-7900.0000692)

Curley EA, Thomas R, Adams CE, Stephen A. 2021 Behavioural and metabolic responses of Unionida mussels to stress. Aquatic Conservation: Marine and Freshwater Ecosystems **31**, 3184-3200. (doi:10.1002/aqc.3689)

Curley EAM, Valyrakis M, Thomas R, Adams CE, Stephen A. 2021 Smart sensors to predict entrainment of freshwater mussels: a new tool in freshwater habitat assessment. Science of the Total Environment **787**, 147586. (doi:10.1016/j.scitotenv.2021.147586)

Cyr F, Paquet A, Martel AL, Angers B. 2007 Cryptic lineages and hybridization in freshwater mussels of the genus *Pyganodon* (Unionidae) in northeastern North America. Canadian Journal of Zoology **85**, 1216-1227. (doi:10.1139/Z07-104)

Daniel WM, Brown KM. 2013 Multifactorial model of habitat, host fish, and landscape effects on Louisiana freshwater mussels. Freshwater Science **32**, 193-203. (doi:10.1899/12-137.1)

Daniel WM, Brown KM. 2014 The role of life history and behavior in explaining unionid mussel distributions. Hydrobiologia **734**, 57-68. (doi:10.1007/s10750-014-1868-7)

Di Maio J, Corkum LD. 1997 Patterns of orientation in unionids as a function of rivers with differing hydrological variability. Journal of Molluscan Studies **63**, 531-539. (doi:10.1093/mollus/63.4.531)

Eagar RM. 1978 Shape and function of the shell: a comparison of some living and fossil bivalve molluscs. Biological Reviews **53**, 169-210. (doi:10.1111/j.1469-185X.1978.tb01436.x)

Edgar RC. 2004 MUSCLE: a multiple sequence alignment method with reduced time and space complexity. BMC Bioinformatics **5**, 1-19. (doi:10.1186/1471-2105-5-113)

Edie SM, Collins KS, Jablonski D. 2022 Specimen alignment with limited point-based homology: 3D morphometrics of disparate bivalve shells (Mollusca: Bivalvia). PeerJ. (doi:10.7717/peerj.13617)

Endler, JA. 1982 Convergent and divergent effects of natural selection on color patterns in two fish faunas. Evolution **36,** 178-188. (doi:10.2307/2407979)

Ferreira-Rodríguez N, Akiyama YB, Aksenova OV, Araujo R, Barnhart MC, Bespalaya YV, Bogan AE, Bolotov IN, Budha PB, Clavijo C, Clearwater SJ, et al. 2019 Research priorities for freshwater mussel conservation assessment. Biological Conservation **231**, 77-87. (doi:10.1016/j.biocon.2019.01.002)

Fox J, Weisberg S. 2019 An R Companion to Applied Regression, Third edition. Sage, Thousand Oaks CA.

Friedman ST, Price SA, Hoey AS, Wainwright PC. 2016 Ecomorphological convergence in planktivorous surgeonfishes. Journal of Evolutionary Biology **29**, 965-78. (doi:10.1111/jeb.12837)

Garamszegi LZ, Møller AP. 2010 Effects of sample size and intraspecific variation in phylogenetic comparative studies: a meta-analytic review. Biological Reviews, 85(4), pp.797-805. (doi:10.1111/j.1469-185X.2010.00126.x)

Gearty W. 2023. Deeptime: Plotting Tools for Anyone Working in Deep Time. R package version 1.0.0. (doi:10.5281/zenodo.7558839)

Gelman A, Hill J. 2007 Data Analysis Using Regression and Hierarchical/Multilevel Models. Cambridge University Press, Cambridge, U.K. (doi:10.1017/CBO9780511790942)

Gillis PL. 2011 Assessing the toxicity of sodium chloride to the glochidia of freshwater mussels: implications for salinization of surface waters. Environmental Pollution **159**, 1702-8. (doi:10.1016/j.envpol.2011.02.032)

Goodding DD, Williams MG, Ford DF, Williams LR, Ford NB. 2019 Associations between substrate and hydraulic variables and the distributions of a sculptured and an unsculptured unionid mussel. Freshwater Science **38**, 543-553. (doi:10.1086/704795)

Gould SJ. 1989 Wonderful Life: The Burgess Shale and the Nature of History. WW Norton & Company, New York, U.S. (doi:10.1017/S0094837300004310)

Graf DL, Cummings KS. 2021 A ‘big data’ approach to global freshwater mussel diversity (Bivalvia: Unionoida), with an updated checklist of genera and species. Journal of Molluscan Studies **87**, eyaa034. (doi:10.1093/mollus/eyaa034)

Graf DL. 1998 Freshwater pearly mussels: pigtoes and Ortmann’s law. American Conchologist **26**, 20-21.

Graf DL. 2007 Palearctic freshwater mussel (Mollusca: Bivalvia: Unionoida) diversity and the Comparatory Method as a species concept. Proceedings of the Academy of Natural Sciences of Philadelphia **156**, 71-88. (doi:10.1635/0097-3157(2007)156[71:PFMMBU]2.0.CO;2)

Graf DL, Cummings KS. 2021 A ‘big data’ approach to global freshwater mussel diversity (Bivalvia: Unionoida), with an updated checklist of genera and species. Journal of Molluscan Studies **87**, p.eyaa034. (doi:10.1093/mollus/eyaa034)

Grant BR, Grant PR. 1993 Evolution of Darwin’s finches caused by a rare climatic event. Proceedings of the Royal Society of London. Series B: Biological Sciences **251**, 111-7. (doi:10.1098/rspb.1993.0016)

Grier NM. 1920 Morphological features of certain mussel-shells found in Lake Erie, compared with those of the corresponding species found in the drainage of the Upper Ohio. Annales of the Carnegie Museum **13**, 145-182.

Grossnickle DM, Brightly WH, Weaver LN, Stanchak KE, Roston RA, Pevsner SK, Stayton CT, Polly PD, Law CJ. 2022 A cautionary note on quantitative measures of phenotypic convergence. bioRxiv. (doi:10.1101/2022.10.18.512739)

Grossnickle DM, Chen M, Wauer JG, Pevsner SK, Weaver LN, Meng QJ, Liu D, Zhang YG, Luo ZX. 2020 Incomplete convergence of gliding mammal skeletons. Evolution **74**, 2662-80. (doi:10.1111/evo.14094)

Gum B, Lange M, Geist J. 2011 A critical reflection on the success of rearing and culturing juvenile freshwater mussels with a focus on the endangered freshwater pearl mussel (*Margaritifera margaritifera* L.). Aquatic Conservation: Marine and Freshwater Ecosystems **21**, 743-751. (doi:10.1002/aqc.1222)

Haag WR. 2010 A hierarchical classification of freshwater mussel diversity in North America. Journal of Biogeography **37**, 12-26. (doi:10.1111/j.1365-2699.2009.02191.x)

Haag WR. 2012 North American Freshwater Mussels: Natural History, Ecology, and Conservation. Cambridge University Press, Cambridge, U.K. (doi:10.1017/CBO9781139048217)

Haag WR, Rypel AL. 2011 Growth and longevity in freshwater mussels: evolutionary and conservation implications. Biological Reviews **86**, 225-47. (doi:10.1111/j.1469-185X.2010.00146.x)

Haag WR, Warren, Jr ML. 1998 Role of ecological factors and reproductive strategies in structuring freshwater mussel communities. Canadian Journal of Fisheries and Aquatic Sciences **55**, 297-306. (doi:10.1139/f97-210)

Haag WR, Williams JD. 2014 Biodiversity on the brink: an assessment of conservation strategies for North American freshwater mussels. Hydrobiologia **735**, 45-60. (doi:10.1007/s10750-013-1524-7)

Hanson JM, Mackay WC, Prepas EE. 1988 Population size, growth, and production of a unionid clam, *Anodonta grandis simpsoniana*, in a small, deep Boreal Forest lake in central Alberta. Canadian Journal of Zoology **66**, 247-253. (doi:10.1139/z88-035)

Harmon LJ, Losos JB. 2005 The effect of intraspecific sample size on type I and type II error rates in comparative studies. Evolution **59**, 2705-10. (doi:10.1111/j.0014-3820.2005.tb00981.x)

Hastie LC, Boon PJ, Young MR, Way S. 2001 The effects of a major flood on an endangered freshwater mussel population. Biological Conservation **98**, 107-15. (doi:10.1016/S0006-3207(00)00152-X)

Hawkins OH, Ortega-Jiménez VM, Sanford CP. 2022 Knifefish turning control and hydrodynamics during forward swimming. Journal of Experimental Biology **225**, p.jeb243498. (doi:10.1242/jeb.243498)

Heino M, Kaitala V. 1996 Optimal resource allocation between growth and reproduction in clams: why does indeterminate growth exist? Functional Ecology **10**, 245-51. (doi:10.2307/2389849)

Hendry AP. 2016 Eco-evolutionary Dynamics. Princeton university press. (doi:10.1515/9781400883080)

Hewitt TL, Wood CL, Foighil DÓ. 2019 Ecological correlates and phylogenetic signal of host use in North American unionid mussels. International Journal for Parasitology **49**, 71-81. (doi:10.1016/j.ijpara.2018.09.006)

Hibbitts TJ, Fitzgerald LA. 2005 Morphological and ecological convergence in two natricine snakes. Biological Journal of the Linnean Society **85**, 363-71. (doi:10.1111/j.1095-8312.2005.00493.x)

Hinch SG, Bailey RC, Green RH. 1986 Growth of *Lampsilis radiata* (Bivalvia: Unionidae) in sand and mud: a reciprocal transplant experiment. Canadian Journal of Fisheries and Aquatic Sciences **43**, 548-52. (doi:10.1139/f86-06)

Hornbach DJ, Kurth VJ, Hove MC. 2010 Variation in freshwater mussel shell sculpture and shape along a river gradient. The American Midland Naturalist **164**, 22-36. (doi:10.1674/0003-0031-164.1.22)

Hothorn T, Bretz F, Westfall P. 2008 Simultaneous inference in general parametric models. Biometrical Journal **50**, 346-363. (doi:10.1002/bimj.200810425)

Howard AD. 1922 Experiments in the culture of fresh-water mussels. Bulletin of the US Bureau of Fisheries **38**, 63-90.

Inoue K, Hayes DM, Harris JL, Christian AD. 2013 Phylogenetic and morphometric analyses reveal ecophenotypic plasticity in freshwater mussels *Obovaria jacksoniana* and *Villosa arkansasensis* (Bivalvia: Unionidae). Ecology and Evolution **3**, 2670-2683. (doi:10.1002/ece3.649)

Jeratthitikul E, Phuangphong S, Sutcharit C, Prasankok P, Kongim B, Panha S. 2019 Integrative taxonomy reveals phenotypic plasticity in the freshwater mussel

Contradens contradens (Bivalvia: Unionidae) in Thailand, with a description of a new species. Systematics and Biodiversity **17**, 134-147. (doi:10.1080/14772000.2018.1554607)

Johnson EH. 2020 Experimental tests of bivalve shell shape reveal potential tradeoffs between mechanical and behavioral defenses. Scientific Reports **10**, 1-2. (doi:10.1038/s41598-020-76358-x)

Karrenberg S, Edwards PJ, Kollmann J. 2002 The life history of Salicaceae living in the active zone of floodplains. Freshwater Biology **47**, 733-48. (doi:10.1046/j.1365-2427.2002.00894.x)

Katoh K, Kuma KI, Toh H, Miyata T. 2005 MAFFT version 5: improvement in accuracy of multiple sequence alignment. Nucleic Acids Research **33**, 511-518. (doi:10.1093/nar/gki198)

Keogh SM, Simons AM. 2019 Molecules and morphology reveal 'new' widespread North American freshwater mussel species (Bivalvia: Unionidae). Molecular Phylogenetics and Evolution **138**, 182-92. (doi:10.1016/j.ympev.2019.05.029)

Kesler DH, Van Tol, NA. 2000 Growth of the freshwater mussel *Pyganodon grandis* (Unionidae) in two west Tennessee borrow pits. Journal of the Tennessee Academy of Science **75**, 71-75.

Kumar SS, Kozarek J, Hornbach D, Hondzo M, Hong J. 2019 Experimental investigation of turbulent flow over live mussels. Environmental Fluid Mechanics **19**, 1417-1430. (doi:10.1007/s10652-019-09664-2)

Lamouroux N, Poff NL, Angermeier PL. 2002 Intercontinental convergence of stream fish community traits along geomorphic and hydraulic gradients. Ecology **83**,1792-807. (doi:10.1890/0012-9658(2002)083[1792:ICOSFC]2.0.CO;2)

Larsson A. 2014 AliView: a fast and lightweight alignment viewer and editor for large datasets. Bioinformatics **30**, 3276-3278. (doi:10.1093/bioinformatics/btu531)

Lauder GV, Wainwright DK, Domel AG, Weaver JC, Wen L, Bertoldi K. 2016 Structure, biomimetics, and fluid dynamics of fish skin surfaces. Physical Review Fluids **1**, 060502. (doi:10.1103/PhysRevFluids.1.060502)

Lee J, Marr J, Guala M. 2022 On Sediment Mass Flux Directionality Induced by Yawed Permeable Vanes under Near-Critical Mobility Conditions. Journal of Hydraulic Engineering **148**, p.04022019. (doi:10.1061/(ASCE)HY.1943-7900.0002006)

Lefevre G, Curtis WC. 1910 Reproduction and parasitism in the Unionidae. Journal of Experimental Zoology 9, 79–116.

Leggett HC, Buckling A, Long GH, Boots M. 2013 Generalism and the evolution of parasite virulence. Trends in ecology & evolution, **28**, 592-596. (doi:10.1016/j.tree.2013.07.002)

Levine TD, Hansen HB, Gerald GW. 2014 Effects of shell shape, size, and sculpture in burrowing and anchoring abilities in the freshwater mussel *Potamilus alatus* (Unionidae). Biological Journal of the Linnean Society **111**, 136-44. (doi:10.1111/bij.12178)

Lopes-Lima M, Bolotov IN, Aldridge DC, Fonseca MM, Gan HM, Gofarov MY, Kondakov AV, Prié V, Sousa R, Varandas S, Vikhrev IV. 2018 Expansion and systematics redefinition of the most threatened freshwater mussel family, the Margaritiferidae. Molecular Phylogenetics and Evolution **127**, 98-118. (doi:10.1016/j.ympev.2018.04.041)

Lopez JW, Vaughn, CC. 2021 A review and evaluation of the effects of hydrodynamic variables on freshwater mussel communities. Freshwater Biology **66**, 1665-79. (doi:10.1111/fwb.13784)

Losos JB. 2011 Convergence, adaptation, and constraint. Evolution **65**, 1827-40. (doi:10.1111/j.1558-5646.2011.01289.x)

Losos JB, Creer DA, Glossip D, Goellner R, Hampton A, Roberts G, Haskell N, Taylor P, Ettling J. 2000 Evolutionary implications of phenotypic plasticity in the hindlimb of the lizard *Anolis sagrei*. Evolution **54**, 301-5. (doi:10.1111/j.0014-3820.2000.tb00032.x)

Losos JB, Jackman TR, Larson A, Queiroz KD, Rodríguez-Schettino L. 1998 Contingency and determinism in replicated adaptive radiations of island lizards. Science **279**, 2115-8. (doi:10.1126/science.279.5359.2115)

Losos JB, Schoener TW, Warheit KI, Creer D. 2001 Experimental studies of adaptive differentiation in Bahamian *Anolis* lizards. Genetica **112–113**, 399–415.

Lytle DA, Poff NL. 2004 Adaptation to natural flow regimes. Trends in Ecology & Evolution **19**, 94-100. (doi:10.1016/j.tree.2003.10.002)

Mackie GL, Flippance LA. 1983 Intra-and interspecific variations in calcium content of freshwater Mollusca in relation to calcium content of the water. Journal of Molluscan Studies **49**, 204-12. (doi:10.1093/oxfordjournals.mollus.a065714)

Maddison WP, Maddison DR. 2021 Mesquite: a modular system for evolutionary analysis. Version 3.70. http://www.mesquiteproject.org.

Medina R, Vitt DH, Shevock JR. 2020 Orthotrichum subgenus *Rivularium* revisited: convergent morphology and repeated evolution of the rheophytic syndrome. The Bryologist **123**, 593-600. (doi:10.1639/0007-2745-123.4.593)

Negus CL. 1966 A quantitative study of growth and production of unionid mussels in the River Thames at Reading. The Journal of animal ecology **35**, 513-532. (doi:10.2307/2489)

Nichols SJ, Silverman H, Dietz TH, Lynn JW, Garling DL. 2005 Pathways of food uptake in native (Unionidae) and introduced (Corbiculidae and Dreissenidae) freshwater bivalves. Journal of Great Lakes Research **31**, 87-96. (doi:10.1016/S0380-1330(05)70240-9)

Nikora V. 2010 Hydrodynamics of aquatic ecosystems: an interface between ecology, biomechanics and environmental fluid mechanics. River research and applications **26**, 367-384. (doi:10.1002/rra.1291)

Olivera-Hyde M, Hallerman E, Santos R, Jones J, Varnerin B, da Cruz Santos Neto G, Mansur MC, Moraleco P, Callil C. 2020 Phylogenetic assessment of freshwater

mussels *Castalia ambigua* and *C. inflata* at an ecotone in the Paraguay River basin, Brazil shows that inflated and compressed shell morphotypes are the same species. Diversity **12**, 481. (doi:10.3390/d12120481)

Ord TJ, Summers TC. 2015 Repeated evolution and the impact of evolutionary history on adaptation. BMC Evolutionary Biology **15**, 1-12. (doi:10.1186/s12862-015-0424-z)

Ortmann AE. 1919 A monograph of the naiades of Pennsylvania. Part III. Memoirs of the Carnegie Museum **8**, 1-384.

Ortmann AE. 1920 Correlation of shape and station in fresh-water mussels (Naiades). Proceedings of the American Philosophical Society **59**, 269-312.

Owen CT, McGregor MA, Cobbs GA, Alexander Jr JE. 2011 Muskrat predation on a diverse unionid mussel community: impacts of prey species composition, size and shape. Freshwater Biology **56**, 554-64. (doi:10.1111/j.1365-2427.2010.02523.x)

Pandolfo TJ, Cope WG, Arellano C, Bringolf RB, Barnhart MC, Hammer E. 2010 Upper thermal tolerances of early life stages of freshwater mussels. Journal of the North American Benthological Society **29**, 959-969. (doi:10.1899/09-128.1)

Paradis E, Schliep K. 2019 APE 5.0: an environment for modern phylogenetics and evolutionary analyses in R. Bioinformatics **35**, 526-528. (doi:10.1093/bioinformatics/bty633)

Parsheh M, Sotiropoulos F, Porté-Agel F. 2010 Estimation of power spectra of acoustic-doppler velocimetry data contaminated with intermittent spikes. Journal of Hydraulic Engineering **136**, 368-378. (doi:10.1061/(ASCE)HY.1943-7900.0000202)

Penn GH. 1939 A study of the life cycle of the freshwater mussel, *Anodonta grandis*. Nautilus **52**, 99-101.

Perles SJ, Christian AD, Berg DJ. 2003 Vertical migration, orientation, aggregation, and fecundity of the freshwater mussel *Lampsilis siliquoidea* The Ohio Journal of Science **103**, 73-78.

Pfeiffer JM, Breinholt JW, Page LM. 2019 Unioverse: a phylogenomic resource for reconstructing the evolution of freshwater mussels (Bivalvia, Unionoida). Molecular Phylogenetics and Evolution **137**, 114-126. (doi:10.1016/j.ympev.2019.02.016)

Pfeiffer JM, DuBose TP, Keogh SM. 2022 Synthesis of natural history collections data reveals patterns of US freshwater mussel diversity and decline. bioRxiv. (doi:10.1101/2022.09.22.509037)

Pfennig DW. 2021 Phenotypic plasticity & evolution: causes, consequences, controversies. Taylor & Francis. (doi:10.1201/9780429343001)

Pieri AM, Inoue K, Johnson NA, Smith CH, Harris JL, Robertson C, Randklev CR. 2018 Molecular and morphometric analyses reveal cryptic diversity within freshwater mussels (Bivalvia: Unionidae) of the western Gulf coastal drainages of the USA. Biological Journal of the Linnean Society **124**, 261-77. (doi:10.1093/biolinnean/bly046)

Popp A, Cope WG, McGregor MA, Kwak TJ, Augspurger T, Levine JF, Koch L. 2018 A Comparison of the chemical sensitivities between in vitro and in vivo propagated juvenile freshwater mussels: Implications for standard toxicity testing. Environmental toxicology and chemistry **37**, 3077-3085. (doi:10.1002/etc.4270)

Prezant RS, Dickinson GH, Chapman EJ, Mugno R, Rosen MN, Cadmus MB. 2022 Comparative assessment of shell properties in eight species of cohabiting unionid bivalves. Freshwater Mollusk Biology and Conservation **25**, 27-36. (doi:10.31931/FMBC-D-21-00001)

R Core Team. 2022 *R*: a language and environment for statistical computing. Vienna, Austria: R Foundation for Statistical Computing.

Rambaut, A, Drummond, AJ, Xie, D, Baele, G, Suchard, MA. 2018 Posterior summarization in Bayesian phylogenetics using Tracer 1.7. Systematic Biology **67**, 901-904. (doi:10.1093/sysbio/syy032)

Randklev CR, Hart MA, Khan JM, Tsakiris ET, Robertson CR. 2019 Hydraulic requirements of freshwater mussels (Unionidae) and a conceptual framework for how they respond to high flows. Ecosphere **10**, e02975. (doi:10.1002/ecs2.2975)

Reed TE, Schindler DE, Waples RS. 2011 Interacting effects of phenotypic plasticity and evolution on population persistence in a changing climate. Conservation Biology **25**, 56-63. (doi:10.1111/j.1523-1739.2010.01552.x)

Revell, LJ. 2012 phytools: an R package for phylogenetic comparative biology (and other things). Methods in Ecology and Evolution **2**, 217-223.

Ricciardi, A, Rasmussen, JB. 1999 Extinction rates of North American freshwater fauna. Conservation Biology **13**, 1220-1222. (doi:10.1046/j.1523-1739.1999.98380.x)

Rincon-Sandoval M, Duarte-Ribeiro E, Davis AM, Santaquiteria A, Hughes LC, Baldwin CC, Soto-Torres L, Acero P A, Walker Jr HJ, Carpenter KE, Sheaves M, Ortí G, Arcila D, Betancur-R R. 2020 Evolutionary determinism and convergence associated with water-column transitions in marine fishes. Proceedings of the National Academy of Sciences **117**, 33396-33403. (doi:10.1073/pnas.2006511117)

Rivera G. 2008 Ecomorphological variation in shell shape of the freshwater turtle *Pseudemys concinna* inhabiting different aquatic flow regimes. Integrative and Comparative Biology **48**, 769-787. (doi:10.1093/icb/icn088)

Sambrook Smith GH, Best JL, Ashworth PJ, Lane SN, Parker NO, Lunt IA, Thomas RE, Simpson CJ. 2010 Can we distinguish flood frequency and magnitude in the sedimentological record of rivers? Geology **38**, 579-82. (doi:10.1130/G30861.1)

Sansom BJ, Atkinson JF, Bennett SJ. 2018 Modulation of near-bed hydrodynamics by freshwater mussels in an experimental channel. Hydrobiologia **810**, 449-463. (doi:10.1007/s10750-017-3172-9)

Sansom BJ, Bennett SJ, Atkinson JF. 2022 Freshwater mussel burrow position and its relation to streambed roughness. Freshwater Science **41**, 315-326. (doi:10.1086/719993)

Sansom BJ, Bennett SJ, Atkinson JF, Vaughn CC. 2020 Emergent hydrodynamics and skimming flow over mussel covered beds in rivers. Water Resources Research **56**, p.e2019WR026252. (doi:10.1029/2019WR026252)

Savazzi E, Peiyi Y. 1992 Some morphological adaptations in freshwater bivalves. Lethaia **25**, 195-209. (doi:10.1111/j.1502-3931.1992.tb01384.x)

Schlager S. 2017 *Morpho* and *Rvcg*—shape analysis in *R*: *R*-packages for geometric morphometrics, shape analysis and surface manipulations. In Statistical Shape and Deformation Analysis: Methods, Implementation and Applications (eds G Zheng, S Li,G Székely), pp. 217–256. AcademicPress, London, UK..

Schluter D, Nagel LM. 1995 Parallel speciation by natural selection. The American Naturalist **146**, 292-301. (doi:10.1086/285799)

Segall M, Cornette R, Godoy-Diana R, Herrel A. 2020 Exploring the functional meaning of head shape disparity in aquatic snakes. Ecology and Evolution **10**, 6993-7005. (doi:10.1002/ece3.6380)

Sepkoski Jr JJ, Rex MA. 1974 Distribution of freshwater mussels: coastal rivers as biogeographic islands. Systematic Biology **23**, 165-188. (doi:10.1093/sysbio/23.2.165)

Serb JM, Sherratt E, Alejandrino A, Adams DC. 2017 Phylogenetic convergence and multiple shell shape optima for gliding scallops (Bivalvia: Pectinidae). Journal of Evolutionary Biology, **30**, 1736-47. (doi:10.1111/jeb.13137)

Sietman BE, Hove MC, Davis JM. 2018 Host attraction, brooding phenology, and host specialization on freshwater drum by 4 freshwater mussel species. Freshwater Science **37**, 96-107. (doi:10.1086/696382)

Simeone D, Tagliaro CH, Lima JO, Beasley CR. 2022 Relative importance of the environment and sexual dimorphism in determining shell shape in the Amazonian freshwater mussel *Castalia ambigua* (Unionida: Hyriidae) along a hydrological gradient. Zoomorphology, **141**, 233-243. (doi:10.1007/s00435-022-00562-8)

Smith LD, Jennings JA. 2000 Induced defensive responses by the bivalve *Mytilus edulis* to predators with different attack modes. Marine Biology **136**, 461-9. (doi:10.1007/s002270050705)

Smithsonian Institution High Performance Computing Cluster. (doi:10.25572/SIHPC)

Sotola VA, Sullivan KT, Littrell BM, Martin NH, Stich DS, Bonner TH. 2021 Short-term responses of freshwater mussels to floods in a southwestern USA river estimated using mark–recapture sampling. Freshwater Biology **66**, 349-61. (doi:10.1111/fwb.13642)

Stanley SM. 1970 Relation of shell form to life habits of the Bivalvia (Mollusca). Geological Society of America Memoirs, **125**, 1–282. (doi:10.1130/MEM125)

Stanley SM. 1975 Why clams have the shape they have: an experimental analysis of burrowing. Paleobiology **1**, 48-58. (doi:10.1017/S0094837300002189)

Stanley SM. 1981 Infaunal survival: alternative functions of shell ornamentation in the Bivalvia (Mollusca). Paleobiology **7**, 384-93. (doi:10.1017/S009483730000467X)

Stayton CT. 2008 Is convergence surprising? An examination of the frequency of convergence in simulated datasets. Journal of Theoretical Biology **252**, 1-14. (doi:10.1016/j.jtbi.2008.01.008)

Stayton CT. 2014 *convevol*: quantifies and assesses the significance of convergent evolution. R package version 1.

Stayton CT. 2015 The definition, recognition, and interpretation of convergent evolution, and two new measures for quantifying and assessing the significance of convergence. Evolution **69**, 2140-53. (doi:10.1111/evo.12729)

Strayer DL. 1981 Notes on the microhabitats of unionid mussels in some Michigan streams. American Midland Naturalist **106**, 411-415.

Strayer DL. 2008 Freshwater mussel ecology: a multifactor approach to distribution and abundance. University of California Press, Berkeley, U.S.A.

Strayer DL. 2014 Understanding how nutrient cycles and freshwater mussels (Unionoida) affect one another. Hydrobiologia **735**, 277-292. (doi:10.1007/s10750-013-1461-5)

Strayer DL, Hamilton SK, Malcom HM. 2021 Long-term increases in shell thickness in *Elliptio complanata* (Bivalvia: Unionidae) in the freshwater tidal Hudson River. Freshwater Biology **1**, 1375-81. (doi:10.1111/fwb.13723)

Strayer DL, Hunter DC, Smith LC, Borg CK. 1994 Distribution, abundance, and roles of freshwater clams (Bivalvia, Unionidae) in the freshwater tidal Hudson River. Freshwater Biology **31**, 239-248. (doi:10.1111/j.1365-2427.1994.tb00858.x)

Surber T. 1913 Notes on the natural hosts of fresh-water mussels. Bulletin of the Bureau of Fisheries. Issued separately as U.S. Bureau of Fisheries Document 778.

Tan YK, Burke AC, and Thomas E. 2022 Out of their shells: digitisation of endangered diversity in orphaned collections spurs access and discovery. Curator **65**, 355-378. (doi:10.1111/cura.12464)

Terui A, Ooue K, Urabe H, Nakamura F. 2017 Parasite infection induces size-dependent host dispersal: consequences for parasite persistence. Proceedings of the Royal Society B: Biological Sciences, **284**, 20171491. (doi:10.1098/rspb.2017.1491)

Trdan RJ, Hoeh WR. 1982 Eurytopic host use by two congeneric species of freshwater mussel (Pelecypoda: Unionidae: *Anodonta*). American Midland Naturalist **108**, 381-388. (doi:10.2307/2425500)

Trontelj P, Blejec A, Fišer C. 2012 Ecomorphological convergence of cave communities. Evolution **66**, 3852-3865. (doi:10.1111/j.1558-5646.2012.01734.x)

Trueman ER, Brand AR, Davis P. 1966 The dynamics of burrowing of some common littoral bivalves. Journal of Experimental Biology **44**, 469-92. (doi:10.1242/jeb.44.3.469)

Tuttle-Raycraft S, Ackerman JD. 2020 Evidence of phenotypic plasticity in the response of unionid mussels to turbidity. Freshwater Biology **65**, 1989-1996. (doi:10.1111/fwb.13595)

U.S. Geological Survey. [USGS] 2020 National Watershed Boundary Dataset (ver. USGS National Watershed Boundary Dataset in FileGDB 10.1 format (published 20200701), accessed July 07, 2020 at https://www.usgs.gov/national-hydrography/access-national-hydrography-products

van Steenis CG. 1981 Rheophytes of the world: an account of the flood-resistant flowering plants and ferns and the theory of autonomous evolution. Sijthoff & Noordhoff, Alphen aan den Rijn & Rockville.

Vaughn CC, Nichols SJ, Spooner DE. 2008 Community and foodweb ecology of freshwater mussels. Journal of the North American Benthological Society **27**, 409-423. (doi:10.1899/07-058.1)

Vehtari A, Gelman A, Gabry J. 2017 Practical Bayesian model evaluation using leave-one-out cross-validation and WAIC. Statistics and Computing **27**, 1413-32.

Vermeij GJ, Dudley EC. 1985 Distributions of adaptations: a comparison between functional shell morphology of freshwater and marine pelecypods. In: Trueman ER, Biology of the Mollusca, Vol. 10. Academic Press, London, U.K. p. 461-478.

Watters GT. 1992 Unionids, fishes, and the species-area curve. Journal of Biogeography **1**, 481-90. (doi:10.2307/2845767)

Watters GT. 1994 Form and function of unionoidean shell sculpture and shape (Bivalvia). American Malacological Bulletin **11**, 1-20.

Wickham H, Averick M, Bryan J, Chang W, McGowan LD, François R, Grolemund G, Hayes A, Henry L, Hester J, Kuhn M, Pedersen TL, Miller E, Bache SM, Müller K, Ooms J, Robinson D, Seidel DP, Spinu V, Takahashi K, Vaughan D, Wilke C, Woo K, Yutani H, 2019 Welcome to the tidyverse. Journal of Open Source Software **4**, 1686. (doi: 10.21105/joss.01686)

Wilson CB. 1916 Copepod parasites of fresh-water fishes and their economic relations to mussel glochidia. Bulletin of the U.S. Fish Commission **34**, 331-374. Issued separately as U.S. Bureau of Fisheries Document 824.

Winter DJ. 2017 rentrez: An R package for the NCBI eUtils API. PeerJ Preprints **5**, e3179v2. (doi:10.7287/peerj.preprints.3179v2)

Wu H, Constantinescu G, Zeng J. 2020 Flow and entrainment mechanisms around a freshwater mussel aligned with the incoming flow. Water resources research **56**, p.e2020WR027983. (doi:10.1029/2020WR027983)

Wu R, Liu X, Guo L, Zhou C, Ouyang S, Wu X. 2022 DNA barcoding, multilocus phylogeny, and morphometry reveal phenotypic plasticity in the Chinese freshwater mussel *Lamprotula caveata* (Bivalvia: Unionidae). Ecology and Evolution **12**, e9035. (doi:10.1002/ece3.9035)

Zale AV, Neves RJ. 1982 Reproductive biology of four freshwater mussel species (Mollusca: Unionidae) in Virginia. Freshwater Invertebrate Biology **1**, 17-28. (doi:10.2307/3259440)

Zelditch ML, Ye J, Mitchell JS, Swiderski DL. 2017 Rare ecomorphological convergence on a complex adaptive landscape: body size and diet mediate evolution of jaw shape in squirrels (Sciuridae). Evolution **71**, 633-49. (doi:10.1111/evo.13168)

Zieritz A, Aldridge DC. 2009 Identification of ecophenotypic trends within three European freshwater mussel species (Bivalvia: Unionoida) using traditional and modern morphometric techniques. Biological Journal of the Linnean Society **98**, 814-25. (doi:10.1111/j.1095-8312.2009.01329.x)

Zieritz A, Hoffman JI, Amos W, Aldridge DC. 2010 Phenotypic plasticity and genetic isolation-by-distance in the freshwater mussel *Unio pictorum* (Mollusca: Unionoida). Evolutionary Ecology **24**, 923-938. (doi:10.1007/s10682-009-9350-0)